Functionalization of DNA Nanostructures for Cell Signaling Applications

by

Ronnie O. Pedersen

Department of Chemistry
Duke University

Date:_____

Approved:

_____
Thomas LaBean, Supervisor

_____
Stephen L. Craig, Co-supervisor

_____
Terrence G. Oas

_____
Steven W. Baldwin

Dissertation submitted in partial fulfillment of
the requirements for the degree of Doctor
of Philosophy in the Department of
Chemistry in the Graduate School
of Duke University

2014

ABSTRACT

Functionalization of DNA Nanostructures for Cell Signaling Applications

by

Ronnie Pedersen

Department of Chemistry
Duke University

Date:_____
Approved:

_____
Thomas LaBean, Supervisor

_____
Stephen L. Craig, Co-Supervisor

_____
Terrence G. Oas

_____
Steven W. Baldwin

An abstract of a dissertation submitted in partial fulfillment of the requirements for the degree of Doctor of Philosophy in the Department of Chemistry in the Graduate School of Duke University

2014

Abstract

Transforming growth factor β (TGF-β) is an important cytokine responsible for a wide range of different cellular functions including extracellular matrix formation, angiogenesis and epithelial-mesenchymal transition. We have sought to use self-assembling DNA nanostructures to influence TGF-β signaling.

The predictable Watson Crick base pairing allows for designing self-assembling nanoscale structures using oligonucleotides. We have used the method of DNA origami to assemble structures functionalized with multiple peptides that bind TGF-β receptors outside the ligand binding domain. This allows the nanostructures to cluster TGF-β receptors and lower the energy barrier of ligand binding thus sensitizing the cells to TGF-β stimulation. To prove efficacy of our nanostructures we have utilized immunofluorescent staining of Smad2/4 in order to monitor TGF-β mediated translocation of Smad2/4 to the cell nucleus. We have also utilized Smad2/4 responsive luminescence constructs that allows us to quantify TGF-β stimulation with and without nanostructures. Our data demonstrate that these functionalized nanostructures are capable of sensitizing cells to TGF-β stimulation and stimulating cellular response at much lower TGF-β concentration.

To functionalize our nanostructures we relied on biotin-streptavidin linkages. This introduces a multivalency that is not necessarily desirable in all designs. Therefore we have investigated alternative means of functionalization.

The first approach is based on targeting DNA nanostructure by using zinc finger binding proteins. Efficacy of zinc finger binding proteins was assayed by the use of enzyme-linked immunosorbent (ELISA) assay and atomic force microscopy (AFM). While ELISA indicated a relative specificity of zinc finger proteins for target DNA sequences AFM showed a high degree of non-specific binding and insufficient affinity.

The second approach is based on using peptide nucleic acid (PNA) incorporated in the nanostructure through base pairing. PNA is a synthetic DNA analog consisting of a backbone of repeating N-(2-aminoethyl)-glycine units to which purine and pyrimidine bases are linked by amide bonds. The solid phase synthesis of PNA allows for convenient extension of the backbone into a peptide segment enabling automatic peptide functionalization of DNA nanostructures. Using biotinylation and AFM, we have investigated how the neutral character of the PNA backbone and the addition of positive lysine residues alters the incorporation in DNA-based nanostructures compared to a DNA control. Results indicate that PNA can successfully be used to functionalize DNA nanostructures and encourage future studies combining PNA functionalization and cell receptor stimulation.

Contents

List of Tables

List of Figures

Abbreviations

AFM: Atomic Force Microscopy

AP: Alkaline Phosphatase

AuNP: gold NanoParticle

DMTMM: 4-(4,6-DiMethoxy[1,3,5]Triazin-2-yl)-4-Methyl-Morpholinium chloride

DNA: Deoxyribo-Nucleic Acid

ECM: Extra Cellular Matrix

ELISA: Enzyme-Linked ImmunoSorbent Assay

FAM: Fluorescein AMidite

GFP: Green Fluorescent Protein

HPLC: High Pressure Liquid Chromatography

MBP: Maltose Binding Protein

PAGE: Poly-Acrylamide Gel Electrophoresis

PDGF: Platelet Derived Growth Factor

PFTase: Protein FarnesylTransferase

PI: Pyrrole–Imidazole

PNA: Peptide Nucleic Acid

SCI: Spinal Cord Injury

SDS: Sodium Dodecyl Sulfate

SPR: Surface Plasmon Resonance

STV: STreptaVidin

TAEM: 20 mM Tris, 2 mM EDTA, 12.5 mM $MgCl_2$, Acetic acid to pH 7.6

TGF-β: Transforming Growth Factor β

TβRI: Tranforming growth factor β Receptor type I

TβRII: Transforming growth factor β Receptor type II

ZBA: Zinc Buffer A (100 mM Tris-HCl, 90 mM KCl, 90 μM $ZnCl_2$, pH 7.5.)

Acknowledgements

Jing Kong synthesized PNA molecules and Nicole Estrich helped with figures 1 and 2. Additionally I would like extend my thanks to my advisor, research group and committee for support and help throughout the project. To professor Elisabeth Loboa for support and help with cell cultures, professor Charles Gersbach for support and help with zinc finger proteins and professor Catalina Achim for support and help with peptide nucleic acids.

1. Introduction

The start of nanotechnology is famously credited to Richard Feynman's speech in 1959 entitled "There is Plenty of Room at the Bottom" [feynman1959]. In this speech Feynman outlines how the laws of physics should allow for smaller and smaller miniaturization to the point where the *Encyclopedia Britannica* could be written on the head of a pin and machines could be made small enough to perform *in situ* medical procedures.

Feynman found part of his inspiration in biology. This was likewise the starting point for K. E. Drexler's 1981 paper on molecular engineering.[1] In this paper Drexler envisioned an approach to molecular manufacturing inspired by protein-based cellular machinery, arguing that the ability to design protein molecules would enable the construction of molecular machines capable of general three-dimensional molecular syntheses.

We can conveniently label this approach – one guided by biological principles – as bionanotechnology, an approach that finds inspiration in biology to accomplish nanotechnological goals like the ones imagined by Feynman.

But what does it mean to be inspired or guided by biology in this context? If we think about cells, they not only define life as we know it, they also represent the most complex and diverse manufacturing systems we know. Relying on a myriad of different energy sources, cells can transform a vast range of input material to an equally vast range of output material while perceiving and responding to informational stimuli. An

essential mechanism in this process is molecular recognition and self-assembly at the nanoscale, as exemplified by the way proteins fold and the way enzymes recognize their substrates.[2] Bionanotechnology seeks to utilize these principles of self-assembly to develop technologies that mimic the capabilities of living cells in production and in information processing. Unlike the historical approach of milling down a macroscale unit with finer and finer tools, the use of self-assembly leads to a bottom-up style of manufacturing where individual nanoscale units come together to form micro- or macroscale assemblies.

As addressed by Drexler, the principal medium of cellular machinery is polypeptides. From an engineering point of view, this presents a problem, as protein folding is not yet fully understood, so we cannot yet design novel proteins with desired structures (let alone desired functions).[3] A solution to this problem, which many researchers have seized on, is to use the biological polymer deoxyribonucleic acid (DNA) as a molecular building material instead of polypeptides. DNA molecules form duplex helices based on Watson and Crick base-pairing.[4] A one-dimensional helix can be expanded into two and even three dimensions by designing DNA molecules that anneal to form branched-junction structures. The use of DNA as a structural material has resulted in the design and construction of a sufficient number of DNA-based nanoscale structures and devices to merit the label "structural DNA nanotechnology." This is the area in which the present dissertation is principally engaged. The predictable self-

assembling behavior of DNA enables the construction of highly complex three-dimensional nanoscale structures in a way that could not be accomplished at present using *de novo* designed proteins as the molecular construction material. Additionally, by utilizing the principle of toehold-mediated strand displacement, an astonishing range of dynamical functions can be incorporated in structures and devices.[5]

Still, a point of criticism that can be brought against DNA-based nanotechnology is that DNA does not serve any structural role in biology and it does not possess the diversity of chemical groups that polypeptides have. One could argue that since DNA-based nanotechnology does not directly imitate the nanotechnology of biology, which is principally based on polypeptides for structural and chemical tasks, it cannot hope to achieve the capabilities of biological systems. To counter this objection one can point to history and the many examples of biology inspiring non-biological technologies. Indeed North Carolina has laid claim to perhaps one of the most noteworthy examples. Here in the state of North Carolina, 110 years ago, the brothers Wilbur and Orville Wright changed the course of history when they performed the first controlled, powered and sustained heavier-than-air flight amongst the sand dunes of the outer banks.[6] The Wright brothers' fancy with powered flight followed many more and less elegant attempts at flying. It also sprang from the ubiquitous human admiration of birds and their ability to soar in the skies above us. The brothers spent much time studying birds in the hopes of elucidating the secret of flight. However, in the end the fixed bi-wing

airplane design of the first Wright Flyer, while relying on universal principles of aerodynamics, was far removed from the flapping wings of a bird. Yet it, and its successors, proved capable of heralding an era of powered heavier-than-air human flight.

In a similar fashion DNA self-assembly represents an approach for creating three dimensional organic structures with nanoscale accuracy that doesn't look quite like anything we see in nature. Still, it is the capability of biological systems to inspire and drive development of bionanotechnology. With this in mind it is pertinent to consider the biological properties of DNA as they form the basis for the nanotechnological potential of the polymer. A review of the overall biological properties of DNA may also suggest subject areas and biological subsystems which could be potential targets for manipulation or study using the molecular tools currently being developed within the field of structural DNA nanotechnology.

2. Biological Properties of DNA

The potential for DNA as a nanoscale construction material is underpinned by its biological properties. In biology DNA is the primary information carrier. Its role can be summed up in the central dogma which states that DNA codes for DNA and for RNA and RNA codes for proteins.[7] That DNA codes for DNA is evident in the way that hereditary information is passed on from parent to progeny. To understand what the rest of the dogma means, we have to know that RNA (ribonucleic acid) is a molecule structurally similar to DNA except it has a hydroxyl group at the 2' ribose position in place of DNA's hydrogen. A given DNA sequence will thus have a complementary RNA sequence to which it can anneal. In this way, a piece of DNA sequence – such as a gene – can be transcribed into a complementary RNA sequence, which can then be translated into a specific protein. Proteins are biological polymers made from 20 types of amino acids, and for any triplet of nucleobases (a codon), the genetic code specifies a specific amino acid. Proteins are the structural and catalytic 'machines' of living cells and thus determine the actions and makeup of the cell. In the following, we will look at how the properties of DNA are intimately tied to its role as the information carrier in living cells.

2.1 DNA in Cells and Molecular Cloning

The central dogma is a universal characteristic of all life as we know it. However, when considering the biological properties of DNA in more detail, we have to

differentiate between the major classifications of life. Biologists group different forms of life based on their similarity and relationship. Humans are distinct from apes but more closely related to them than they are to dogs. All three are distinct from plants and again these four share characteristics distinct from an Escherichia coli bacterium. At the very root of the classification of life, we find three so-called domains. These are Archaea, Bacteria, and Eucarya with members of Eucarya often referred to as eukaryotes .[8] Members of all three domains have the cell as the basic unit of life. A cell is a lipid membrane encapsulating the molecular machinery required for executing the central dogma as well as a metabolism. One defining feature of eukaryotes is that they have an additional internal lipid compartment, the nucleus, encapsulating their DNA. This is distinct from Archaea and Bacteria, and for this reason and others, these two domains have often been grouped together as prokaryotes.[9] In the following, we will be primarily concerned with common features and will only distinguish between eukaryotes and bacteria, disregarding the interesting but less studied Archaea. In bacteria, the entire genomic sequence is usually a single circular dsDNA condensed in one area of the cell. For E. coli, the size of this molecule is 4.6 Mb (million base pairs). In addition, bacteria often have smaller auxiliary pieces of dsDNA called plasmids. These are smaller circular molecules that can be replicated independently and transferred between different bacteria and thus can be used to transfer genetic traits such as antibiotic resistance. This is at the heart of molecular cloning and biotechnology. By inserting a gene of interest in

a plasmid and 'transfecting' it into a bacterium, the gene will then be replicated as the cell divides.[10] This technique is made possible by the use of restriction endonucleases which are a class of enzymes that cleave DNA at specific sequences.[11] Type II endonucleases typically cleave both strands of palindromic sequences, meaning sequences that read the same backward and forward. In the context of DNA, this is understood in the way that the sequence that reads 5′ to 3′ on one strand reads the same in the 5′ to 3′ direction on the complementary strand. By convention, genetic sequences are written 5′ to 3′. For example, the restriction endonuclease EcoRI recognizes the sequence 5′-G · AATTC-3′ and cleaves the backbone of both the written strand and the identical complementary strand (between the G and A). This creates a duplex with a short overhang (4 bases, in this case) called a sticky end. If a genetic sequence is cut from a genome with a certain restriction enzyme and mixed with purified plasmids cut with the same enzyme, the sticky ends will be complementary and can bridge the cut plasmid by hybridizing sticky ends to sticky ends. Endonucleases typically hydrolyze the oxygen-phosphorus bond on the 5′ side of the phosphorus, meaning that the 3′ end of the product will have a hydroxyl group and the 5′ end will terminate at the phosphate group. This configuration allows for ligase enzyme to covalently ligate the backbone once the sticky ends have annealed. Since ligation is an addition reaction between the phosphate and hydroxyl group it can be prevented by removing the phosphate on the 5′ end with phosphatase enzyme. Enzyme mediated ligation can be an important tool in

DNA nanotechnology as the nicks found in oligonucleotide based structures can be ligated following annealing based assembly, creating a sturdier structure.[12]

Eukaryotic cells have larger genomes than bacteria, from tens of millions of base pairs (bp) to more than 100 billion bp, distributed on several different DNA molecules termed chromosomes.[13, 14] These extremely long DNA molecules are organized on several different hierarchical levels during the cell cycle with the most compacted form visible through light microscopy during S phase as irregular X shapes. The first step of organization is achieved by spooling DNA onto alkaline proteins called histones. This creates a unit called a 'nucleosome' containing 146 bp that is visible in electron microscopy as beads on a string.[15] Compaction of DNA by histones plays an important role in regulating gene expression as more compact DNA are less available for RNA polymerases to bind. Another level of transcriptional control observed in some vertebrates – but not all eukaryotes – is based on methylation of cytosine on carbon 5. This chemical modification of DNA generally serves to repress genetic expression. Both histone-mediated compaction and methylation can change during a cell's life cycle but can also be passed on through several generations. Thus, the effective genetic expression is altered without altering the underlying DNA sequence.[16]

2.2 DNA Replication

The most important biological aspect of DNA's structure is arguably the ability to accurately transmit genetic information to offspring. As noted by Watson and Crick in

their seminal paper from 1953, the double-helical structure immediately suggests a mechanism for DNA replication. This mechanism is based on a semiconservative scheme where unwinding of the double helix allows each single strand to function as a template for the synthesis of new strands. Completion of a round of replication thus results in two helices, each containing one strand carried over from the parent duplex and one newly synthesized strand. If we consider this scheme, we can identify three processes that need to occur. The duplex needs to unwind. The resulting supercoil needs to be alleviated. And finally, new strands need to be synthesized using the parent strands as templates. Each of these processes is catalyzed by a different group of enzymes.

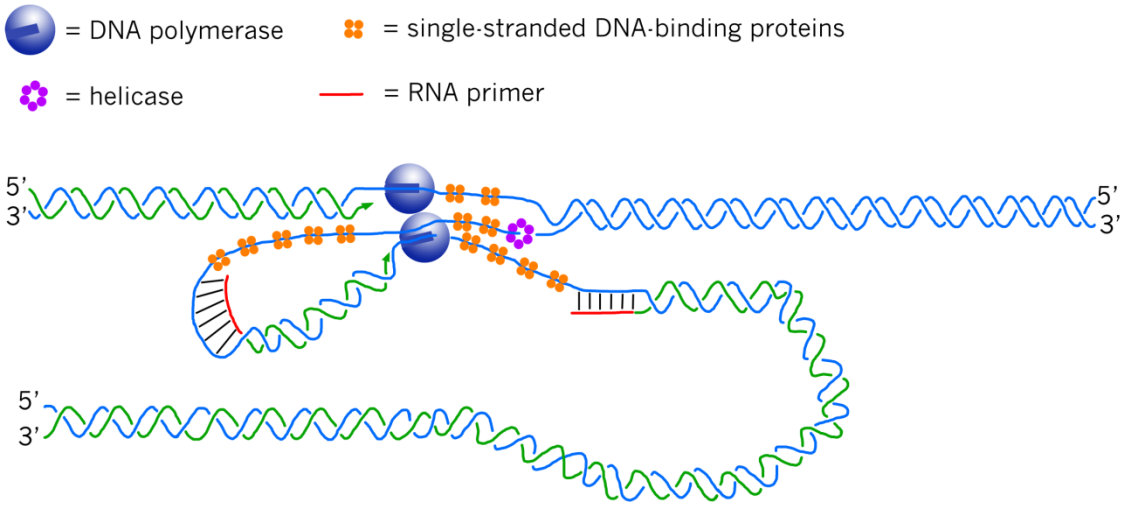

Figure 1 - DNA replication. DNA polymerase enzymes processively synthesizes a new DNA strand template by the nucleotide sequence in the parent strand.

In bacterial cells, replication is initiated at a specific site on the genome called the origin. Starting at this site, helicase enzymes utilize stored chemical energy by

hydrolyzing adenosine triphosphate (ATP) in order to peel the complementary DNA strands apart, while single-strand DNA-binding proteins bind the single strands and help prevent reannealing. The "bubble" created within the double-helix has two junctions called replication forks, and helicases run processively along the DNA in both directions extending the loop.[17] In both circular prokaryotic and large eukaryotic genomes, this process results in supercoiling which is alleviated by topoisomerase enzymes. In both prokaryotes and eukaryotes, topoisomerase enzymes are divided into type I and type II. Type I works by cleaving just one of the two strands creating what is called a nick in the backbone (a single-strand break). This is accomplished by a nucleophilic attack from a tyrosine hydroxyl group on a phosphorus atom in the sugar-phosphate backbone creating a transient covalent bond between enzyme and DNA. With the backbone nicked, either the duplex can now perform a controlled rotation or the intact single strand can be passed through the nick depending on the enzyme. Type II topoisomerases cleave both DNA strands of a duplex using two tyrosine residues. By holding the ends in place, a different part of the duplex is allowed to pass through the break, thus releasing or introducing supercoil. This reaction cycle is completed with ATP hydrolysis.[18] DNA polymerases are the primary enzymes responsible for DNA replication. These enzymes only catalyze the addition of deoxynucleoside triphosphates (dNTP) to the 3′ end of a growing strand using exposed single strand as a template for dNTP selection. This has two implications. The first is that a short primer strand is

needed for a DNA polymerase to work. A primer is synthesized by a primase enzyme and consists of RNA which is later excised and replaced with DNA. The second implication is that DNA polymerase only works in the 5′ to 3′ direction as the 3′ group makes a nucleophilic attack on the α-phosphate of the incoming dNTP. This results in a semi-discontinuous replication scheme where the two strands are replicated in different ways. One strand, called the leading strand, is initiated with one primer and extends continuously as the parent duplex is unwound. The other strand, called the lagging strand, can only be synthesized in short fragments as the synthesis is in the opposite direction of the moving replication fork. These short fragments are called Okazaki fragments and are 1,000–2,000 nucleotides long in E. coli and 100–200 fragments long in eukaryotes.[19] Besides catalyzing addition of dNTPs, all DNA polymerases in E. coli also have 3′ to 5′ exonuclease activity meaning that they can excise nucleotides in this direction. This is done when a noncomplementary nucleotide is erroneously added to the growing chain, thus improving the fidelity with which replication occurs. In E. coli, the specific polymerase responsible for substituting the RNA primers with DNA is called polymerase I. This enzyme also contains 5′→ 3′ exonuclease activity enabling it to extend from a nick by excising nucleotides on the 5′ side as it moves along. It can thereby remove the RNA primers, and subsequently, ligase can covalently link the fragments.

The incredible processivity of polymerases has great potential in DNA based nanotechnology as these enzymes can function as molecular motors running on DNA tracks and even moving loads around.[20]

2.3 Polymerase Chain Reaction

A synthetic form of DNA replication that has been of paramount importance is the polymerase chain reaction (PCR) technique. This method reliably amplifies miniscule amounts of DNA in a test tube within hours. This is accomplished by using a heat-stable polymerase and adding a large excess of both forward and reverse primers to a DNA target. Cycling between melting the duplex DNA, annealing primers, and letting the polymerase extend results in an exponential replication of the sequence bordered by the primers. See Figure 2.[21]

In the first step, a mixture of target DNA, nucleotides, primers, and heat-stable polymerase is heated to 94 °C in order to melt the target duplex. Heat-stable polymerase – such as Taq polymerase from the bacterium Thermus aquaticus – prevents the enzyme from denaturing during this step. (2) In the second step, the temperature is lowered to allow the primers to anneal to the target single-stranded DNA. The forward primer anneals to the 3′ end of the template strand and the reverse primer anneals to the 30 end

of the complementary strand.

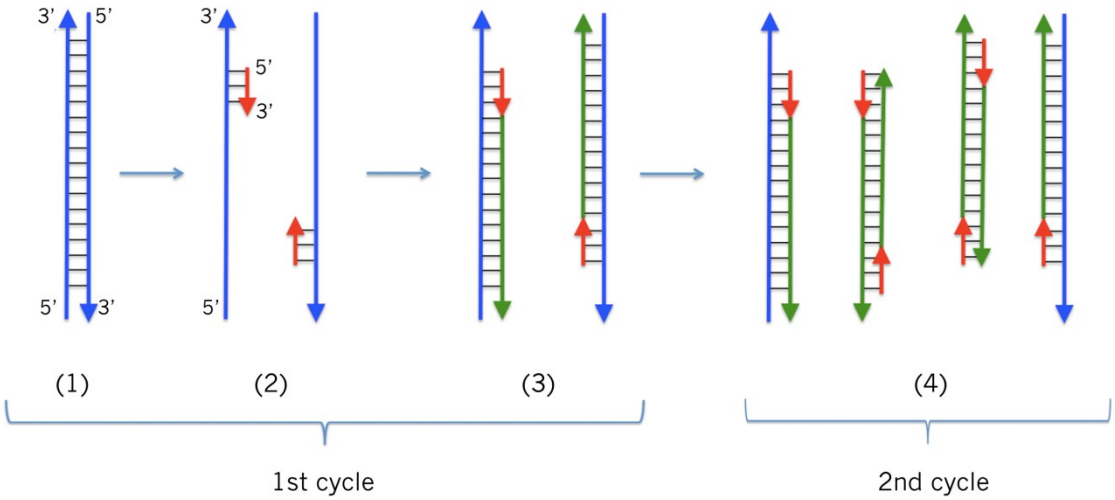

Figure 2 - Polymerase chain reaction. In each cycle the duplex is melted and then short oligonucleotide primers are annealed. The primers are then extended to form new duplexes and the cycle repeated.

The temperature chosen may depend on the melting temperature of the primers but will typically be around 55 °C. The high concentration of primers prevents the target DNA from reforming a duplex. (3) In the third step, the temperature is raised to the optimum working temperature of the polymerase. For Taq, this is 72 °C. The polymerase then extends the primers in the 5′ to 3′ direction. The first round of replication results in the new strands that extend beyond the region bordered by the primers in the 5′ direction. Subsequent rounds of replication from newly synthesized strands generate a sequence defined by primer location.

2.4 Transcription and Translation

Transcription is the process of synthesizing messenger RNA (mRNA) molecules based on the sequence of genes on a DNA molecule. Analogous to DNA replication, this is accomplished by an RNA polymerase that reads the template sequence in the 3′ to 5′ direction and synthesizes an mRNA molecule in the 5′ to 3′ direction. One of the sharp differences between prokaryotes and eukaryotes is the fact that there is only one known RNA polymerase in prokaryotes but three distinct RNA polymerases are known in eukaryotes.[22] This is mirrored in the fact that eukaryotes have more complex RNA-mediated control of expression. In E. coli, RNA polymerase associates with transcription factor proteins to initiate transcription of a gene. For this to occur, the transcription complex recognizes a specific sequence by binding non-covalently to the individual nucleobases. Both strands in a genome contain genetic information. In the context of a specific gene, the strand that is being 'read' by the polymerase – the complementary strand – is called the noncoding strand or the antisense strand. The strand that is identical in sequence to the resulting mRNA is called the coding strand or the sense strand.

Transcription is terminated when reaching a specific sequence, sometimes through the association of additional protein factors. The mRNA is processed by ribosomes where amino acids linked to transfer RNAs (tRNA) complementary to

specific codons (nucleotide triplets) are transferred to a growing polypeptide chain. The final product is a protein specified by the original gene sequence in the DNA molecule.[23]

The ribosome in itself represents one of the most intricate and fascinating examples of nanoscale robotics and has inspired the design of DNA nanostructures that can perform controlled polymeric assembly encoded by a DNA template.[24, 25]

2.5 Genetic Recombination

As the information carrier of life, DNA need not only facilitate accurate transmission of information but also allow for genetic diversity, the substrate of evolution. One process attributing to this is homologous recombination which is the recombination of two different DNA duplexes with a stretch of identical sequence. In other words, two different DNA duplexes exchanged their binding partners and then they are cleaved and the pieces recombined.[26] Different organisms have different enzymatic pathways facilitating this process but one common feature is the formation of a Holliday junction.[27] Figure 3. This four-arm junction illustrates the topological diversity of DNA that makes it suitable not only as a carrier of information but also as a nanometer-scale building material.

3. Nanotechnological Properties of DNA

3.1 DNA Tiles

The birth of structural DNA-nanotechnology dates back to a paper by N. C. Seeman published in 1982.[28] In this paper Seeman accounts for the construction of immobile DNA junctions and envisions how such molecular assemblies might form 2- and 3-dimensinal networks through sticky-end ligation. He imagined such networks might facilitate X-ray diffraction of both proteins and the junctions themselves. Part of his inspiration for this came from the Holliday junction motif. However, due to the sequence similarity between strands in a Holliday junction, a single junction unit – or tile – would be immobile. In other words, the junction point would move, eventually resulting in two separate duplexes. See Figure 3. Required for solving this issue were oligonucleotides appropriately complementary without having sequence symmetry.

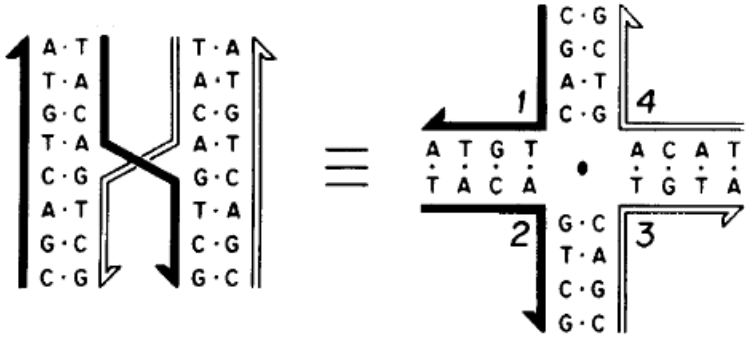

Figure 3 - Two different Illustrations of the same Holliday Junction motif. The junction can move due to sequence symmetry. Reproduced with permission.[28]

This was realized a year later when Seeman's research group reported the construction of the first immobile 4-arm junction[29] and Seeman and colleagues subsequently assembled both 5-, 6-, 8- and 12-arm junctions.[30,31]

Aiming at using these components as building blocks for larger aggregates double crossover DNA tiles of various compositions has been developed with increased rigidity.[32] Figure 4.

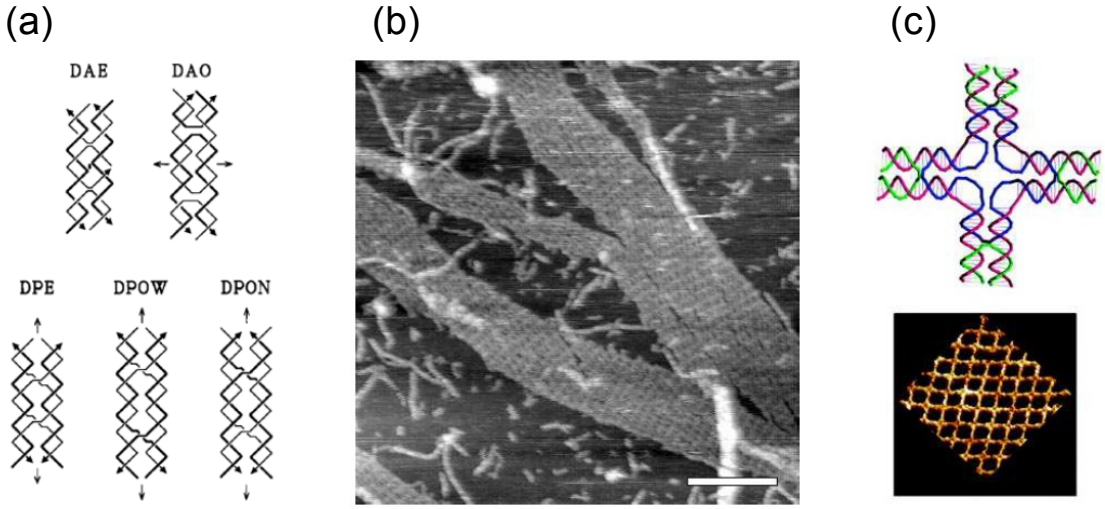

Figure 4 DNA tiles. (a) Different types of double crossover tiles. The complexes are made up of two helices that cross over at two positions. The first distinction between the different types is made based on parallel or anti parallel arrangement of the two helices. The second distinction is made based on whether there is an even or uneven number of half turns between the crossover positions. The third and final distinction is for parallel assemblies with an uneven number of half turns between crossovers, the last half turn can be either a wide or a narrow groove. The different configurations have different symmetries designated with arrows. By adding overhangs to the corners of these assemblies it was possible to form 2-dimensional grids. Reproduced with permission .[33] (b) Grid formed from DAE molecules. Scale bar is 300 nm. Reproduced with permission .[34] (c) Top: model of four-arm junctions. Bottom: AFM image of 2-dimensional grid assembled from four-arm junctions. Reproduced with permission.[35]

This rigidity was hypothesized to allow for predictable aggregation (designed assembly), experimentally verified by the assembly of the first 2-dimensional DNA lattice.[34] Several other grids based on different tiles have been developed e.g. Hao Yan *et al.* developed a four-arm tile, based on connected four-way junctions, used to create an periodic assembly and template silver nanowires.[35] An issue with tile based assemblies is that they are periodic and thereby not fully addressable. In other words you can selectively functionalize or modify individual strands within a tile but the introduced modification will be repeated throughout the final assembly. This has been circumvented by introducing sequential assembly of individual tiles by annealing tiles independently and then assembling in arrays at temperatures below the tile melting temperature.[36] This strategy relies on the low melt temperature of the short single stranded "sticky" ends that mediate assembly of individual tiles. The requirement for a low melting temperature places a requirement on the length of these segments and thereby the number of unique segments that can anneal in one step. In other words it forces the introduction of multiple steps for the assembly of larger structures thereby lowering yield.

3.2 DNA Origami

A DNA-nanotechnological breakthrough was reached in 2006 with a paper by P. W. K. Rothemund.[37] In it, Rothemund describes the first implementation of the technique of DNA-origami, a method that allows for the self-assembly of 2D structures

through the use of one single stranded DNA scaffold and hundreds of small staple strands used to "staple" the scaffold into a desired shape. The appeal of this technique stems from the fact that large fully addressable structures can be assembled with high yield and relative ease.

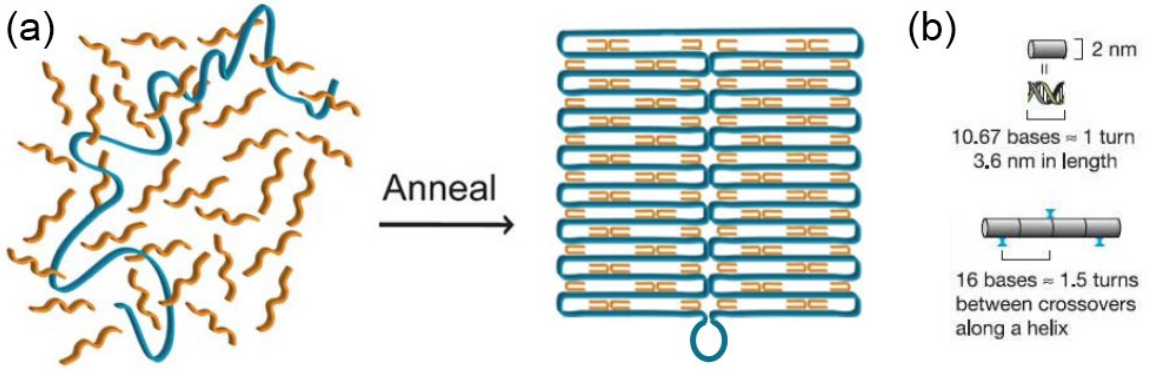

Figure 5 - DNA origami (a) Illustration of assembly principle with multiple short oligo strands "stapling" together a long single stranded scaffold. Reproduced with permission.[38] (b) Physical basis of structure approximation. A duplex is 2 nm wide and one turn is taken to be 10.67 bases or 3.6 nm. Reproduced with permission.[37]

The first step in making an origami structure is to approximate the desired shape by a geometrical arrangement of DNA helices an integer number of turns in lengths. These helices are connected with crossovers, i.e. positions where a single strand from each helix crosses over to form part of an adjacent helix. Due to the twist of the DNA molecule the crossover points have to be spaced an odd number of half turns apart. Rothemund tested 1.5 and 2.5-turn spacings and found the spacing of crossovers to influence the interhelix gap, with 1.5-turn spacing conferring a gap value close to 1 nm. The second step is to raster fold the main scaffold strand in such a way that is passes through all the imagined helices. In doing this a second set of scaffold crossovers are

formed with the restriction that when progressing in one direction scaffold crossovers have to be an odd number of half turns apart. Conversely, when reversing direction the scaffold crossovers have to be an even number of half turns apart. Design of structures is greatly simplified by the use of programs such as caDNAno and CanDo and it has been shown that the construction principle can be expanded into three dimensions with different kinds of helix packing.[39-42]

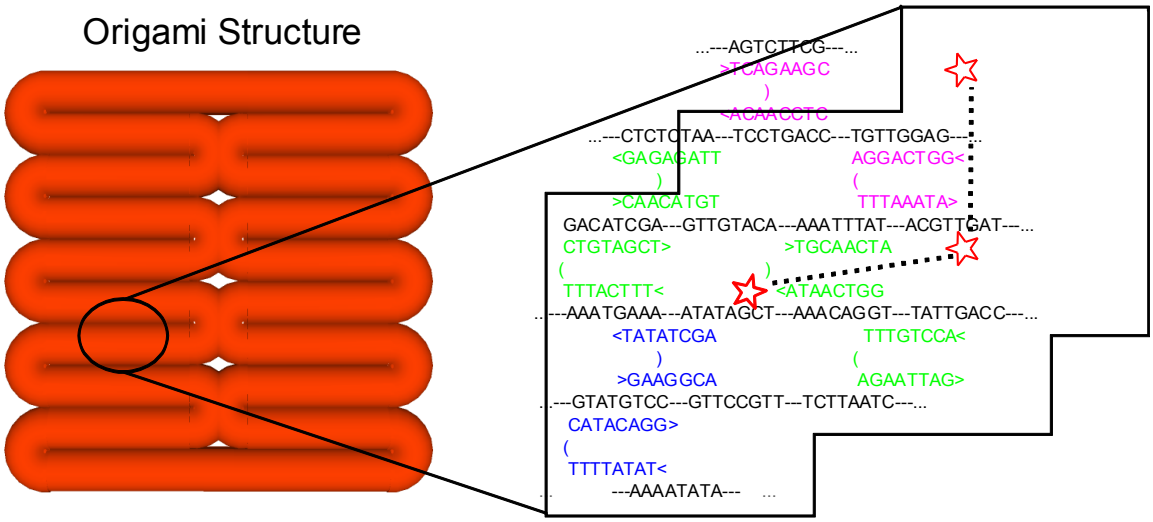

Figure 6 - Distances within origami structure. To the right is the sequence structure of origami with standard crossover. Individual oligo strands are color coded and the scaffold strand sequence is black. Red stars illustrate potential closest spaced 5′ functional groups added to the oligo strands. With the duplex model and gap distance in figure 5 distances α and β are 5.0 and 6.2 nm.

Each individual oligonucleotide strand in an origami can function as a handle to which a chemical functionality can be attached thus allowing the origami structure to function as a molecular scaffold or "breadboard". The smallest scale or the "resolution" that one can work with in this case is defined by each individual oligo. Figure 6

illustrates this. If a functional group is added to the 5′ end of the oligo and each duplex is 2 nm wide with a 1 nm gap in between duplexes and the length of a base pair is 3.6 nm / 10.67 base pairs then the distance from functional group to the next closest functional group is 5.0 to 6.2 nm. This defines the lower limit, or the "resolution" of the origami structure when functioning as a molecular scaffold.

4. Sensitization of Transforming Growth Factor-β Signaling by Multiple Peptides Patterned on DNA Nanostructures

4.1 Transforming Growth Factor β signaling

The first discovery of TGF-β was made in 1978 by Joseph E. De Larco and George J. Todaro .[43] They identified a novel component in extracts of murine sarcoma virus-transformed mouse fibroblasts that induced cell division in monolayers and colony formation in soft agar. It quickly became apparent that a similar factor was present in extracts from other tumor cells and that it worked in concert with Epidermal Growth Factor to transform the morphology and growth characteristics of treated cells. Furthermore, it was shown that the factor was a polypeptide and that there was not just one but three different isoforms.[44-46] Subsequent research has divulged the canonical signaling pathway of the three isoforms TGFβ-1, -2 and -3. Homodimers of these different isoforms assemble a ternary complex of two type I and two type II receptors (TβRI and TβRII respectively). However, TGF-β2 exhibit lower affinity to the receptor complex compared with TGF-β1 and TGF-β3 due to a substitution of Arg25 and Arg94 in these two isoforms to Lys25 and Lys94 in TGF-β2.[47, 48] Despite these differences it has been believed that assembly of the ternary complex occurs in the same general manner with TGF-β first binding to TβRII homodimers and then recruiting TβRI homodimers.[47, 49] However, more recent findings have indicated that TGF-β2 shows a higher affinity to

TβRI suggesting that the mechanism of complex formation might be isoform dependent.[50]

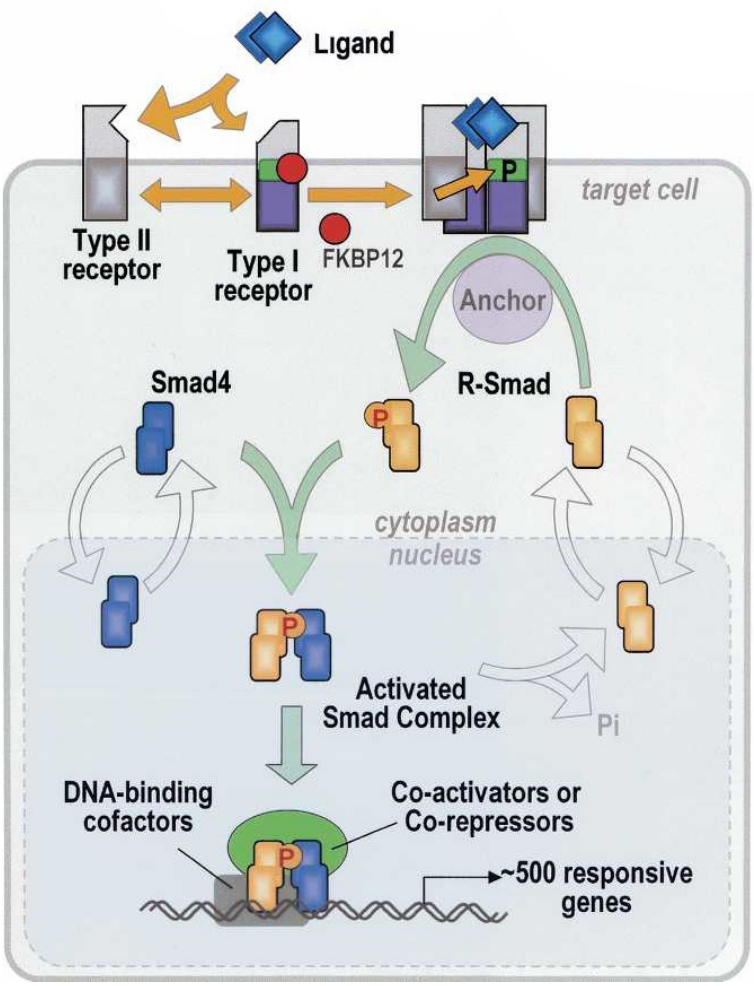

Figure 7 - TGF-β pathway. Homodimer TGF-β binds type II and type I receptors (TβRII and TβRI) forming a ternary complex consisting of type II and type I receptor dimmers. Phosphorylation of TβRI by TβRII decreases affinity of TβRI towards inhibitor protein FKBP12 and increases affinity towards R-Smads. Association with R-Smads results in R-Smad phosphorylation and subsequent complex formation with Smad4 and translocation to the nucleus where the complex functions as transcription factor in association with other co-factors, -activators and -repressors. Reproduced with permission.[51]

Formation of the ternary complex induces cross phosphorylation of TβRI by TβRII.[52] TβRII Phosphorylates serine and threonines in the GS domain of TGFβ type I receptors (TβRI) which increases the binding affinity for Smad2 and Smad3 and decreases the affinity for the inhibitory protein FKBP12.[53] Additionally Smad2 is recruited through interaction with SARA (*S*mad *a*nchor for *r*eceptor *a*ctivation) which binds both Smad2 and TGFβ receptors.[54, 55] TβRI then phosphorylates Smad2 and Smad3 (R-Smads) at a SXS motif located at the C-termini. This induces disassociation from the ternary complex and formation of either dimer or trimer complexes with Smad4 in a 2:1 or 3:1 ratio of Smad2 or Smad3 to Smad4.[56-58] This complex then translocates to the nucleus through nuclear pore complexes (NPC).[59] Only relatively small molecules of about < 30kDa can passively diffuse through NPC's whereas larger molecules require active transport often mediated by transport receptors.[60] Smads may be actively shuttled across the nuclear membrane through interaction of a nuclear localization sequence (NLS) in the N-terminal with NPC proteins .[61] Smad4 has also been shown to contain a nuclear export sequence (NES) that is blocked following R-Smad association thus sequestering Smad4 to the nucleus.[62] However, Smad4 is not essential to all TGF-β stimulated responses.[63]

In the cell nucleus the Smad2/3:Smad4 complex functions as a transcription factor.[51] All the R-Smad proteins (except a splice variant of Smad2) contain a DNA binding β-hairpin that recognizes the motif CAGAC and GC rich sequences.[64-66]

However, this interaction is not strong enough to form a stable complex with DNA and so association with DNA binding co-factors and master transcription factors determine binding locations in the genome.[51,67] This helps explain the multiple different outcome results following TGF-β stimulation in different cell lines at different stages of development.[68] Further expanding on the intricate response is the fact that TGF-β not only functions through the canonical Smad pathway but also affects several other signaling pathways including c-Jun N-terminal kinase, rho-like guanosine triphosphatase, phosphatidylinositol-3-kinase, mitogen-activated protein kinases and TGF-β-activated kinase 1.[69,70]

4.2 Structure of the Ternary Complex

Assembly of the ternary complex is initiated by binding of TGF-β to its receptors. Groppe *et al.*[71] reported a cooperative assembly mechanism for TGF-β3, with the cytokine binding to TβRII with a K_D of 0.5 μM and to TβRI with a K_D of 188 μM but with TβRI binding to the preformed complex of TGF-β3 and TβRII with a K_D of 0.6 μM. This contrasts with Sergei Radaev *et al.*[50] who reported a K_D between TGF-β3 and TβRII of 0.14 μM and a tenfold lower K_D between the preformed complex of TGF-β3:TβRII and TβRI of 0.014 μM. This secondary dissociation constant is similar to the 0.016 μM reported between TGF-β2:TβRII and TβRI in the same study. This represents a large increase in affinity compared to 11.2 μM and 22.4 μM reported between TGF-β2 and receptor type I and II respectively.

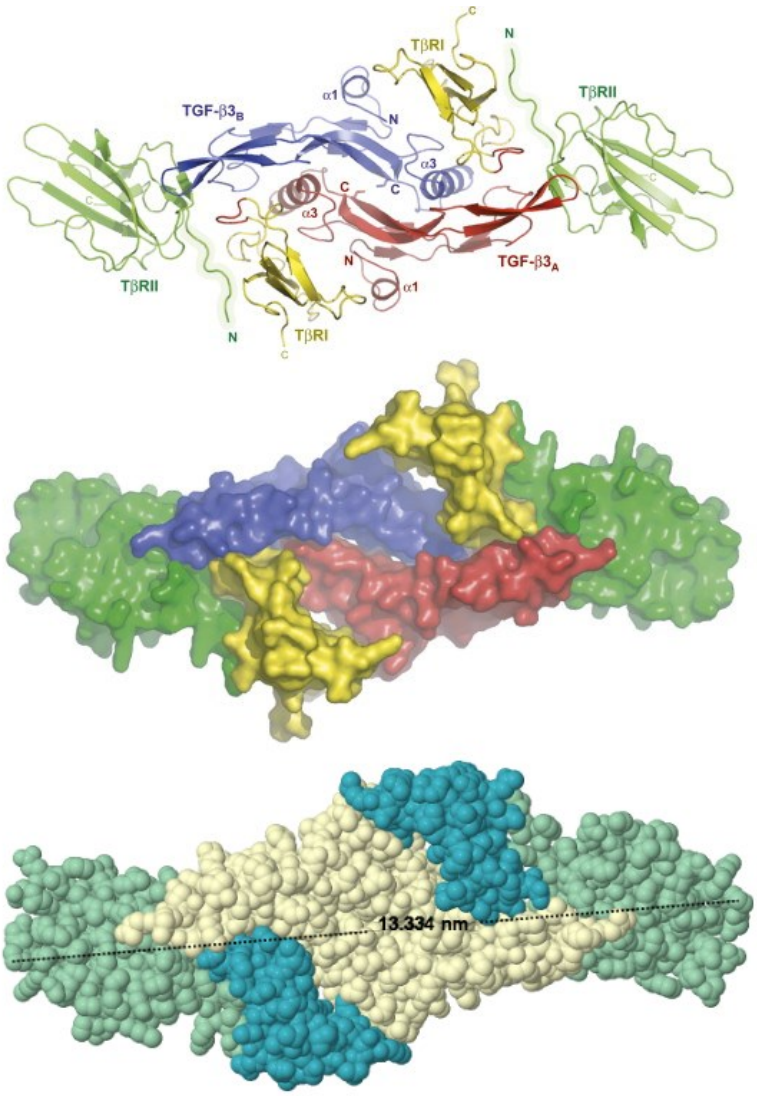

Figure 8 - Crystal structure of the TGF-β, TβRI and TβRII ternary complex. Top: Ribbon diagram of TGF-β3 assembly labeled with the different subunits. Individual TGF-β subunits are labeled TGF-β3A and TGF-β3B. Two important elements mediating assembly are the flexible N-terminus of TβRII (highlighted with diffuse green border) which becomes ordered in the ternary complex and the pre-helix extension of TβRI (highlighted in red) that docks at the cytokine:TβRII interface. Middle: surface representation of TGF-β3. Reproduced with permission .[71] Bottom: Space fill of TGF-β1 assembly with distance measurement in the plane parallel to the membrane illustrating the dimensions of assembly (PDB: 2PJY).

While crystal structures have not been determined for the TGF-β2 ternary complex, structures for the TGF-β1 and TGF-β3 show a common ligand recognition mode with the tips of the cytokine dimer binding TβRII, and TβRI binding with a pre-helix extension against the TβRII:TGF-β3 interface. Figure 8.

Affinity between TβRII and the 1 and 3 isotype ligand is driven by salt bridges between Glu and Asp residues in the receptor and Arg residues in ligand and some hydrophobic contacts as well. The interface between TGF-β1 and -β3 and TβRI is primarily hydrophobic with a ~10° rotation of the receptor in the TGF-β3 complex relative to the TGF-β1 complex resulting in a decrease of buried solvent accessible area from 1518 Å^2 to 1118 Å^2. The contact interface between the two receptor types buries 740 Å^2 of solvent accessible area. Of importance is a prehelix extension in TβRI that forms a hydrogen bond between an Arg residue and Asp residue in TβRII. These residues are highly conserved across species. Additionally seven residues in a disordered N-terminal extension of TβRII become ordered in the ternary complex bind to TβRI through hydrophobic interactions.

4.3 DNA Nanostructures in Cell Culture

Structural DNA nanotechnology has made great advances in the creation of self-assembled addressable nano structures by taking advantage of the predictable interactions of DNA base pairing.[72-74] Especially the method of scaffolded DNA origami, which relies on an excess of many short "staple" strands to fold a long, single-stranded

scaffold into almost any desired shape, has proven successful as a robust means of patterning inorganic, organic and biological molecules with nano-scale precision.[75, 76]

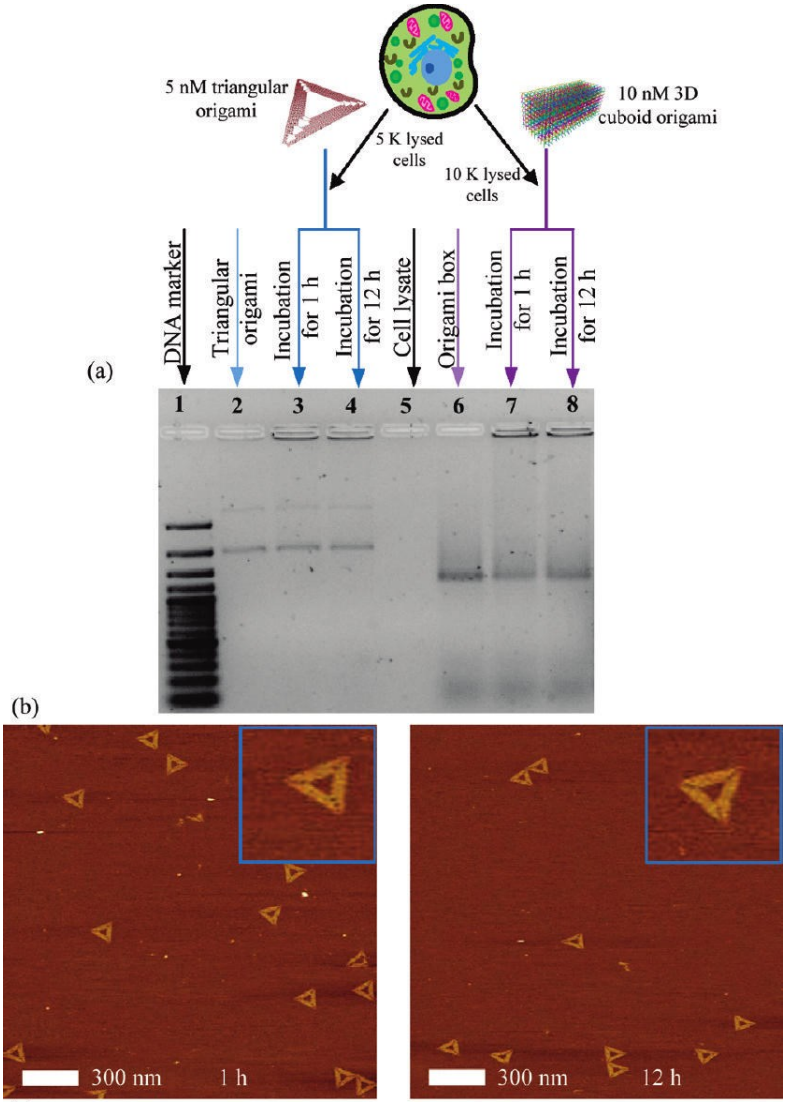

Figure 9 - Integrity of DNA origami incubated in cell lysate. (a) Triangular or cuboid origami was incubated for 1 or 12 hours in mammalian cell lysate and then run a on PAGE gel. Little to no degradation is evident from the intensity of the bands. (b) Bands were cut out and origami samples extracted and further analyzed for structural integrity by AFM. Reproduced with permission.[77]

The biological and biocompatible nature of DNA allows for these versatile structures to interface with cellular systems without prohibitive cytotoxicity. Recent research has demonstrated that DNA nanostructures enjoy increased resistance to enzymatic digestion,[78] and they retain their structural integrity for extended periods of time in cell lysate as evidenced by the work of Mei *et al.*[77] They investigated the integrity of DNA origami structures incubated in cell lysate from a range of different mammalian cells. They found little degradation of samples as evidenced by PAGE analysis and by AFM of the PAGE bands. See Figure 9.

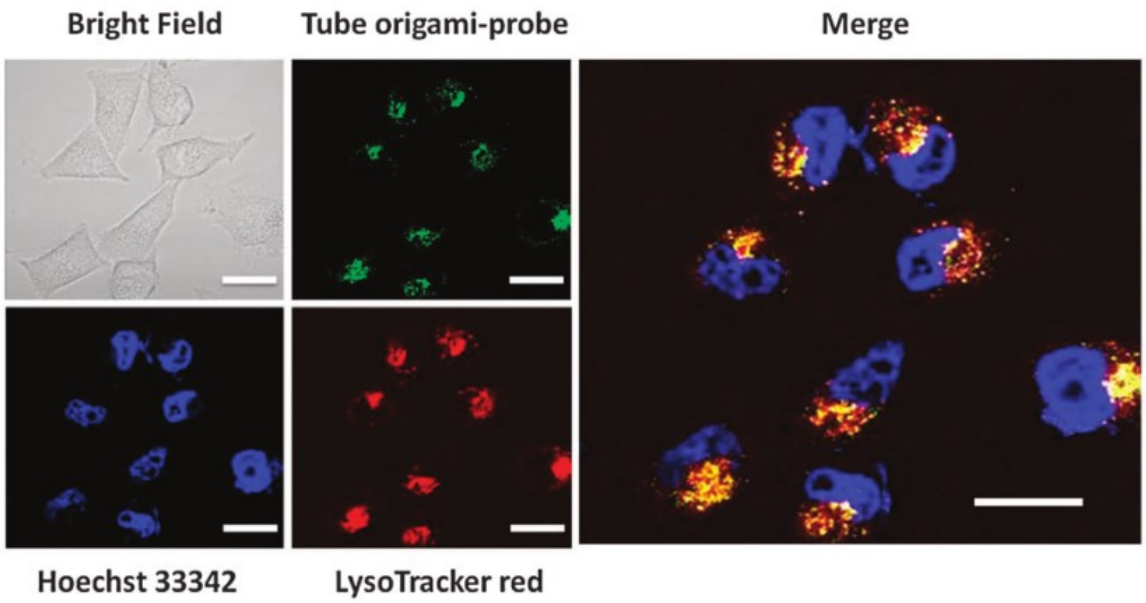

Figure 10 - Intracellular localization of DNA origami structures following passive uptake. Reproduced with permission.[79]

Shen *et al.* analysed intracellular localization and degradation of DNA origami in mammalian cells and found that tubular origami structures were taken up by cells and co-localized with lysosomes.[79] They used cyanine fluorophores that exhibit strong

fluorescent emission upon binding to DNA. By pre-incubating tubular origami structures with these fluorophores and then treating cells with the fluorophore loaded origami they could trace intracellular localization. Figure 10. Additionally, upon degradation of the DNA, the fluorescence emission is greatly reduced and the authors observed a 50% decrease in the fluorescence from the fluorophore loaded origami structures in the timespan of 24 hours following cellular uptake.

Aptamer functionalized DNA nanostructures have been found to be active in blood plasma[80] and resistance to degradation can be further improved by various covalent modifications of DNA oligonucleotides.[81] The stability of DNA nanostructures in biological environments has allowed for their application in the targeting of living cells,[82, 83] and it has been shown that DNA icosahedra and origami structures can function as drug carriers for doxorubicin.[84, 85] Both DNA wireframe tetrahedra and origami structures have been coated with CpG oligonucleotides and used as potent vehicles for immunostimulation.[86, 87] One of the advantages of using DNA nanostructures is the ease with which they can be modified as illustrated by the creation of a tunable, artificial extracellular matrix (ECM) constructed from DNA motifs decorated with fibronectin domains.[88]

4.5 DNA Nanostructures for TGF-β Sensitization

Since many cell surface receptors activate through ligand mediated oligomerization followed by phosphorylation of intracellular receptor domains, we

hypothesized that extracellular DNA nanostructures might confer even greater control over cellular behavior through the preclustering and thus activating or sensitizing of cell surface receptors. To test this hypothesis, we set out to test preclustering of transforming growth factor-β (TGFβ) receptors using multiple copies of a receptor binding peptide patterned on DNA nanostructures. TGFβ plays an important role in the feedback control system between ECM and cells and, as such, is an attractive target with significant implications in tissue engineering.[89]

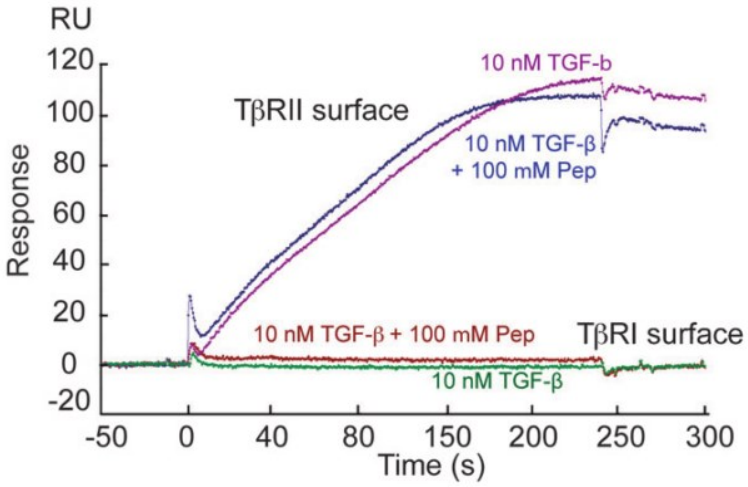

Figure 11 - Surface Plasmon Resonance (SPR) graph displaying response of TβRII and TβRI surface to TGF-β and TGF-β + peptide. TβRI surface shows no response to TGF-β with or without peptide. TβRII shows binding to TGF-β but the extend of binding is independent of peptide indicating that the peptide binds outside the TGF-β binding site. Reproduced with permission.[90]

Lingyin Li *et al.* used phage display to developed a TβRI and TβRII binding peptide that binds the extracellular domain outside the ligand binding domain.[90] They furthermore demonstrated preclustering of TβRI and TβRII by functionalizing a gold surface with the peptide and culturing NMuMG cells on it, resulting in increased

sensitivity of the cells to TGF-β.[91] A major shortcoming of such surface-based systems is that although the overall concentration of peptide bound to the surface can be varied, the specific nanoscale density or clustering of peptide cannot be known or controlled.

Here, we control the nanoscale patterning of the TβR binding peptide of Li *et al.* upon DNA origami by sandwiching tetravalent streptavidin molecules between biotinylated peptide and biotinylated origami. Figure 12.

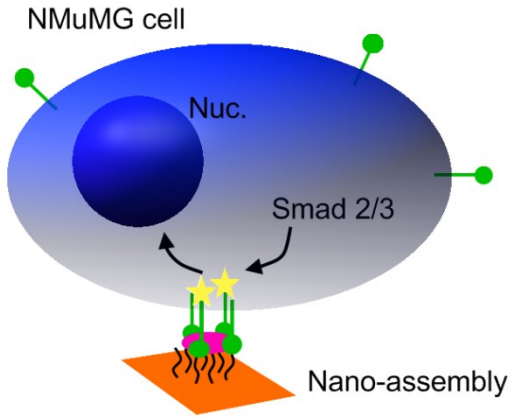

Figure 12 - Illustration of peptide patterned nanostructure binding and clustering TGF-β receptors and sensitizing cell to TGF-β stimulus.

Tall rectangular origami of Rothemund's original design[37] (RRO) was modified by leaving out 12 centrally located staple strands (strands denoted as: t-1r14f, t-1r18f, t-1r16f, t-1r20f, t- 1r14e, t1r14f, t-1r16e, t1r16f, t-1r18e, t1r18f, t-1r20e, t1r20f). New strands were designed allowing for 5' modifications to be displayed on one face of the structure, and 10 strands were biotinylated creating a central patch of biotin moieties. Figure 13a illustrates a schematic of the streptavidin as blue dots located on orange rectangular origami, and Figure 13b illustrates a sideview of the nanoassembly.

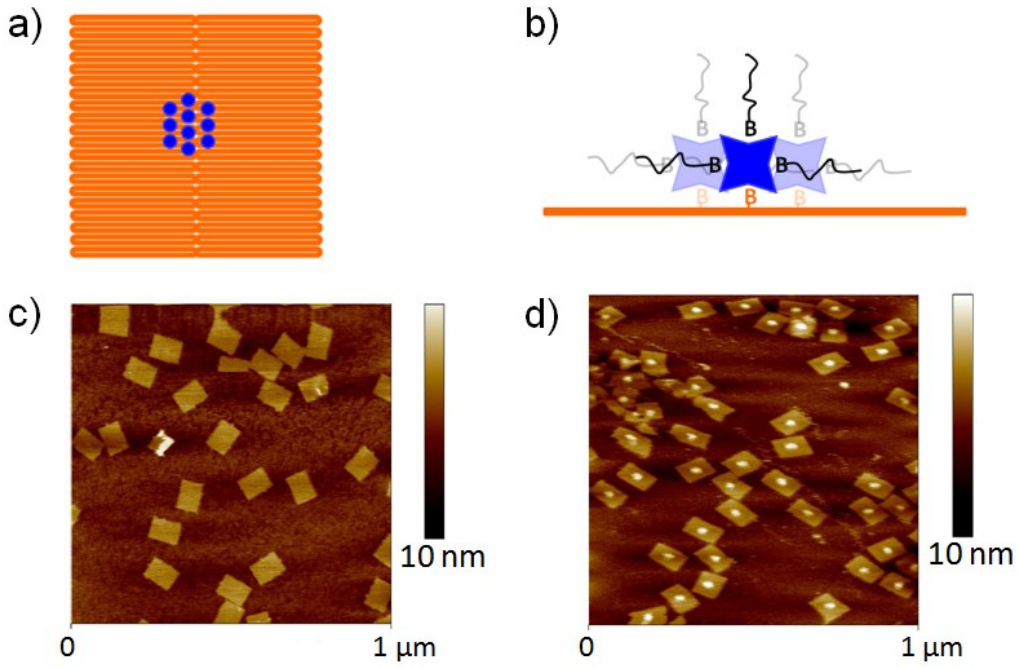

Figure 13 - (a) Schematic of the DNA origami RROt with biotin/streptavidin sites marked in blue. (b) side schematic of the nanoassembly. (c) Origami structures before assembly with streptavidin and peptide. (d) Nanoassembly after spin purification. Peptide–streptavidin complex is visible in the center of the origami structure.

The multivalency of streptavidin results in the potential for up to three peptides to be displayed at each origami biotinylation site assuming a 1-to-1 binding between biotins on the origami and streptavidin. This assumption is reasonable when we consider the geometry of biotinylation sites on the origami compared to the geometry of streptavidin. The protein is a tetramer with four biotin binding sites spaced no more than 3.8 nm apart (PDB entry 3RY1).[92]

On the other hand, the closest spacing of biotin on the modified origami is two helices over. With a 2 nm helix diameter and 1 nm interhelix spacing, this results in a distance of approximately 5 nm. It is thus unlikely for a streptavidin tetramer to bridge

between two origami bound biotins. Therefore it is reasonable to assume that each origami biotinylation site will result in the binding of up to three biotinylated peptides. Nanoplatforms were assembled stepwise. In order to purify assemblies from excess component building blocks, multiple spin-filtration steps were performed using filters selected to retain the nanoassemblies but to allow unassembled, individual components to flow through. To investigate the structural integrity of the nanoassemblies after spin-filtration steps, we performed atomic force microscopy (AFM). Figure 13c shows an AFM image of the annealed origami containing the modified staple strands and Figure 13d shows the final nanoassemblies following spin filtration; the peptide−streptavidin complex is visible as a centrally located patch on the origami rectangles.

During activation of the TGFβ pathway, phosphorylation of TβRI exposes a Smad protein binding site which results in Smad2 and Smad3 phosphorylation. Phosphorylated Smad2/3 forms a complex with Smad4 and are then translocated to the nucleus where they act as transcription factors in association with other proteins. Initiation of the signaling pathway can thus be monitored by examining the translocation of Smad proteins into the nucleus. This is accomplished by staining fixed cells with a primary Smad antibody and secondary Fluorescent antibody. Li *et al.* reported that growing NMuMG cells on surfaces presenting TβR-binding peptides sensitize the cells by preclustering TβR and causing endogenous TGFβ in the culture medium to trigger a signaling event leading to a translocation of the Smad2/3 proteins to

the cell nucleus.[91] In our initial experiments in which cells were treated with TGFβ and peptide-bearing nanoassemblies, we found that endogenous levels of TGFβ in NMuMG cell cultures were not sufficient to elicit a detectable response. Titrating TGFβ we also found reduced sensitivity in cells compared to that reported by Li *et al.* with no Smad translocation observed using concentrations below 50 pM of added TGFβ. Figure 14 shows NMuMG cells treated with four different concentrations of TGF-β. In the first panel where the cells have been treated with 50 pM TGF-β the Smad2/4 stain is localized throughout the non-regular chaped cell body. This contrasts with the 80 pM treatment where we can see the stain localized in the spherical nucleus with a more faint trace of stain in the non-spherical cell body.

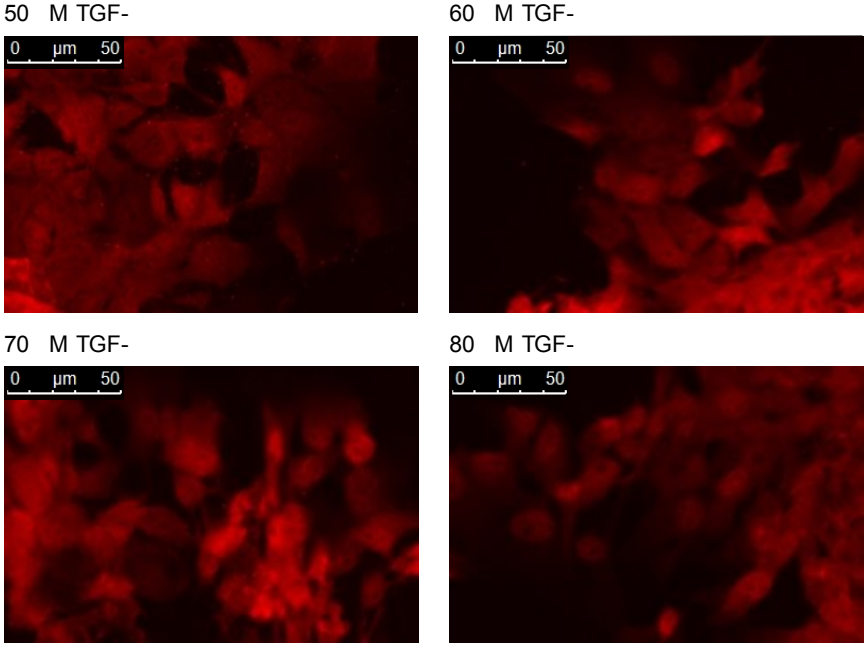

Figure 14 - NMuMG cells treated with varying concentrations of TGF-β and stained for Smad2/4. While translocation is observed clearly at 80 nM no translocation is observed at 50 nM concentration.

This prompted us to add a background level of 40 pM TGFβ along with nanoassemblies in order to detect a positive perturbation of the signaling pathway.

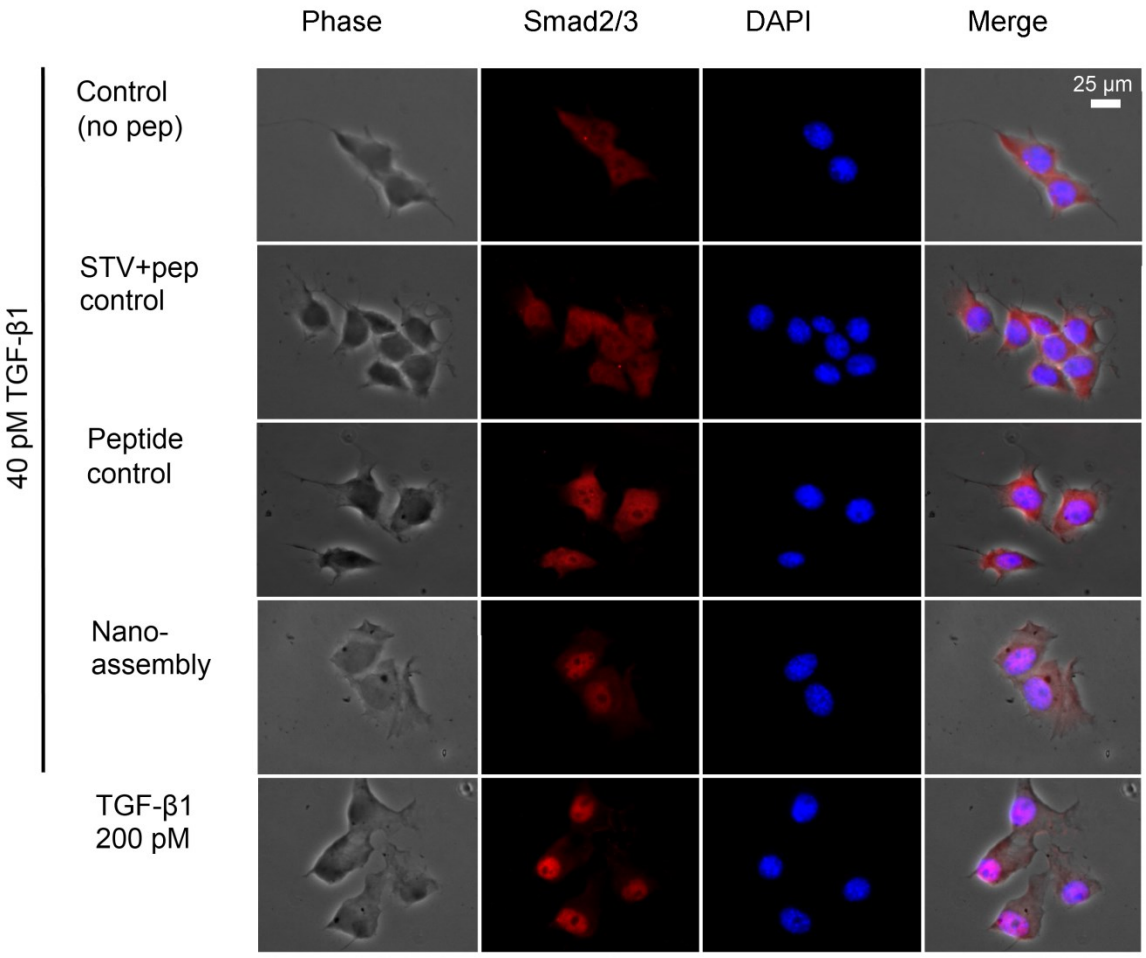

Figure 15 - Representative micrographs of NmuMG cells cultured for 18 h and then fixed and stained with DAPI and antibody against Smad2/3 (red stain). Top row is a control culture with a background level of 40 pM TGFβ added. As can be seen, the red stain is diffuse throughout the cell body with no apparent localization in the cell nucleus. Similar results are seen in the second and third rows showing controls with added peptide at 12 nM and premixed peptide and streptavidin in a 4 to 1 ratio with streptavidin at 3 nM. The fourth row from the top shows cells treated with nanoassemblies. As can be seen in the Smad2/3 column, this treatment results in translocation of Smad2/3 into the nucleus. This mimics the effect observed when cells are treated with a high dose (200 pM) of TGFβ, as in the fifth row.

Figure 15 shows representative micrographs of NMuMG cells cultured for 18 h with or without nanoassemblies. In cells exposed to 40 pM TGFβ, no translocation of the Smad proteins to the cell nucleus was observed. This contrasts with cells exposed to 200 pM TGFβ where the Smad2/3 stain predominantly overlaps with a DAPI stain of the nuclear DNA. To test the efficacy of our nanoassemblies, cells were exposed to 300 pM nanostructure and 40 pM background TGFβ. This resulted in Smad2/3 translocation into the nucleus as evidenced by colocalization of Smad2/3 stain and DAPI DNA stain. Controls were also done with streptavidin and peptide premixed before addition to the cell culture as well as samples containing peptide alone. The multivalency of streptavidin could conceivably lead to limited clustering when the tetrameric protein binds up to four biotinylated peptides. However, as the micrographs in Figure 15 show, no Smad2/3 translocation is observed when premixed streptavidin and peptide is added to the cell culture. Neither of these control conditions activated Smad translocation.

In order to achieve a quantitative measure of the biological pathway induction, we employed a luciferase assay responsive to Smad mediated TβR stimulation. Cells were transfected and then exposed to either 200 pM TGFβ or 40 pM TGFβ and nanoassemblies. Concluding from Figure 15 that no Smad2/3 translocation takes place when treating cells with peptide or streptavidin+peptide, these conditions were included as negative controls. Figure 16 shows relative luminescence values.

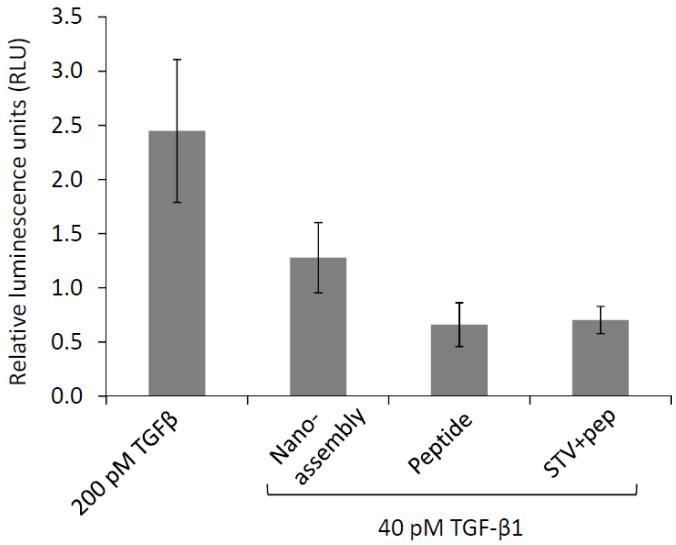

Figure 16 - Luminescence from cell samples treated with 200 pM TGFβ, nanoassembly and 40 pM TGFβ, peptide and 40 pM TGFβ, and pep- streptavidin complex and 40 pM TGFβ. Error bars represent standard deviation.

Samples treated with nanoassemblies showed significant activation of the Smad pathway compared to the negative control samples treated with peptide alone or peptide and streptavidin preincubated. The highest level of pathway activation was seen in the positive control sample exposed to 200 pM TGFβ. This indicates that our nanoassemblies are sensitizing NMuMG cells to TGFβ. We hypothesize that this occurs because preclustering of the receptors by the nanoassemblies results in decreased entropic cost compared to the normal pathway where receptor clustering occurs after TGFβ binding. It is conceivable that the efficacy of the nanoassembly could be increased by replacing the noncovalent biotin-streptavidin linkage with a direct covalent coupling between the peptides and the DNA origami. This would also allow for tighter control of peptide position and multiplicity than provided by the tetravalent streptavidin.

Additionally, a covalent attachment would make it easier to eliminate free peptide in the assembly samples which might further improve preclustering of receptors.

5. Functionalization of DNA Nanostructures with Zinc Finger DNA Binding Peptides

DNA binding proteins represents an attractive strategy for functionalizing DNA nanostructures as fusion constructs of such proteins would be able to add the catalytic activity of enzymes or the antigen affinity of antibodies to specific sites on DNA nanostructures by binding to select sequences on the nanostructures. Zinc fingers are small protein domains that typically interact with other molecules such as DNA or other proteins. Zinc is either necessary for correct folding of the domains or for the specific interaction with targets.

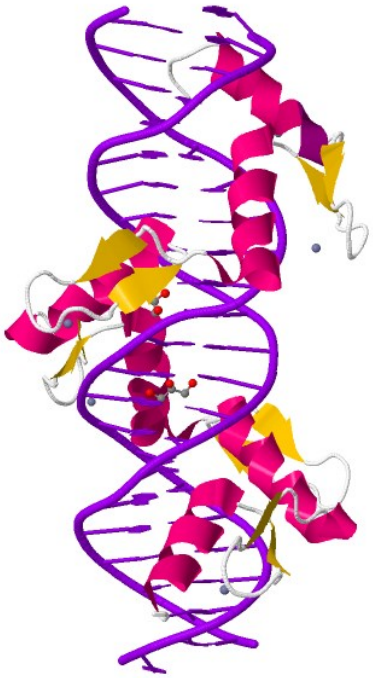

Figure 17 - Structure of a six-finger zinc finger peptide bound to DNA. PDB: 2I13

The classic DNA-binding zinc finger was first described by Klug and colleagues as part of the *Xenopus laevis* transcription factor TFIIIA.[93] It comprises two cysteine residues at the N-terminus end and two histidine residues at the C-terminus and is as such classified C2H2. These four residues coordinate a zinc atom which is crucial for the correct folding of the domain. The N-terminus adopts a β-hairpin conformation. The C-terminal part of the domain forms an alpha-helix. This helix fits into the major groove of duplex DNA and protruding side chains form both nonspecific and sequence specific contacts with the DNA molecule. A zinc finger domain can thus recognize a specific sequence of 3 to 5 nucleotides. The strength of the motif is that additional domains can be added successively in a modular fashion to create a protein which recognizes a longer DNA sequence with high specificity and affinity.[94] Barbas and colleagues showed that up to 6 naturally occurring zinc finger domains in succession can specifically recognize 18 basepair long sequences both in an eukaryotic genome and in vitro (Figure 17).[95] They have further developed a library of 16 GXX recognizing domains and shown that they can cut and paste these together to target arbitrary 6x(GXX) sequences.[96] This potentially represents an unexploited avenue for construction and targeting of DNA nano-structures, as it allows for engineering precise sequence affinity into any desired fusion protein construct.

5.1 Zinc Finger Constructs

To test this DNA nanostructure functionalization strategy we expressed three different zinc finger constructs of zinc finger domains fused to maltose binding protein (MBP). The MBP domain allows for purification using a maltose column and also provides a visual cue in AFM. Additionally a Factor Xa cleveage site enables the separation of zinc finger and MBP domains. Three different constructs were expressed. 6F is a 6 finger domain fused to MBP that recognizes the sequence GGG GCC GGA GCC GCA GTG (E2C). 2x6F is made up of two 6 finger domains. One domain recognizes the same sequence as 6F and the other domain recognizes the sequence GACTCCGGCTCCGGCTCC (E3). These two domains are linked with a nine residue glycine/serine linker region and fused to a MBP domain. 2x3F has two DNA binding domains like 2x6F but only has 3 finger subunits in each DNA binding domain that recognizes the sequence GGG GCC GGA. The 6F protein should allow for assessing the binding efficiency of the six zinc finger subunit by to DNA nanostructures by visualizing the MBP domain with AFM. The rationale for having two separate binding subunits in the 2x6F and 2x3F proteins is to use the proteins as orthogonal linkers between different DNA nanostructures. This could allow for the assembly of larger structures by circumventing the problem of charge repulsion in larger DNA based structures while having both a six and three finger based protein would allow for

comparison of the efficiency of linking as a function of number of "fingers" in the DNA binding domains.

5.2 TX tile Design and Assembly

To test assembly of DNA nanostructures by 2x6F we designed a TX tile based array with binding sites for the six finger domain. The outer strands of the tile were modified with protruding hairpins containing the zinc finger target sequence and two pairs of flanking nucleotides. 4 T's were incorporated to terminate the hairpin loop.

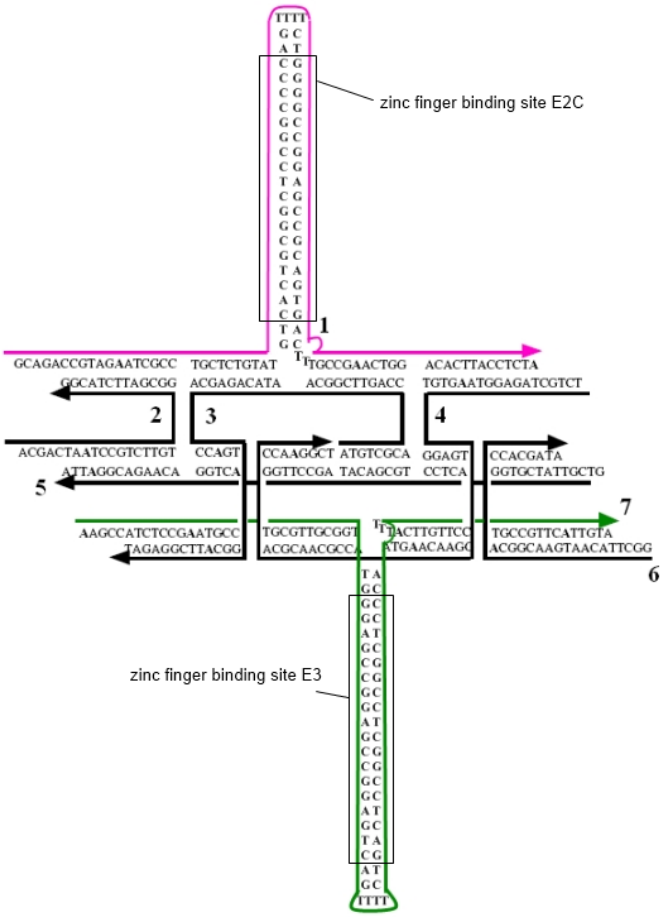

Figure 18 - DNA structure and sequence of a single TX tile with zinc finger binding sites. Several tiles anneal by single stranded overhang to form linear arrays.

Different target sequences were included in hairpins protruding in the plane on either side of the tile. The goal of having two different targets on either side of the arrays is to bridge different arrays with proteins consisting of 2 6-finger domains linked with a 9 residue glycine/serine linker. TX arrays have previously been used to demonstrate orthogonal linking using aptamers and anti-aptamer antibodies. However, zinc finger proteins have potential to achieve such linking with a higher degree of versatility and ease (Figure 19).

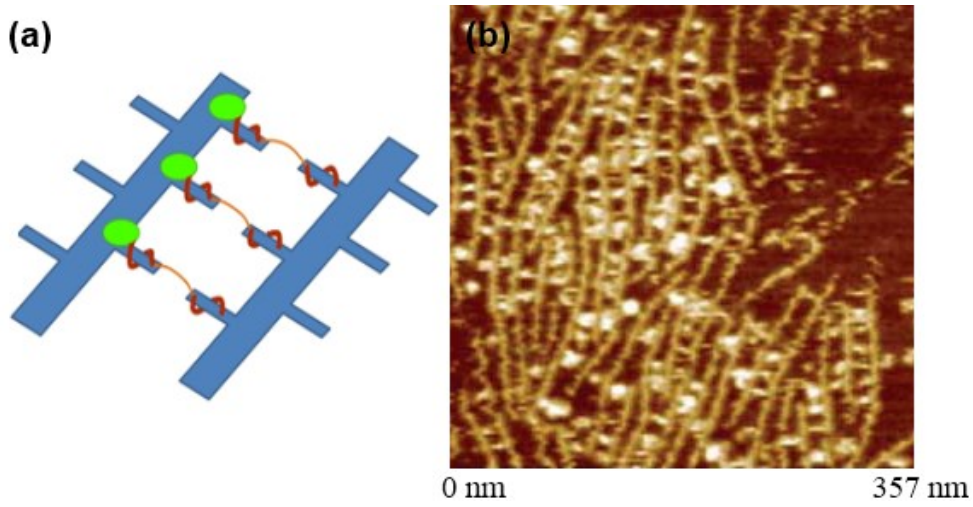

Figure 19 - (a) Cartoon illustration of two zinc finger domains (dark red) linked together (orange) with a terminal Maltose Binding Protein (MBP) domain (green) connecting two different DNA arrays (blue). (b) AFM image from Li *et al.* showing arrays bridged with antibodies and aptamers. Reproduced with permission.[97]

Structural integrity of the linear arrays was verified by atomic force microscopy. Figure 20 show that linear arrays are formed and appear corrugated in accord with the protruding hairpin structure. The line in Figure 20b specifies a cross-section measurement indicating that the width of the arrays is approximately 20 nm. This is

consistent with the tile design when including the 22 nucleotide side arms but excluding any gap between helices. As the spacing between cross-overs are 21 to 31 nucleotides apart, comparable to the 32 nm in origami structures, the gap size would be expected to be similar. It is likely that the width measurement does not accurately reflect the entire width of the structure including side arms as the side arms are not as structurally robust as the core tile array.

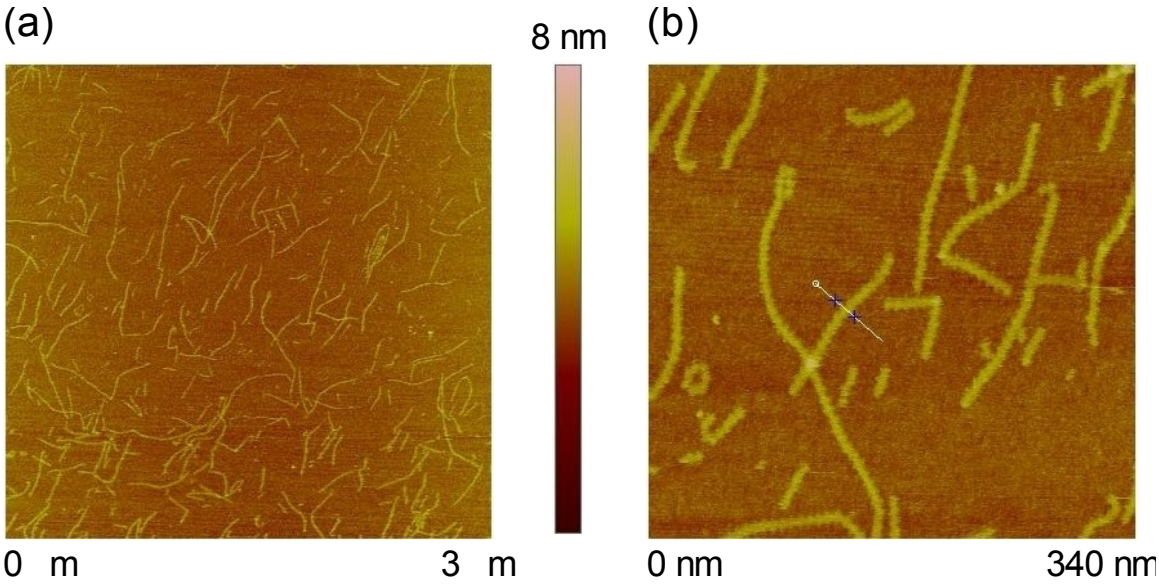

Figure 20 (a) TX linear arrays on mica. (b) Zoom of the sample from a.

5.3 Expression and Relative Specificity of Zinc Finger Constructs

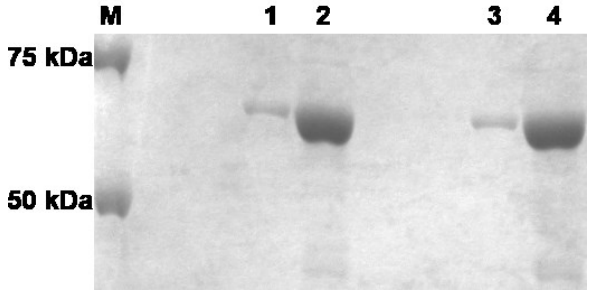

Figure 21 Representative Coomassie stained SDS-PAGE gel of 6F construct. The theoretical mass of the construct is 65 kDa. Lane 1and 2: 6F construct after maltose column affinity purification. Lane 3 and 4: 6F construct after 30 kDa spinfilter purification.

Proteins were expressed in *E.* Coli and purified by running cell lysate through an amylase column and then eluting the protein with a solution of maltose. An additional concentration step was done using 30 MWCO spin filters. To assess the purity of the samples we performed SDS-PAGE. Figure 21 indicates that a high degree of purity was achieved following elution from the amylase column. To assess the activity of expressed proteins enzyme-linked immunosorbent assays (ELISA) were conducted with STV coated plates to which biotinylated DNA hairpins were bound and then incubated with cell lysate followed by alkaline phosphatase (AP) fused anti-MBP antibodies. AP catalyzes the reaction of para-nitrophenylphosphate to para-nitrophenol and the concentration of para-nitrophenol can be accurately measured by its absorption at 405 nm.

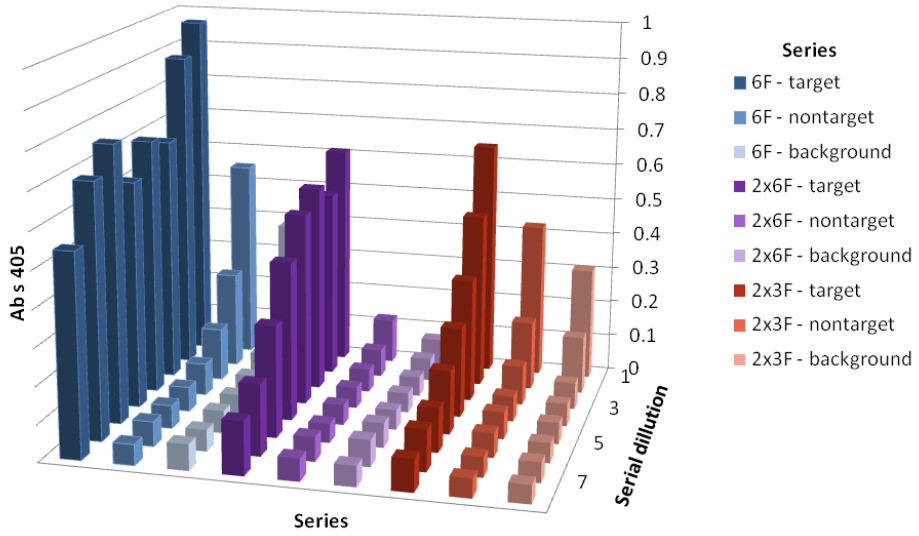

Figure 22 - ELISA analysis of zinc finger binding. Fresh cell lysate is diluted along the z-axis. Different series correspond to different DNA targets as specified in experimental methods section. Background is done without a biotinylated DNA target.

Figure 22 shows ELISA results. All three constructs were tested. The z axis represents a serial dilution of centrifuge clarified lysate of *E. coli* cells containing the relevant plasmid. Different series represent different DNA targets as specified in the right margin. The non-target sequence is of the form $(GXX)_6$. As such it would be expected to show a higher affinity for the proteins than a random sequence. At higher dilutions we see specific binding to the target sequence and little difference between background and nontarget.

5.4 DNA Nanostructure and Protein Association

Association between protein and TX linear arrays were investigated with AFM. Several different buffer schemes were tested including: 1) Adding protein in zinc buffer

A (ZBA) to TX arrays in TAEM buffer. 2) Adding protein in ZBA to TX arrays in ZBA(Mg) buffer. 3) Adding $ZnCl_2$ to premade TX arrays in TAEM buffer for final $ZnCl_2$ concentration of 90 μM and then adding protein in ZBA. The initial experiments were done with 2x6F proteins on mica. Proteins appear as approximately 1 nm protrusions. This is smaller than the approximate 6x4x2 nm dimensions of MBP and could be due to partial denaturation of the protein on the mica surface. Figure 23 shows AFM micrographs of TX arrays annealed in TAEM with added $ZnCl_2$ incubated with 6F proteins constructs. No apparent binding of protein to the TX arrays is visible.

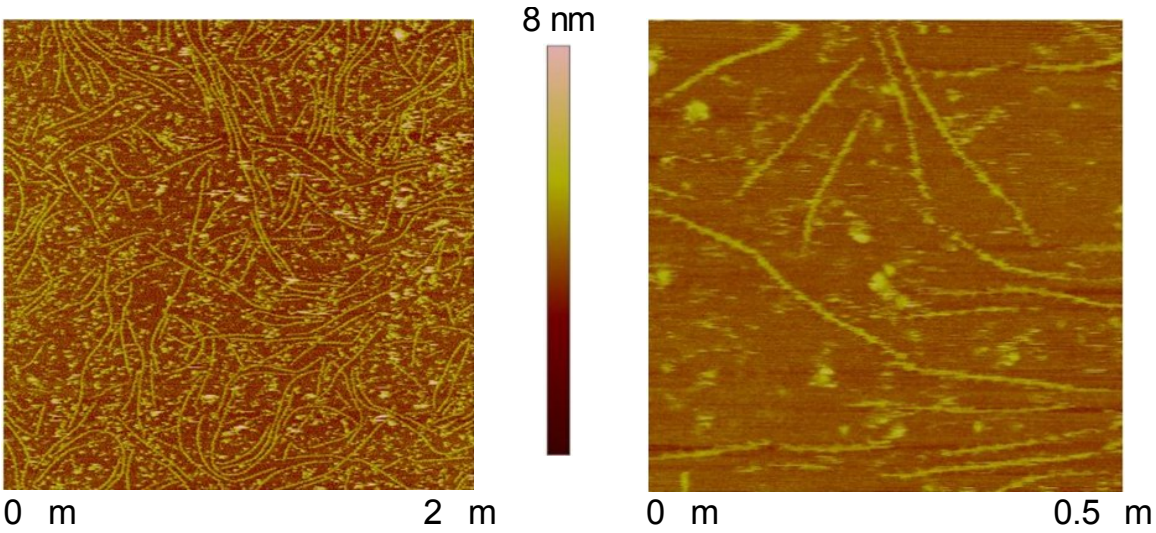

Figure 23 - AFM of TX arrays in TAEM buffer with 90 μM $ZnCl_2$ incubated with 6F peptide.

The fact that no binding was observed between TX arrays and zinc finger proteins when assayed with AFM, but binding was observed using the ELISA assay, led us to believe that it might be the interaction with the mica surface that impeded binding between the duplex binding site and the zinc fingers. This prompted us to change the

nanostructure motif. Using a rectangular origami instead of TX arrays would allow for a "vertical" binding site protruding away from the surface. It could be that the TX design impedes binding of the zinc finger because the binding site is "horizontal", which means it binds to the mica surface. Perhaps this "pushes" bound protein off the duplex or arrays with protein bound don't bind to the mica surface very well resulting in no imaging of them.

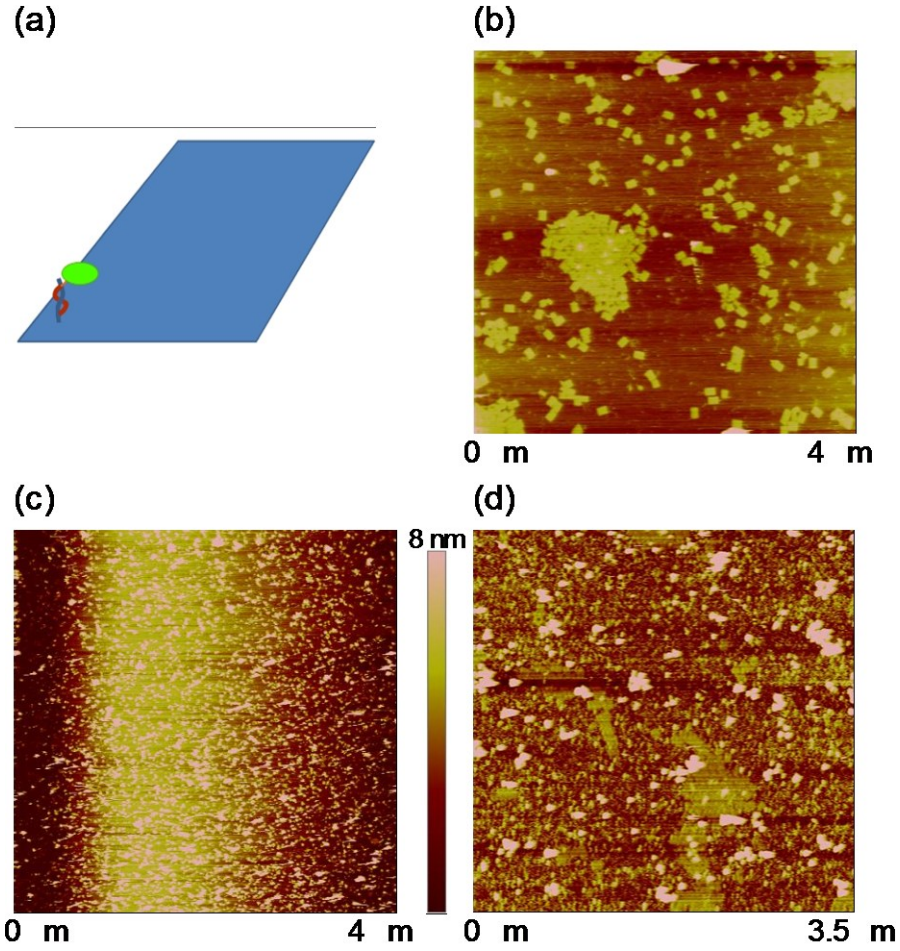

Figure 24 Origami and 6F zinc finger proteins. (a) Illustration of origami structure with "vertical" binding site. (b) Origami structures annealed in TAEM buffer and spin filtered with ZBA. Structures retain structural integrity in ZBA buffer. (c) 5 nM

6F protein incubated on mica. (d) Origami sample spinfiltered with ZBA and incubated with 47 nM 6F half an hour before imaging.

Figure 24 illustrates origami design for detection of 6F binding as well as AFM results. A single staple strand was modified with a hairpin protrusion containing the 6F binding site. Figure 24b-d illustrates origami structure annealed in TAEM buffer and then spin-filtered with ZBA exchanging the buffer, 6F protein by itself at 5 nm and origami sample incubated with the protein. The high degree of binding to the surface at a low protein concentration of just 5 nM illustrates an issue with the AFM approach. With a reported K_D of 5-10 nM for the six finger zinc finger binding motif we would ideally like to use protein concentrations in the micromolar range for a high degree of bound target sites. However, this makes it impossible to visualize binding in the AFM. Two different approaches could help alleviate this problem. One is to alter the mica surface so as to prevent non-specific deposition of protein on the surface. Another is to try and bind the protein to the nanostructure at sufficient concentration and then purify the nanostructure with bound protein. This is dependent on a reasonably slow off rate for the protein to remain bound during and after purification.

5.5 Zinc Finger Study by Nakata *et al.*

Nakata *et al.* reported on zinc finger proteins binding to a modified origami structure.[98] They used the zinc finger motifs zif268 and AZP4 and an origami structure with cavities containing multiple binding sites. Figure 25a shows the origami design with a four hairpins localized in a central cavity with each hairpin containing a zinc

finger binding site. They mixed this structure with 250 nM biotinylated zinc finger protein and 250 nM streptavidin. Then they imaged the sample using AFM as seen in Figure 25b. It can be seen that they observe *much* less non specific binding to the surface that we have observed. This could be caused by their use of a smaller zinc finger construct without the MBP domain. However, they also express a fusion construct with a fluorescent Cerulean domain of 27 kDa that likewise does not seem to cause substantial nonspecific surface binding.

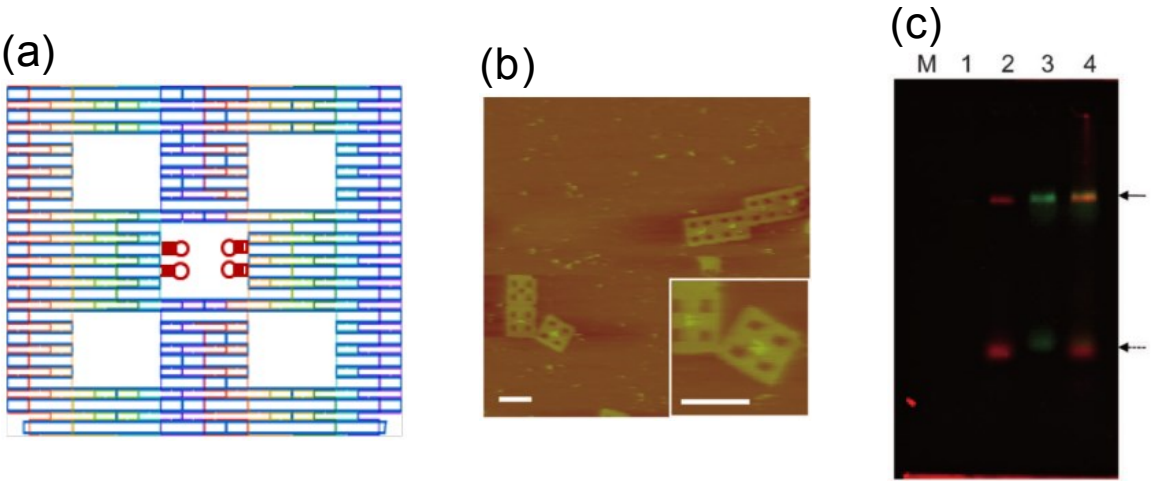

Figure 25 - Zinc finger binding to origami by Nakata *et al.* (a) Schematic illustration of the origami structure employed to bind zinc finger proteins. The four red hairpins in the center cavity contain binding sites. (b) AFM of origami bound to biotin tagged zinc finger protein bound to streptavidin. Scale bar = 100 nm (c) Fluorophore tagged zinc finger proteins incubated with origami. Lane 1: origami with no binding sites incubated with zif268. The fluorescent protein does not travel into the gel. Lane 2: Origami with binding site incubated with zif268. A red band is visible from both the origami and the excess staple strands both of which contain binding sites. Lane 3: Origami with binding site incubated with AZP4. Lane 4: Origami with both binding sites incubated with both AZP4 and zif268. Orange color indicate that both the red and green fluorescently tagged zif268 and AZP4 co-migrate with the origami band. Reproduced with permission.[98]

The authors only show one AFM micrograph with bound zinc fingers in the central cavity of a couple of origami structures. They also couple a fluorophore the zinc fingers and incubate with each construct with its respective origami before running the samples on a gel. Figure 25. No migration is seen of the fluorescent proteins when incubated with an origami without binding sites (Lane 1 Figure 25c) but when incubated with origami containing the relevant binding sites fluorescent bands co-localize with the origami and staple strand bands.

A clear difference in their approach is the use of four binding sites located in a cavity. The presence of four sites should greatly increase the total affinity between structure and protein but it also lowers the "resolution" of the functionalization technique in the sense that a larger area is needed. In other words, instead of knowing exactly which DNA strand in the structure is functionalized you have four strands covering a larger area where any one or more these strands *could* be bound to a zinc finger construct.

5.6 Conclusion

DNA binding proteins are an attractive means of adding protein functionality to DNA nanostructures. However, nanostructures typically don't function in the high concentration, dynamic context of the intracellular space. Hence binding affinity and off rates becomes very important for assembling durable and lasting structures. We have expressed zinc finger constructs that successfully bind their duplex targets in an ELISA

assay. However, investigation of binding to modified nanostructures by AFM is impeded by the high degree of non-specific surface binding.

The successful demonstration by Nakata *et al.* comes at the cost of "resolution" by requiring multiple binding sites on the nanostructure. This is of crucial importance since the potential scientific benefits of self-assembled DNA nanostructures is dependent on the spatial control of structures to within a few nanometers. Additionally the underdetermined nature of multiple binding sites makes other techniques comparatively more attractive such as biotin-streptavidin based methodologies.

6. Functionalization and Modification of DNA Nanostructures with Peptide Nucleic Acid

6.1 Functionalization of DNA Nanostructures.

6.1.1 Introduction

During the last two decades, nucleic acids have emerged as a promising material for nanotechnology due to the highly predictable and programmable Watson-Crick hybridization of complementary nucleic acid sequences.[72] The high fidelity and hybridization allows the formation of diverse structures through sequence design.[99] Of particular success has been an approach known as DNA origami in which a single-stranded scaffold if folded via a large number of short synthetic strands.[37, 76, 100] Current synthetic methods for producing natural and artificial nucleic acids with specific chemical modifications allow the access to milligrams of material, which is adequate for fundamental studies and practical applications.[101]. The easy control of the geometry, diverse range of shapes, and high resolution of the nucleic acid structures has in recent years lead to an expansion of the field into the broader domain of biomaterials finding use in both tissue culture,[88, 102] drug delivery[84, 85] and immunotechnology.[86, 87, 103]

Crucial for the practical use of these structures is a convenient way to functionalize specific locations. Several research groups have explored various means of functionalization. A commen approach relies on incorporating DNA oligos that have been chemically modified with solid phase phosphoramidite chemistry during synthesis. For example incorporation of oligos with terminal thiol groups allows binding

to gold nanoparticles (AuNP). Due to their electronic, optical and magnetic properties, AuNPs have been extensively incorporated into different nano structures formed from thiol-modified DNAs.[38, 104-108] DNA oligos modified with terminal amines or click-chemistry partners allows for chemical modification of resulting nanostructures with NHS-esters and trough click chemistry.[109] Enzymatic modifications of DNA oligonucleotides with terminal transferase allows for addition of deoxynucleotides to the 3′ end of one oligonucleotide or to several different ones in parallel. In addition, the appended deoxynucleotide can carry a wide variety of chemical groups that are thus displayed on the final assembled nanostructure.[110] As opposed to termini modification of DNA oligos, internal purines can be sequence specifically alkylated using pyrrole–imidazole (PI) polyamide enabling modification with functional groups such as biotin.[111] See Figure 26.

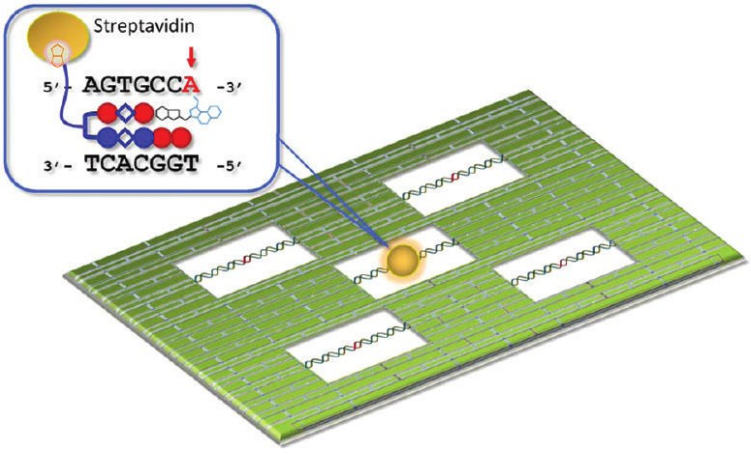

Figure 26 - Illustration of pyrrole–imidazole polyamide mediated sequence specific functionalization of double helices in a DNA Nanostructure. Reproduced with permission.[111]

PI polyamides are capable of sequence specific binding to the minor grove of the double helix.[112] By functionalizing a PI polyamide with 1-(chloromethyl)-5-hydroxy-1,2-dihydro-3H-benz[e]indole , Sugiyama and colleagues were able to covalently bind to the N2 position on a adenine adjacent to a specific six nucleotide sequence incorporated in a DNA nanostructure. Additional functionalization with biotin enabled visualization and analysis of the modification using AFM.

Proteins naturally have a great range of functionalities and catalytic activities and also share buffer compatibility with DNA. As such they are extremely desirable components to incorporate in DNA nanostructures. Previously it has been shown that incorporation of an antigen allows for programmed patterning of antibodies on DNA nanostructures.[113] A simpler approach utilized the ligand recognition of aptamers to attach thrombin and platelet derived growth factor (PDGF) to DNA nanostructures.[114]

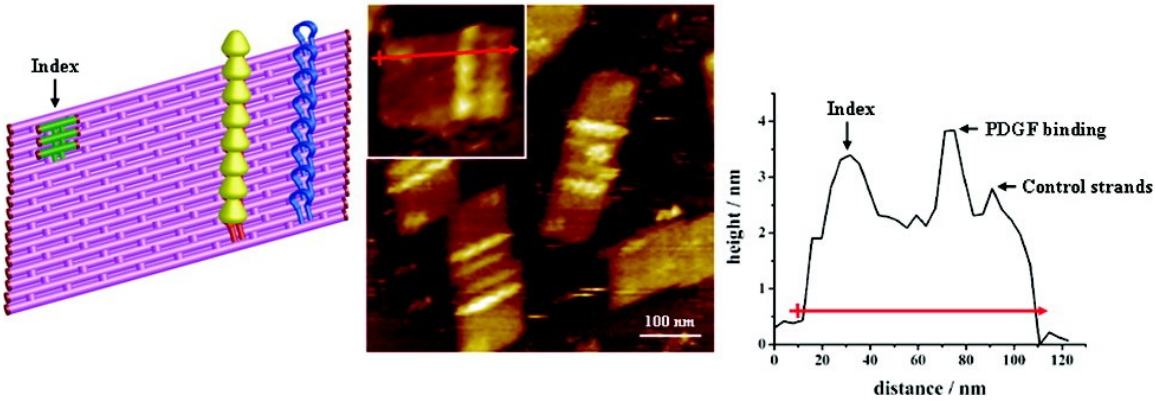

Figure 27 - Illustration and AFM image showing PDGF bound to aptamer functionalized DNA origami structure. Illustration on the left show rectangular DNA origami with red aptamers binding yellow PDGF proteins and blue control strands not binding PDGF. The insert in the middle AFM image delineates the height trace shown to the right. Reproduced with permission.[114]

Yan and colleagues incorporated PDGF and thrombin binding aptamers in DNA origami structures and showed specific binding of the ligands resulting in two-dimensional multiprotein nanoarrays. See Figure 27. The same thiol modification of DNA oligonucleotides used to link AuNPs to DNA was used to make maleimide-based modifications of the DNA structures. For example, a maleimide-linked nitrilotriacetic acid (NTA) was coupled to a thiol group; Ni^{2+} binding to NTA in turn allowed the binding of his-tagged proteins to the Ni^{2+}-NTA complex.[115] Thiols can also be used for covalent coupling to amine groups using maleimide-N-hydroxysuccinimide heterobifunctional linkers.[116] The N-hydroxysuccinimide reactive group has been used to incorporate snap- and halo-tags allowing for covalent incorporation of fusion proteins into DNA nanostructures.[117, 118] Heterobifunctional linkers based on this reactive group have also been used to link cytochrome c covalently to oligonucleotides allowing for self assembly of a DNA tetrahedra around the protein.[119] Distefano and colleagues similarly encapsulated green fluorescent protein (GFP) in a DNA tetrahedral but relied on addition of an azide-modified isoprenoid diphosphate to a C-terminal peptide tag on GFP using protein farnesyltransferase (PFTase). Following this step GFP is coupled to an alkyne modified DNA oligo and through the Huisgen cycloaddition ("click") reaction.[120]

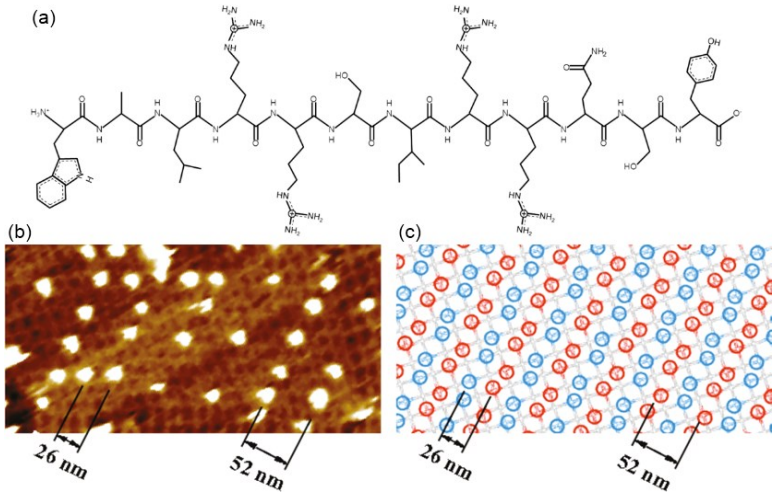

Figure 28 - Gold binding peptide incorporated in DNA nanostructure. (a) Peptide WALRRSIRRQSY (b) AFM of two dimensional array functionalized with peptide on opposing sides. Bound AuNP's favor one side. (c) Map of array illustrating peptides displayed on opposing sides of array as blue and red circles. Reproduced with permission.[121]

Illustrating the diverse functionality of peptides is the in vitro evolution of peptides for recognition of inorganic material.[122] LaBean and colleagues used DMTMM to link the C-terminal of the gold binding peptide WALRRSIRRQSY to oligonucleotides. These could then be incorporated in a tile based two-dimensional array and subsequent addition of AuNP's showed preferential binding to peptides without the use of thiol chemistry.[121] See Figure 28.

6.1.2 Peptide Nucleic Acid

Recently attention has been directed toward using peptide nucleic acids (PNA) for extending the chemical versatility of DNA nanostructure. PNA is a synthetic DNA analog consisting of a backbone of repeating N-(2-aminoethyl)-glycine units to which purine and pyrimidine bases are linked by amide bonds.[123] See Figure 29.

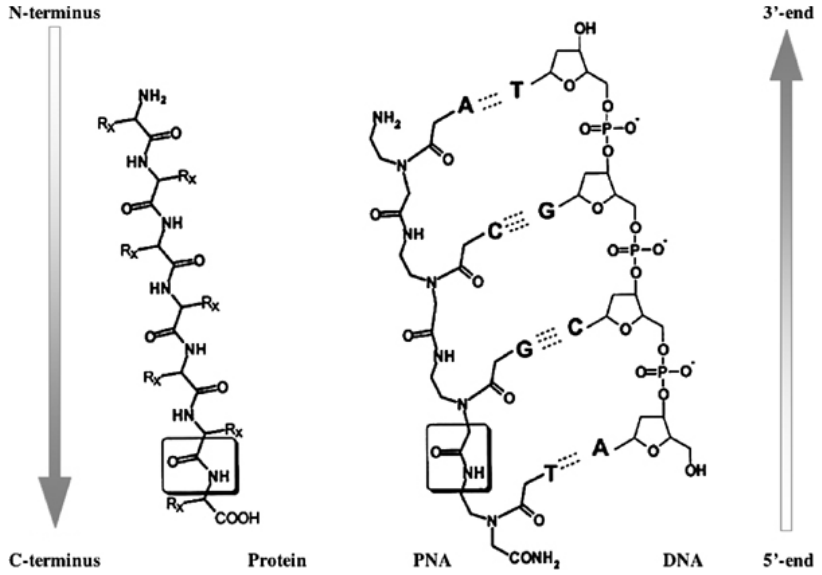

Figure 29 - Illustration of PNA structure compared to peptide and DNA structure. The amide bond common to PNA and peptide backbone is boxed in. PNA sequences are written from N to C terminal by convention and preferentially binds to DNA in the anti-parallel orientation illustrated here. Reproduced with permission.[124]

The neutral backbone affords PNA characteristics different from those of DNA, such as increased affinity towards complementary strands at low salt concentrations.[125] Since PNA is synthesized by the same solid phase chemistry as peptides, it is simple to make PNA-peptide chimeras and consequently to incorporate peptides at well-defined locations in DNA nanostructures.[126]

Hao Yan and colleagues used a three dimensional DNA nanocage to bind to bind PNA-peptide chimeric molecules that were also functionalized with dyes allowing enabling them to assay binding in the nanocage. See Figure 30. Although their peptide sequences where only three residues long, this project illustrates the potential for using the highly predictable nature of DNA folding to overcome the difficulty in predicting

peptide folding. The ability to orient catalytic peptides in three dimensional space could open up for the design of novel biological catalysts.

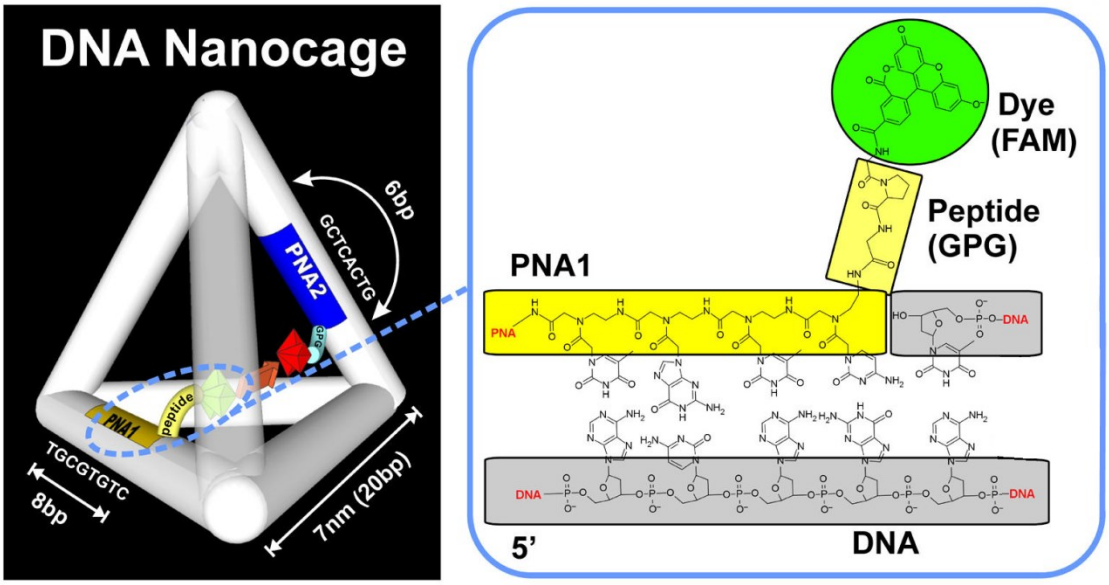

Figure 30 - Illustration of PNA-peptide chimera binding in a DNA nanocage. Incorporation of a dye allows for tracking the binding of two different PNA-peptide chimeras. Reproduced with permission.[126]

The unique properties of PNA can also be used to construct nanostructures with different handedness than that of DNA•DNA duplexes[127] and with low tolerance of base mismatches useful in detection systems.[128, 129] One of the most interesting features of PNA molecules is that their high affinity for complementary DNA allows for sequence specific invasion of DNA duplexes.[123, 130, 131] This property can be used to create nanoscale assemblies using double stranded DNA as a scaffold[132, 133] or as a way to manipulate dynamic nanostructures by addition of PNA without the use of predesigned toeholds.[134, 135] PNA holds promise for greatly expanding of the toolbox of DNA nanotechnology

both by introducing chemical reactivity in the form of peptides and by aiding in the fine tuning of nanostructure designs.

6.2 Experimental Design

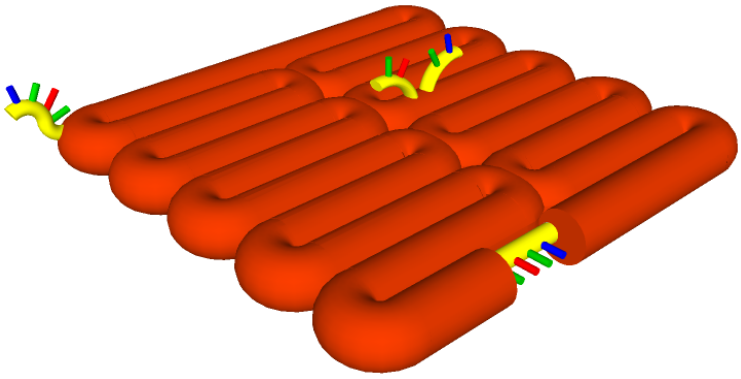

Figure 31 – Illustration of RROb. Three different PNA binding sites on the DNA origami structure have been designed to investigate inclusion of PNAb. Orange cylinders represent the DNA duplex forming the structure. Yellow cylinders represent single stranded regions complementary to PNA. The binding site in the front of the picture that is "inline" with the orange duplex cylinders are located on the m13 scaffold. Notice that this model is not to scale nor does it accurately depict no. of bases. However, it is meant to better convey the location and the conformation of binding sites.

We have investigated the incorporation of PNA in DNA nanostructures using a 16-base PNA molecule with three lysines (Lys) at the C end (PNAb). See Figure 32. The lysines' sidegroup has a pK_a of 10.5; hence at pH 8.00 each PNA strand has three positive charges. We also included a biotin group at the N end of the PNA. To test the incorporation of this PNA molecule into DNA structures, we employed a two dimensional DNA origami structure of Rothemunds original design herein labelled RRO (regular rectangular origami) following previous convention.[37] We modified RRO to

include three PNA binding sites at the locations and with the configurations identified in Figure 31 giving the structure names RROb.

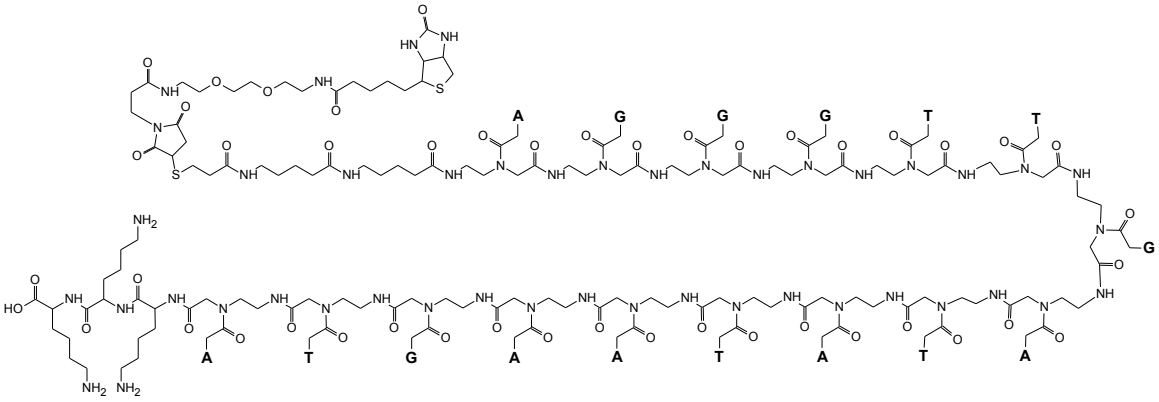

Figure 32 PNAb structure and sequence.

We labeled the binding sites centre, side and corner. The side site consists of a stretch of exposed, uncomplemented M13 scaffold strand along the edge of the rectangular structure complementary to the PNA sequence. The centre site is placed in the centre of the two dimensional origami and consists of overhangs from two staple strands forming a V-shaped binding site; each overhang is complementary to half of the PNA molecule. The corner site is located at the corner and consists of an overhang from a staple strand and has a sequence fully complementary to that of the PNA molecule. The attachment of the PNA to these sites was assayed using streptavidin (STV), which can bind with high affinity to biotin.

The increased stability of a hetero DNA•PNA duplex when compared to a DNA•DNA duplex allows PNA to invade a DNA duplex. This invasion represents a method for DNA modification that is orthogonal to the widely used toehold-mediated

strand displacement for the introduction of controlled dynamic behavior in nano devices.[5] However, the relative stability of the DNA•PNA and DNA•DNA duplexes is highly dependent on ionic strength. Hence we decided to first evaluate the kinetics of invasion of a DNA duplex by the PNA molecule and its dependence on salt concentration. We employed the method of initial rates and a DNA duplex labeled with a fluorophore and a quencher to monitor by fluorescence the dissociation of the DNA duplex in the presence of PNA. Building on knowledge learned from this kinetic experiment, we designed a linear TX array[136, 137] to display invasion sites in order to visualize invasion of the biotinylated PNA strand. See Figure 33.

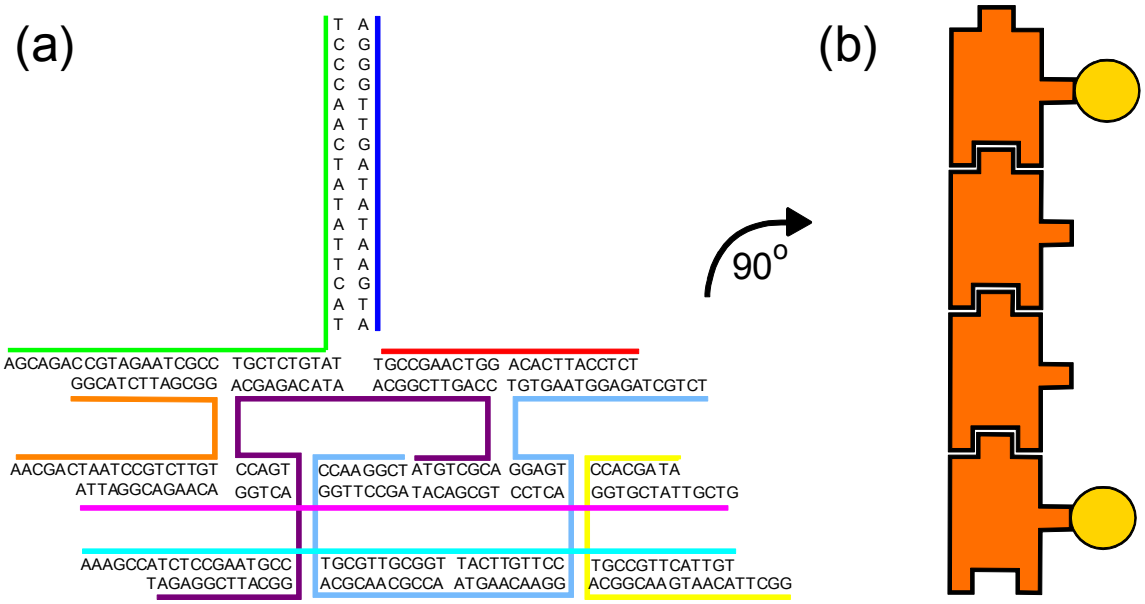

Figure 33 - (a) TX tile fully illustrated with sequences. The top protruding duplex allows for invasion of complementary PNA strand. (b) Multiple tiles assemble into linear arrays. In this illustration four tiles are linked togehter. This enables estimation of the efficiency of PNA invasion when using biotinylated PNA as the bound streptavidin can be counted in AFM. STV is illustrated here as yellow circles at the first and last tile in a four tile array.

6.3 Results and Discussion

6.3.1 Melting Curves

The melting curves were measured to evaluate thermodynamic stability of a DNA•PNA duplex compared to a DNA•DNA duplex. The enhanced thermal stability of the DNA•PNA duplexes over the DNA•DNA duplexes were observed in solutions of different salt concentrations. The melting temperatures T_m of PNA•DNA duplex under different salt concentrations are above 75 °C in all cases, which is much higher (by 19-38 °C) than that of the DNA•DNA duplex (Table 1). The melting temperatures of this 16-bp duplexes are in agreement with the literature values of 15-bp duplexes.[138] Representative melting curves are shown in Figure 34.

Table 1 Melting temperatures (˚C) of DNA•DNA and DNA•PNA duplexes in 1X TAE buffer at 3 μM and different concentration of $MgCl_2$. PNA sequence: TGAATATAGTTGGGA. Complementary DNA sequence: TCCCAACTATATTCAT

Conc. Of $MgCl_2$	DNA:DNA	PNA:DNA	ΔT_m
1	40	78	38
6	56	77	21
12.5	57	76	19

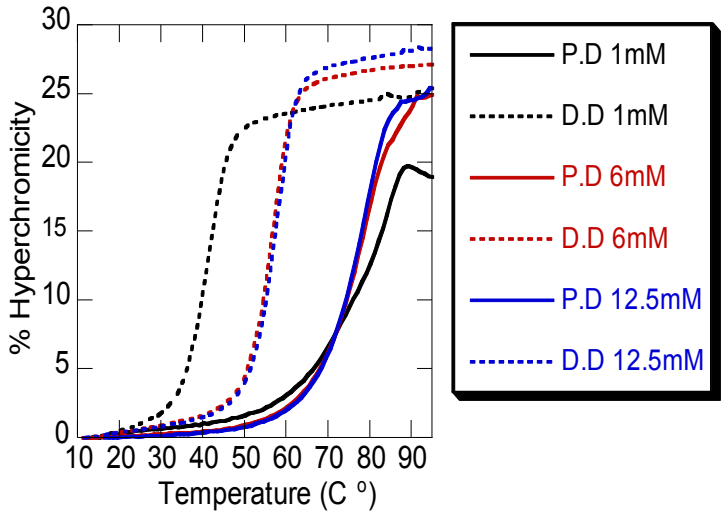

Figure 34 - Melting curves of PNA•DNA (solid line) or DNA•DNA (dotted line) duplex in 1, 6 or 12.5 mM $MgCl_2$. Strands were at a concentration of 3 μM.

The melting curve of DNA•DNA duplex has a slightly sharper transition around the melting temperature of duplex than the PNA•DNA duplex, which demonstrated a higher cooperativity of the base pairs in DNA•DNA duplex than that of the PNA•DNA duplexes. However, the melting curves of PNA•DNA shifted significantly to higher temperature, indicating the great thermodynamic driving force of the strand invasion of PNA in DNA nanostructures. When the salt concentration decreases from 12.5 to 1 mM, the thermal stability of PNA•DNA decreases while that of DNA•DNA increases, leading to a higher thermodynamic driving force of strand invasion at lower salt concentration. The same result is further observed in the fluorescence assay of duplex invasion under different salt concentration.

6.3.2 Binding of PNA to DNA Nanostructures

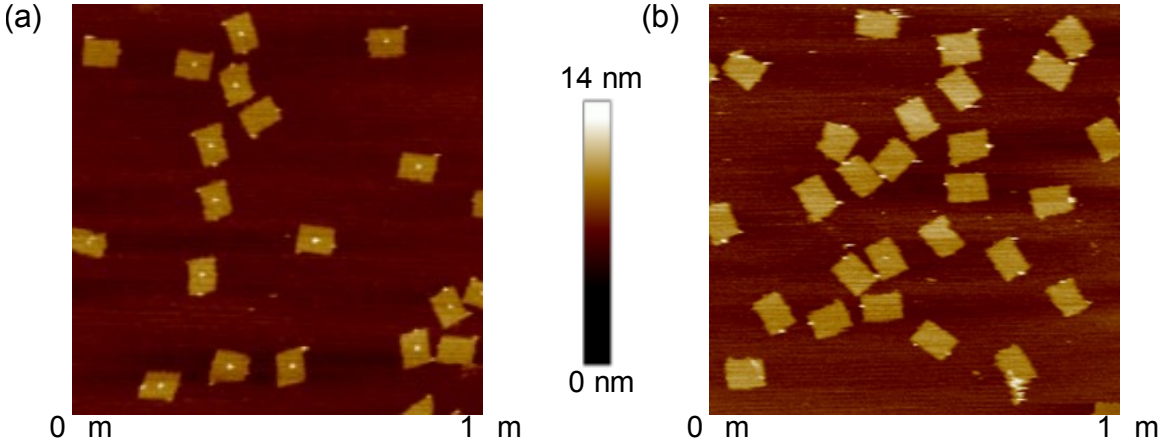

Figure 35 - Binding of PNA or DNA to RRO was evaluated by counting STV at different locations. Each micrograph was treated individually the mean displayed with error bars representing standard deviation.

To evaluate the thermodynamics of PNA binding relative to three different binding sites on a two dimensional DNA origami we annealed the origami with equivalent conc. of biotinylated PNA. Samples were then incubated with 1-2 μM STV for 1-2 hours and imaged with AFM. Figure 35 a and b shows representative images of structures with biotinylated PNA and a control with a biotinylated DNA probe. A total of 10 different micrographs were collected and analysed. The number of structures and binding events counted are listed in Table 2. For each individual micrograph the binding rate was calculated. The mean value is displayed in Figure 36.

Table 2 Total number of counted origami structures and bound STV's at different binding sites.

	PNA	DNA
Origami	596	883
Center Site	510	5
Edge Site	322	458
Corner Site	344	276

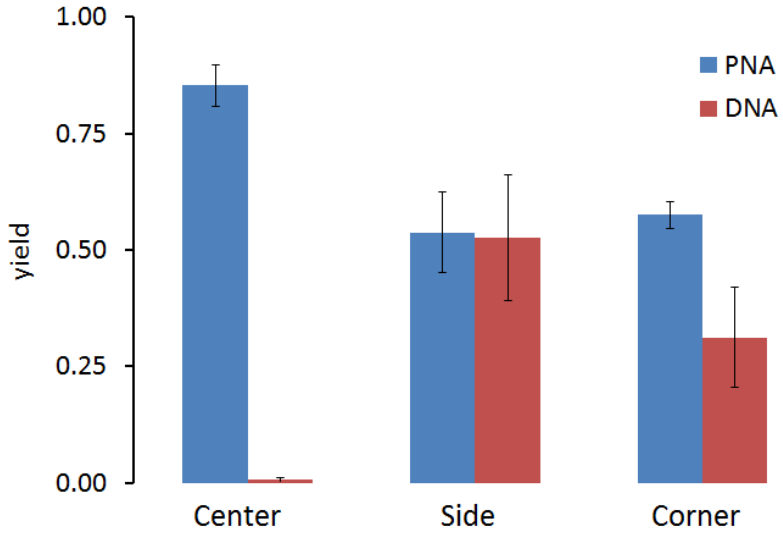

Figure 36 - Binding of PNA or DNA to RRO was evaluated by counting STV at different locations. Each micrograph was treated individually the mean displayed with error bars representing standard deviation.

An oligomer of 16 nucleotides generally does not have high enough affinity to its complementary strand to effectively target DNA nanostructures. However, Figure 35a shows that our PNA molecule targets the centre site with a high degree of binding and

significantly higher than the two other sites. The 16 nucleotide DNA sequence on the other hand achieves almost zero binding at the centre site. This is in agreement with previous reports of diminished hybridization at the centre of RRO which Jungmann *et al.* ascribed to an increased off rate.[139, 140] We ascribe the very low level of binding observed here to the combination of location on the origami and conformation of the centre binding site. The V-shaped binding conformation was originally introduced by Ke *et al.* to aid in AFM identifying 40 nt long probes,[139] but we conclude that this conformation is ill suited for shorter probes. It is conceivable that fraying originating at the V vertex can quickly expand to full dissociation. Interestingly we do see a higher binding of the DNA control probe to the side site compared to the corner site. We ascribe this to the additional base stacking at the ends of the DNA probe and believe that including base stacking pairs at the ends of probe targets could increase the affinity of future target designs. The positive PNA strand shows a higher degree of binding to the corner site than the DNA probe but about the same degree of binding to the side site. This is most likey due to a disruption at the ends of the PNA molecule resulting from the added lysine residues at the C terminal end and the added C10 spacer on the N terminal. The biggest difference is observed at the center site where we observe almost no DNA binding but 85 percent PNA binding. We believe this is due to an inversion of the electrostatic force between the PNA probe and the origami surface compared to the DNA probe and the surface. Unlike the corner site that protrudes freely into solution

and can thus avoid close contact with other parts of the structure and the side site that only sees one neighboring duplex. The center site sits in the middle of the negative charged origami and the conformation of the binding site is such that the entirety of the probe is brought closer to the origami surface thus increasing the electrostatic force of either sign. Johnson-Buck *et al.* propose that DNA nanostructures enrich the immediate surrounding environment in positive counterions at low ionic strength creating a diffuse layer of positive counter ions.[141] Our present results suggest that this layer is not enough to prevent fraying of the DNA probe at the binding site vertex leading to dissociation and conversely that the positively charged PNA remain highly attracted to the origami surface.

The charge of the DNA backbone becomes an increasing challenge in large dense three dimensional nanostructures requiring slow anneals of up to 178 hours with high salt concentration.[39, 41] Our results indicate that positive PNA probes of even shorter lengths could be used as crucial "anchor" strands enabling even larger structures or shorter more convenient anneals.

6.3.3 Duplex Invasion

We further wished to investigate the propensity for our positively charged mixed base PNA probe to invade a nanostructure embedded DNA duplex. To do this we first did a fluorescence assay of the invasion into a fluorophore and quencher labeled single duplex. This allowed us to determine the initial rates of the invasion reaction while

varying the concentration of both duplex and PNA and thus isolate the exponent in the rate equation; $r = k[DNA]^X[PNA]^Y$ where [DNA] is the concentration of pre-annealed DNA duplex and [PNA] is the concentration of added PNA. Figure 37a shows representative graphs of the initial concentration of dissociated duplex following addition and mixing of PNA at 1 mM $MgCl_2$.

(a)

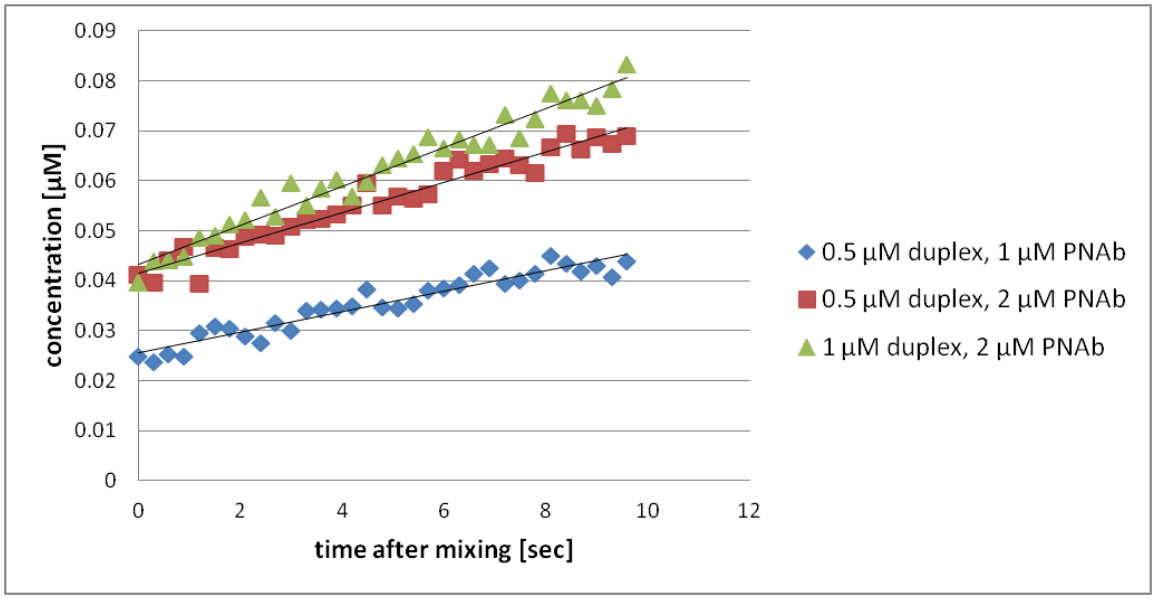

(b)

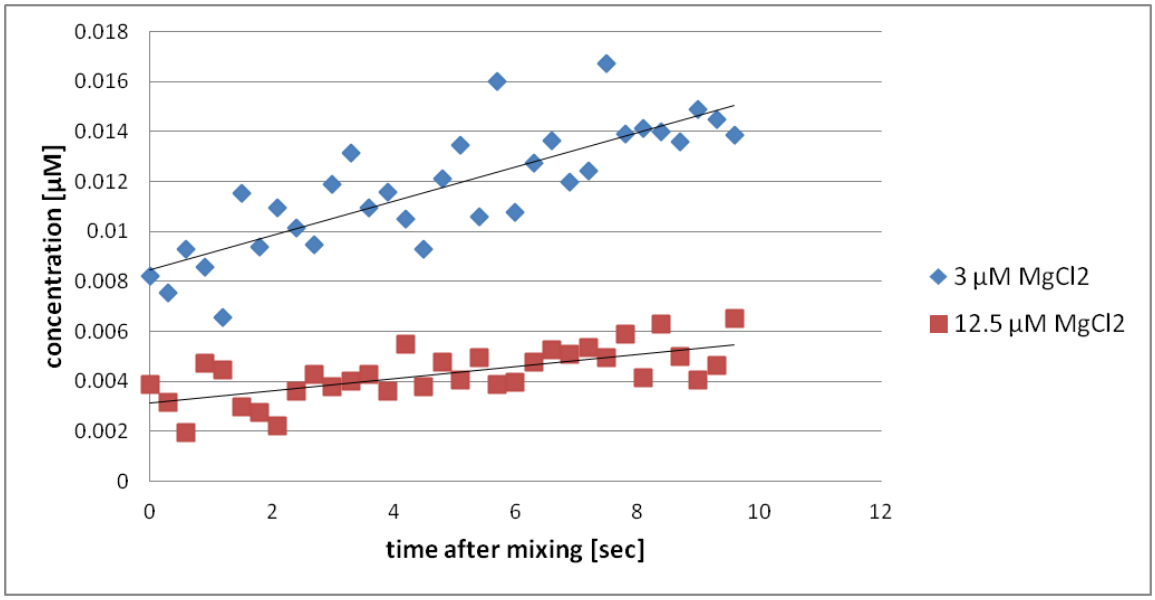

Figure 37 - (a) Representative graphs of initial concentration of dissociated duplex following mixing with different start concentrations. PNAb is mixed into a solution of pre-annealed AGGGTTGATATAAGTA(Iowa Black RT) and (Cy5)TACTTATATCAACCCCT. (b) Representative graphs of initial concentrations following mixing at different $MgCl_2$ concentrations.

Table 3 Initial rates of dissociation of duplex DNA following addition of PNAb under different initial reactant concentrations and $MgCl_2$ concentrations.

	Initial rates [μM/sec]	R^2 of linear fit
0.5 μM duplex, 1 μM PNAb, 1 μM $MgCl_2$	0.0022	0.9372
	0.0017	0.9278
	0.0021	0.9160
0.5 μM duplex, 2 μM PNAb, 1 μM $MgCl_2$	0.0033	0.9365
	0.0034	0.9711
	0.0031	0.9548
1 μM duplex, 2 μM PNAb, 1 μM $MgCl_2$	0.0048	0.9566
	0.0038	0.9642
	0.0040	0.9524
0.5 μM duplex, 1 μM PNAb, 3 μM $MgCl_2$	0.0007	0.8962
	0.0005	0.8094
	0.0005	0.8810
0.5 μM duplex, 1 μM PNAb, 12.5 μM $MgCl_2$	0.0003	0.7875
	0.0002	0.4584
	0.0003	0.4507

With three different concentrations we have have three different rates; r_1, r_2 and r_3 defined as the average of the rate of the three replications of each condition. Using the method of initial rates we can isolate the exponents in the rate equation:

$$\frac{r_2}{r_1} = \frac{k[DNA]_2{}^X[PNAb]_2{}^Y}{k[DNA]_1{}^X[PNAb]_1{}^Y} = \frac{[PNAb]_2{}^Y}{[PNAb]_1{}^Y} \Rightarrow$$

$$Y = \frac{ln\left(\frac{r_2}{r_1}\right)}{ln\left(\frac{[DNA]_2}{[DNA]_1}\right)}$$

Likewise we use the ratio of r_3 to r_2 to determine the second exponent. Isolating the exponents results in values of 0.34 and 0.72 for X and Y respectively. This indicates a ratio of 2:1 PNA to DNA in the rate limiting step in accordance with previous reports on the invasion of poly-T PNA oligos into much longer DNA duplexes[142] and could also indicate the formation of a PNA_2:DNA triplex. Although PNA is known to form stable antiparallel duplexes with complementary DNA and especially homopurine PNA has been shown to form a 1:1 PNA:DNA duplex,[143] previous studies have also reported on the formation of homopyrimidine PNA_2:DNA triplexes,[142] cytosine rich homopyrimidine PNA:DNA_2 triplexes,[144] alternating thymine-guanine PNA:DNA duplexes[144] and conversely alternating thymine-guanine PNA_2:DNA triplexes.[145] A prominent factor in this variety of stoichiometric configurations is the increased stability of PNA Hoogsteen basepairs.[146]

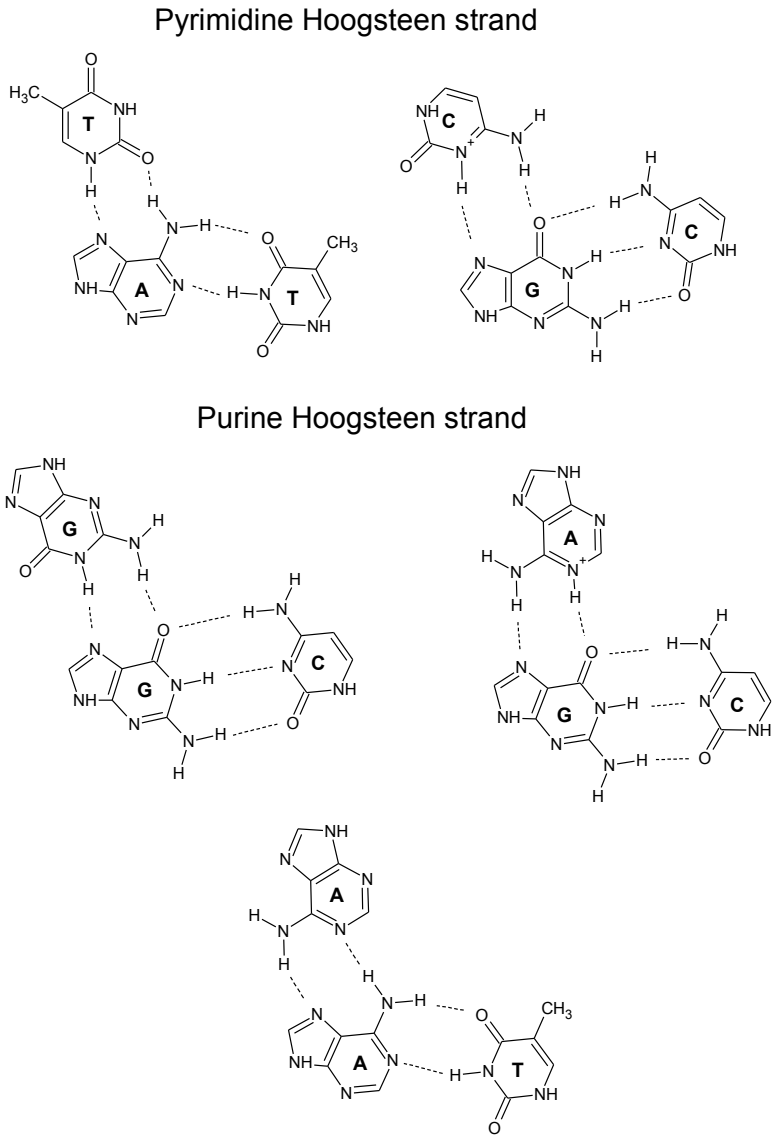

Figure 38 - Basepair triads with Hoogsteen basepairs at the top. Notice that formation of the C:G Hoogsteen pairs requires protonation of the N3 of cytosine and the A:G requires protonation of N1 of adenine. Hence the propensity for this assembly can be probed by altering pH. Reproduced with permission.[146]

The canonical Hoogsteen basepairing scheme results in a triplex with a Watson Crick purine-pyrimidine pair and pyrimidine binding in the major groove via Hoogsteen pairing but purine strands can also form Hoogsteen basepairs. See Figure 38.

In DNA triplexes the Hoogsteen strand binds parallel to the strand with which it basepairs. Likewise in homopyrimidine PNA_2:DNA triplexes where the Hoogsteen strand binds in a parallel fashion to the homopurine DNA strand. However, these complexes are additionally stabilized by hydrogen bonds between the phosphor bound oxygen of the DNA strand and the amide hydrogen on the Hoogsteen strand. [147]

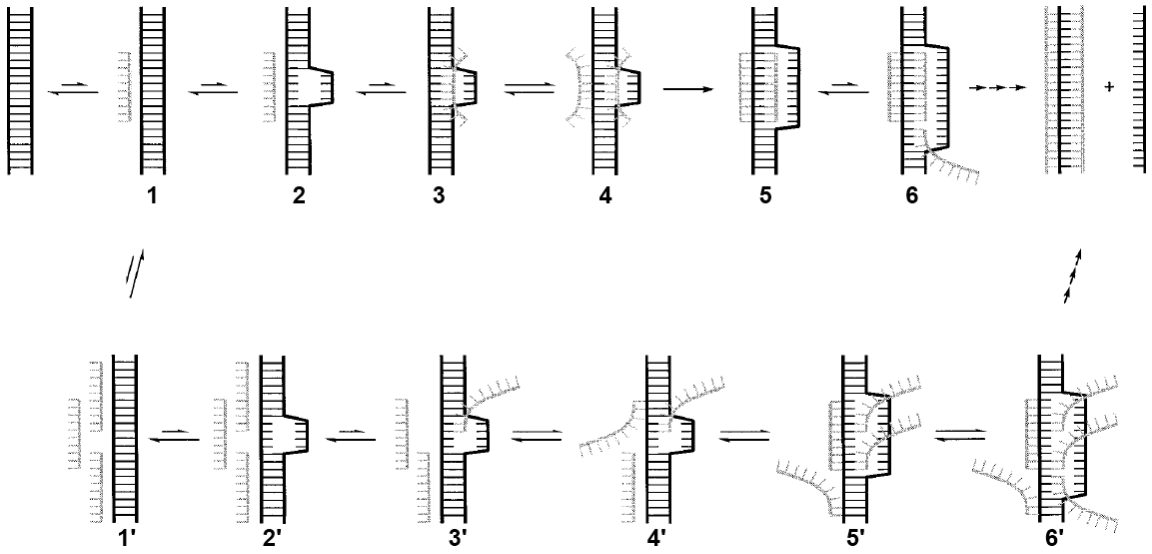

Figure 39 - Kinetic scheme from Wittung *et al.* Reproduced with permission.[142]

Wittung *et al.* investigated the invasion of a homopyrimidine PNA into a DNA duplex but despite the final triplex they did not reach a conclusion concerning the rate limiting intermediate. The top row in Figure 39 illustrates one idea with an initial base dissociation in the DNA duplex followed by association of the first PNA strand and then a second PNA strand. Wittung *et al.* argue that the association of the second PNA strand (species 4) should energetically not be slower than species 2. To accommodate a rate limiting step with multiple PNA's they also suggest a second scheme (Figure 39 bottom

row) consisting of several PNA's associating with the DNA duplex both by invasion and Hoogsteen basepairing. In this scheme species 5′ and 6′ represent metastable structures with several PNA's bound that slowly rearrange to the final product.

The different possible confirmations make it difficult to probe the rate limiting step in the duplex invasion reaction. In the present case we are concerned with evaluating the salt dependence of the reaction and our rate equation allows for a relative investigation of this.

Table 4 Rate constants for PNA invasion at different $MgCl_2$ concentrations.

	1 mM $MgCl_2$	6 mM $MgCl_2$	12.5 $MgCl_2$
k ($s^{-1} M^{-1}$)	0.0025	0.00072	0.00034

Considering this we then tried altering the concentration of $MgCl_2$. Figure 37b shows representative graphs of the initial rates of duplex dissociation. Using the exponents determined we calculate the rate constants at different salt concentrations. See Table 4. We observe an increase in the rate constant of almost an order of magnitude when going from 1 mM $MgCl_2$ to the 12.5 mM that is usually used for annealing DNA nanostructures. Utilizing this information we annealed TAE arrays with duplex invasion sites at 12.5 mM $MgCl_2$ and then buffer exchanged the assembled structures with 1 mM $MgCl_2$ at 4 °C. We then added biotinylated PNA equimolar to the concentration of

invasion sites and incubated for >2 hours before depositing on mica with 12.5 mM $MgCl_2$ and 1-2 μM STV and imaged with AFM.

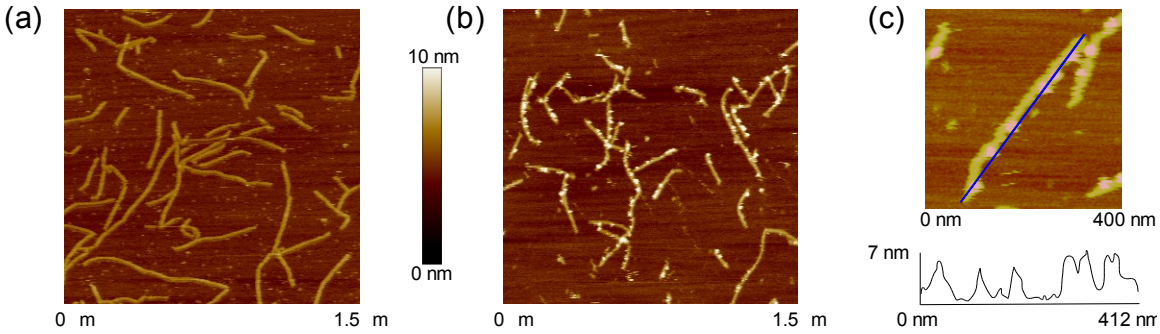

Figure 40 AFM of PNA invasion in TX array (a) Control sample with biotinylated DNA. (b) TAE arrays incubated at 1 mM MgCl2 with biotin-PNA and then imaged with STV. (c) Zoom of array with section contour. The section is 412 nm and includes 6 STV's.

The control sample with biotinylated DNA added shows no STV localization to the arrays (Figure 40a) but the PNA sample shows the protein localized as beads on a string following invasion into the duplex by biotinylated PNA (Figure 40b). Figure 40c shows a zoom of an array with attached STV and a 412 nm section along the array. Each tile is 52 nucleotides long. At 0.33 nm per nucleotide in duplex DNA that makes for ~17 nm per tile and 24 tiles in the 412 nm long array. With 6 STV's bound this gives a yield of ~25% invasion sites successfully targeted. While a substantial variance is observed (Figure 40b) it seems clear that the level of duplex invasion within a nanostructure is substantially lower than the kinetics would suggest. While PNA holds promise as an orthogonal means of introducing dynamic behaviours in nano devices, more

experiments are needed in order to careful model duplex invading potential of PNA in the context of DNA nanostructures.

6.3.4 Conclusion

We have shown that positively charged PNA molecules behave differently than DNA in the context of DNA nanostructures as evidenced by the altered binding distribution on a two dimensional DNA origami. Positive PNA probes can exploit the large density of negative charge at the centre of DNA based nanostructures to more effectively bind targets with shorter complementary sequences. A feature that is essential when exploiting the lower scale-limit of DNA based nanotechnology and DNA based biomaterials. Furthermore the potential for strand invasion increases the toolbox for creating dynamic nanoscale DNA devices. However, more research is needed to better understand and model the invasion mechanism in order to create accurate and predictable nanoscale machinery.

7. Medical Impact and Future Directions

One of the areas where TGF-β plays an important part is in wound healing. Following injury, a wide range of intracellular and intercellular pathways must be coordinated to restore tissue integrity. Wound repair is classically divided into three different stages. One; inflammation, two; new tissue formation and three; remodeling.[148]

1) The first stage of "inflammation" typically lasts till about 24-48 hours after the injury. This stage is characterized by a type of cell fragments called platelets, clustering together and forming a plug. The coagulation cascade is then initiated resulting in fibrin being deposited on the plug, stopping blod loss and ahcieving haemostasis. Additionally the immunesystem is activated by invading pathogens and neutrophils are recruited to the site of injury.

2) The second stage called "new tissue formation" occurs 2-10 days after injury and involves cellular proliferation and migration leading to restoration of the epithelium. It also involves extensive production of extra cellular matrix (ECM) especially in the form of collagen. This new ECM is primarily produced by fibroblast cells as a response to TGF-β and other cytokines. This stage also sees the initiation of new blood vessel formation through the migration of endothelial cells. A process known as angiogenesis which is likewise stimulated by TGF-β and other cytokines. [149]

3) The final stage is "remodeling" which begins 2-3 weeks after injury and can last for more than a year. During this stage many cells either undergo apoptosis or migrate out of the wound area. This leaves a disorganized collagen matrix with a sparse population of fibroblasts constituting the scar tissue.

The wound healing process is important in pathological conditions where it doesn't function properly. This is the case in chronic wounds such as diabetic ulcers that are becoming more prevalent as more and more people develop diabetes.[150] It was

estimated that 285 million people worldwide had diabetes in 2010 and this number is expected to rise to 439 by 2030. An increase from 6.4 to 7.7%.[151]

The process of wound healing can also pose problems in other situations. In spinal cord injuries (SCI) a primary impediment for neuronal axon regrowth is the formation of collagen rich scar tissue.[152] SCI recovery can be advanced by disrupting scar formation either by blocking the enzymatic pathway of collagen synthesis or by treatment with TGF-β inhibitory antibodies.[152, 153] However, the wide range of cellular tasks that TGF-β partakes in means disrupting this signaling pathway can have detrimental consequences for recovery. For example; failure of angiogenesis leads to secondary degeneration of both neurons and glial cells but this process can be ameliorated by stimulating angiogenesis through treatment with cytokines.[154] Since TGF-β is an important signaling molecule in angiogenesis, treatment with inhibitory antibodies towards TGF-β can be expected to have substantial negative consequences through the inhibition of angiogenesis.

Wound healing isn't just relevant in the case of actual visible wounds. An almost identical process occurs in practically any tissue that receives destructive stimuli. For example; following a myocardial infarction a similar process takes place in the heart tissue leading to the formation of scar tissue. Complications stemming from this formation kills close to 100,000 people in the US every year.[148] If we can understand the wound healing process better and develop a technology that allow us to modulate it, we

could hope to address some of these issues. Be it in inducing the scar forming process in chronic wounds, or attenuating it following a heart attack.

The wound healing process is orchestrated through the release of signaling chemicals by the cells in the wound area. These molecules are predominantly polypeptides classified as cytokines. Investigations of the expression of several such signaling molecules show distinct temporal patterns following injury. For example: In rat skin-burn injuries, Type I collagen expression remains low until a couple of days after injury when it starts to increase, consistent with the production of collagen in the second stage of wound healing. TGF-β displays a biphasic expression pattern that hints at its diverse functionality as a signaling molecule.[155]

In wound healing TGF-β plays a central role in both inducing expression of collagen, and more broadly inducing fibrosis and also inducing angiogenesis. This means that TGF-β manipulation can potentially both be used to promote wound healing and to prevent detrimental scar formation in cases such as spinal cord injury. The challenge is to have cell specific and temporal control. It might be advantages to limit collagen formation by fibroblast cells without preventing angiogenesis by endothelial cells. Application of TGF-β ligand to the wound results in an area wide stimulation as does application of TGF-β neutralizing antibodies.

Our DNA nanostructure based technology holds promise as a way to modulate TGF-β stimulation as it allows for cell stimulation without modification of the systemic

level of TGF-β. This especially has potential as a therapeutic strategy if we can target our nano-assemblies to cell subpopulations. This has already been achieved with different structures trough convenient incorporation of aptamers.[156] Further research should focus on proving sub-population specific interaction and sensitization of nano-assemblies as this holds great promise for medical applications.

8. Experimental

8.1 Sensitization of Transforming Growth Factor-β Signaling by Multiple Peptides Patterned on DNA Nanostructures

8.1.1 Nanostructure Assembly

Rothemund's tall rectangle origami[37] was modified by redesigning and then biotinylating a select set of staple strands. 5 nM M13 ssDNA scaffold (Bayou Biolabs) were annealed with 5x concentration of staple strands (Integrated DNA Technologies) in 1x TAE/Mg2+ (Tris, 40 mM; acetic acid, 20 mM; EDTA, 2 mM; and magnesium acetate, 12.5 mM; pH 8.0) and annealed from 90 to 4°C over the course of 2 hours. Nano-assemblies were assembled in stepwise fashion and separated from unassembled components using Microcon 100,000 MWCO filter2 spin units. Streptavidin was incubated overnight and biotinylated peptide LTGKNFPMFHRN-biotin (Eton Bioscience) was incubated for at least two hours at room temperature. Freshly prepared assemblies were added to cell cultures for a final estimated concentration (assuming no loss during filtration the step) of 300 pM.

8.1.2 AFM

5ul of diluted sample was pipetted onto freshly cleaved mica. AFM images were obtained on a Digital Instruments Nanoscope III (Vecco, USA) using NP–S oxide-sharpened silicon nitride tips (Vecco, USA) with a Multimode head and fluid cell in tapping mode under buffer.

8.1.3 Cell Culture

NMuMG cells were obtained from Duke University cell culture facility. They were cultured in DMEM media with 10% FBS, 50 units/ml penicillin, 50 μg/ml streptomycin and 10 μg/ml human or bovine insulin at 37°C and 5% CO2.

8.1.4 Immunofluorescence

Cells were grown on circular microscope cover slips (Ted Pella) in 24-well plates with 40 pM added background TGFβ (ProSpec) and specified treatments. The cells were treated with nano-assemblies for 18 hours before fixing. They were fixed in 4% paraformaldehyde/PBS for 15 min at 4°C, then permeabilized in 0.125% Trition X-100/PBS for 15 min at room temperature followed by blocking in 3% BSA/PBS for 30 min. Monoclonal mouse anti-Smad2/3 (clone 18, BD Biosciences Pharmingen, 1:200) was spotted onto parafilm and microscope slides inverted onto droplets and incubated overnight at 4°C. Following washing with PBS, secondary antibody Rhodamine Red-X goat anti-mouse IgG (H+L) (Life Technologies) was incubated for 1 hour at room temperature. After washing with PBS the samples were then stained with 300nM DAPI for ~5 min before washing again in PBS and mounting with Fluoromount-G (Southern Biotech).

8.1.5 Luminescence Assay

Smad2/3 response was quantified using Cignal SMAD Reporter Assay Kit (SABiosciences) which was transfected with Fugene6 (Promega) and developed with

Dual-Glo Luciferase assay system (Promega). Manufactures instructions were followed with reverse transfections (transfectant added first, followed by addition of cells) done in Opti-MEM media (Life Technologies) with 3% FBS and 1% NEAA (Life Technologies). Transfected cells were assayed in growth media with background TGFβ conc. of 40 pM. All data were collected as the mean of triplicate measurements, and the entire experiment was repeated three times. Luciferase luminescence was normalized to renilla luminesce controlled by a constitutively active promote as per the manufacterer's instructions (SABiological).

8.2 Functionalization of DNA Nanostructures with Zinc Finger Binding Peptides

8.2.1 Design of TX Tile

Design of the TX tile was based on a previous published structure. [157] The outer strands of the tile were modified with protruding hairpins containing the zinc finger target sequence and two pairs of flanking nucleotides. 4 T's were incorporated to terminate the hairpin loop. Custom oligo nucleotides were purchased from Integrated DNA Technology (www.idtdna.com) and purified by PAGE. Structures were formed by mixing strands at approximate stoichiometric ratio in TAEMg (20 mM Tris, 2 mM EDTA, 12.5 mM $MgCl_2$, acetic acid to pH 7.6) to a final concentration of 1 μM in 50 μl. The mixture was then placed in a 94 °C water bath and left to cool to room temperature during approximately 24 hours.

8.2.2 Protein Expression

Protein was expressed and purified with the pMAL expression system from New England Biolabs (www.neb.com). Concentration was determined by measuring the absorbance and 280 nm and using the method of Gill and Hippel to calculate an extinction coefficient.[158] Increasing the concentration was done with a 10 MWCO spin filter column from Amicon.

8.2.3 ELISA Assay of Protein Expression

Streptavidin coated 96 well plates were incubated with target sequence biotin-GGC CAC TGC GGC TCC GGC CCC GAG TTT TCT CGG GGC CGG AGC CGC AGT GGC C and non-target sequence biotin-GGC GAC TCC GGC CGC CTC GGC GAG TTT TCT CGC CGA GGC GGC CGG AGT CGC C. Saturated with albumin and washed with PBST (137 mM NaCl, 2.7 mM Kl, 10 mM Na_2HPO_4, 2 mM KH_2PO_4, 0.1 % tween 20). Dilution series of freshly lysed cells expressing the constructs were then incubated for half an hour. Afterwards the 96-well plates were incubated first with anti-MBP antibodies raised in mice and then with anti-mouse antibodies raised in goat and fused to Alkaline Phosphatase (AP). Addition of AP developer (0.5 mg/ml pNPP disodium salt hexahydrate, 10 % w/v diethanolamine, 0.5 mM $MgCl_2$) to the wells initiates the reaction which ran for approximately 1 hour where-after absorbance at 405 nm was recorded.

8.3 Functionalization and Modification of DNA Nanostructures with Peptide Nucleic Acid

8.3.1 PNA Synthesis

The PNA oligomer was synthesized by solid phase peptide synthesis using the Boc-protection strategy.[159] MBHA resin was downloaded with Boc-L-Lys-(4-MeOBzl)-OH (NovaBiochem) to an estimated loading of 0.05 mequiv/g. Boc group on resin is deprotected with 5 % *m*-cresol in trifluoroacetic acid (TFA). According to the sequence of the PNA oligomer, a Boc-protected PNA monomer (A, G, T, or C) (ASM Research Chemicals) was coupled to the resin using O-Benzotriazole-N,N,N′,N′-tetramethyluronium hexafluoro-phosphate (HBTU) (Peptides International) as a coupling agent. Unreacted $-NH_2$ sites on resin were capped by acetic anhydride. Finally, 5-aminovaleric acid (C_4) as a linker and 3-mercaptopropionic acid (C_2) as a source of –SH group were coupled at the end of the PNA oligomer to allow the functionalization of biotin. PNA oligomers were cleaved from the resin with TFA and trifluoromethanesulfonic acid (TFMSA), precipitated in diethyl ether, and dried with nitrogen. PNA oligomers were purified by reversed-phase HPLC using a C18 silica column on a Waters 600 model. Absorbance was measured at 260 nm with a Waters 2996 Photodiode Array Detector. Characterization of the oligomers was performed by MALDI-ToF mass spectrometry on an Applied Biosystems Voyager Biospectrometry Workstation with Delayed Extraction and an R-cyano-4-hydroxycinnamic acid matrix (10 mg/mL in 1:1 water/acetonitrile, 0.1% TFA). PNA sequence synthesized for this

study is Lys_3-ATGAATATAGTTGGGA-$C_4C_4C_2$. m/z for the PNA molecule $(M+H)^+$ were calculated and found to be 5127.2/5130.0. PNA solutions were prepared in nanopure water (>18.3 MΩ cm^{-1}) and stored at -18 °C to avoid depurination reactions. The concentration of PNA stock solution were determined by UV-Vis spectrophotometry using $\varepsilon(260)$ = 6600, 8600, 11 700, and 13 700 cm^{-1} M^{-1} for each C, T, G, and A monomer, respectively. For biotinylation the PNA was first reduced using immobilized TCEP (Thermo Scientific) and then biotinylated with EZ-Link Maleimide-PEG2-Biotin2 (Thermo Scientific). The final product was purified by reverse phase HPLC.

8.3.2 UV-Vis Melting Curves

UV melting curves were recorded at 260 nm in the temperature range of 10-95 °C for both cooling and heating modes, at the rate of 1 °C/min. Prior to the measurement of the melting profiles, solutions of 3 μM of each ssPNA in 1XTAE and different concentration of $MgCl_2$ were kept at 95 °C for 10 min before cooling down. T_m is the inflection point of a sigmoidal function used to fit the melting curve. DNA strands were purchased from Integrated DNA Technologies.

8.3.3 Nanostructure Assembly

All DNA strands were purchased from Integrated DNA Technologies. Origami samples were annealed from 90 to 20°C over two hours in TAE/Mg^{2+} (Tris, 40 mM; acetic acid, 20 mM; EDTA, 2 mM; and magnesium acetate, 12.5 mM; pH 8.0) with 5 nM M13 scaffold, 50 nM staple strand and 200 nM PNA or DNA control strands. Following

anneal the samples were spun filtered with Microcon 100,000 MWCO filter spin units at 4°C and subsequently kept on ice until prepped for AFM. TAE arrays were annealed with 200 nM of each strand from 90 to 20°C over 8 hours. Following anneal the sample was buffer exchanged into TAE buffer with 1 mM $MgCl_2$ at 4°C. PNA or DNA control oligo was then added to 200 nM and incubated for more than 2 hours. Then bought to 12.5 mM $MgCl_2$ before imaging with AFM.

8.3.4 AFM

Origami samples were mixed with 1-2 μM STV and incubated at room temperature for 1-2 hours. Then 5 μl sample was deposited on freshly cleaved mica. TAE array samples were put directly on freshly cleaved mica and then STV was added to a concentration of 1-2 μM. AFM images were obtained on a Digital Instruments Nanoscope III (Vecco, USA) using NP–S oxide-sharpened silicon nitride tips (Vecco, USA) with a multimode head and fluid cell in tapping mode under buffer.

8.3.5 Fluorescence

Fluorescence data were collected using a Cary Eclipse Fluorescence Spectrophotometer from Varian, with temperature controller set to 23°C. Excitation and emission wavelengths were 648 and 668 nm with a 5 nm bandwidth. Complementary DNA strands with fluorophore "Cy5" and quencher "Iowa Black RQ" were purchased from IDT and pre-annealed in TAE buffer with specified $MgCl_2$ concentration by incubating at 90 °C for 5 min and then cooling to room temperature. PNA was added and mixed

within a 10 sec period and data points were recorded every 0.1 sec and subsequently averaged with a three data point period. Fluorescence data was translated to concentration values by setting base level to 0 μM dissociated duplex and recording maximum fluorescence following thermal melting and annealing of duplex with PNA and taking this to correspond with full dissociation of DNA duplex. A 10 second period following mixing was used to fit a linear equation giving the initial rate of reaction. All rates were measured in triplicate and the average used to calculate the exponents in the rate equation.

Appendix A – Additional Micrographs

Supplemental Micrographs of NMuMG Cells Treated with Nanostructures and Controls

Below follows additional micrographs of cell treated with nano assemblies and controls. Top of each image is Smad2/3 stain, middle is DAPI stain and bottom is a merged image of the two preceeding.

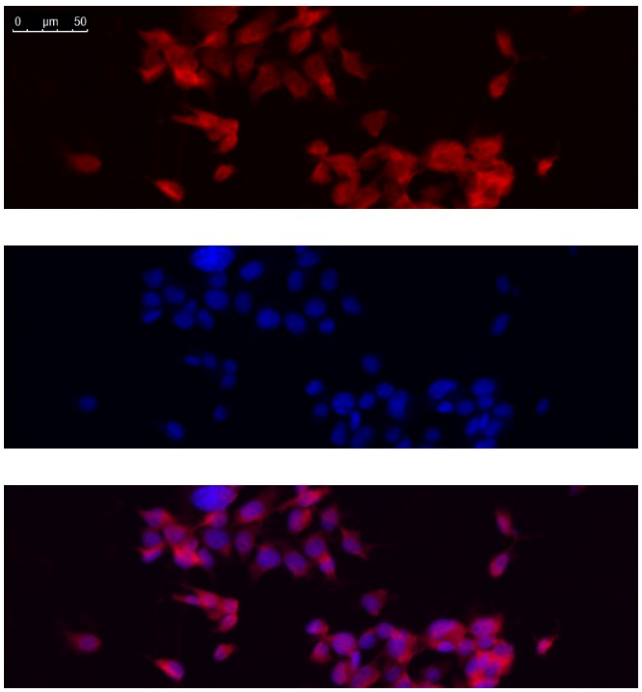

Figure 41 Control sample with background TGFβ level of 40 pM. Top: Smad3/4 stain. Middle: DAPI stain. Bottom: merged.

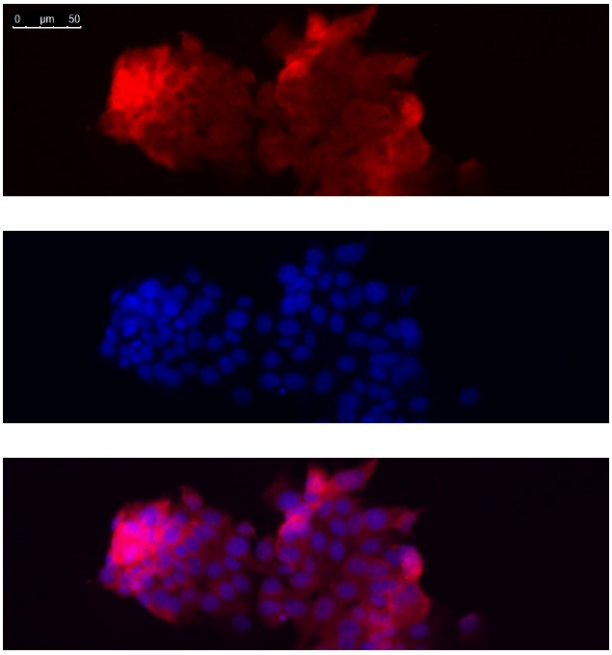

Figure 42 Control sample treated with 3 nM streptavidin and 12 nM peptide premixed and 40 pM TGFβ. Top: Smad3/4 stain. Middle: DAPI stain. Bottom: merged.

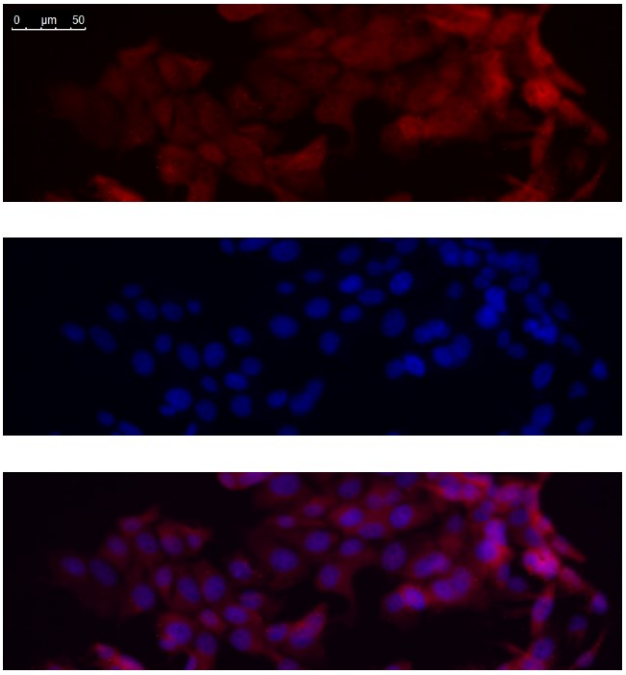

Figure 43 Control sample treated with 12 nM peptide and 40 pM TGFβ. Top: Smad3/4 stain. Middle: DAPI stain. Bottom: merged.

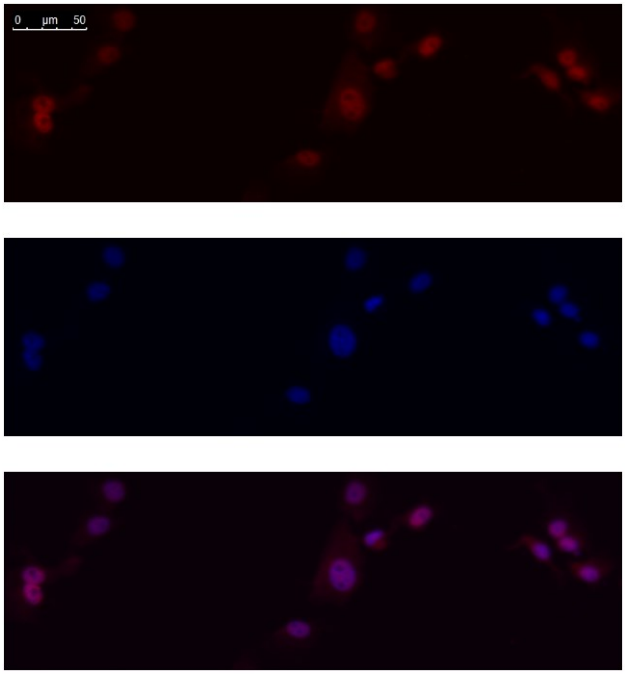

Figure 44 Sample treated with nano assembly and 40 pM TGFβ. Top: Smad3/4 stain. Middle: DAPI stain. Bottom: merged.

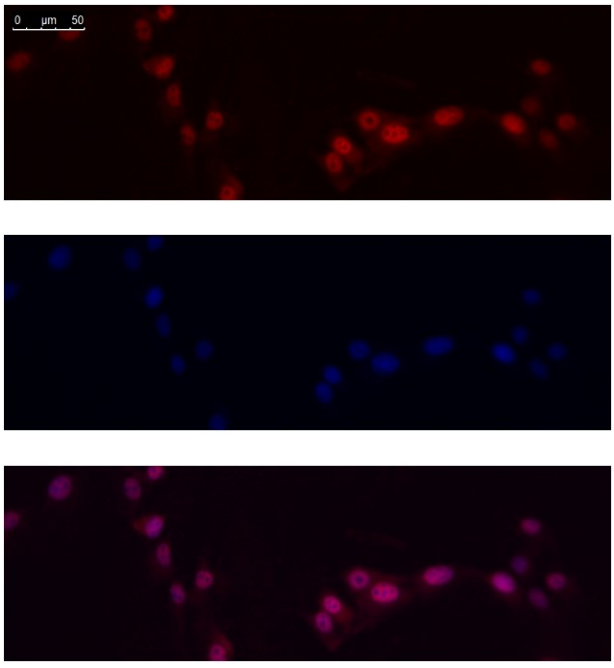

Figure 45 Positive control treated with 200 pM TGFβ. Top: Smad3/4 stain. Middle: DAPI stain. Bottom: merged.

AFM Micrographs of Biotinylated PNA Incorporated in Origami

Fully formed structures wholly in each micrograph were counted. Structures not fully formed were not counted and are marked with a yellow cross. Centre located streptavidin is marked with a red circle, side located with a blue circle and corner located with a green circle.

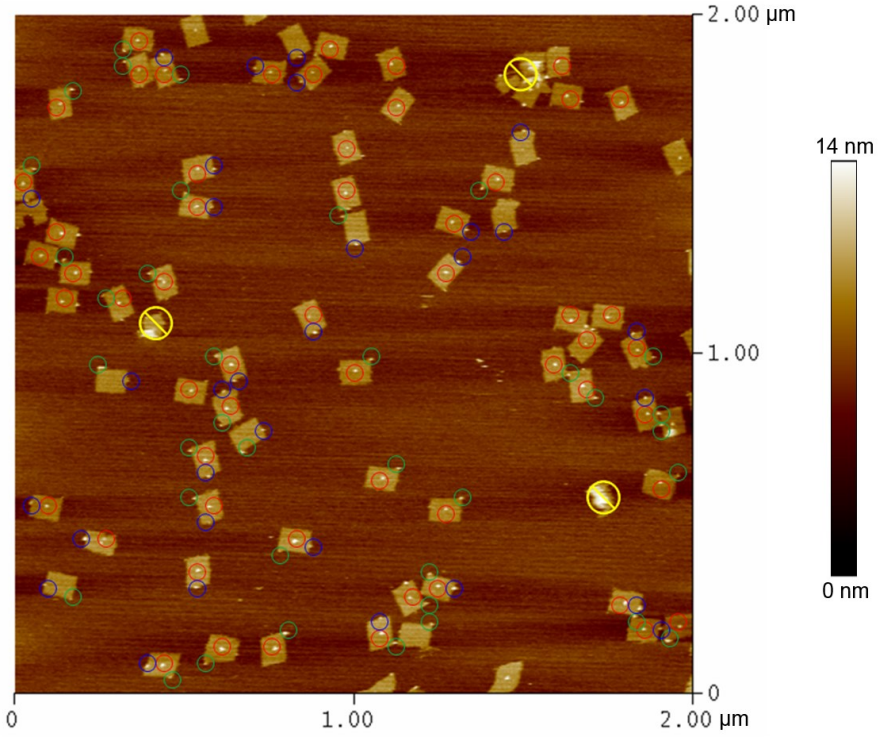

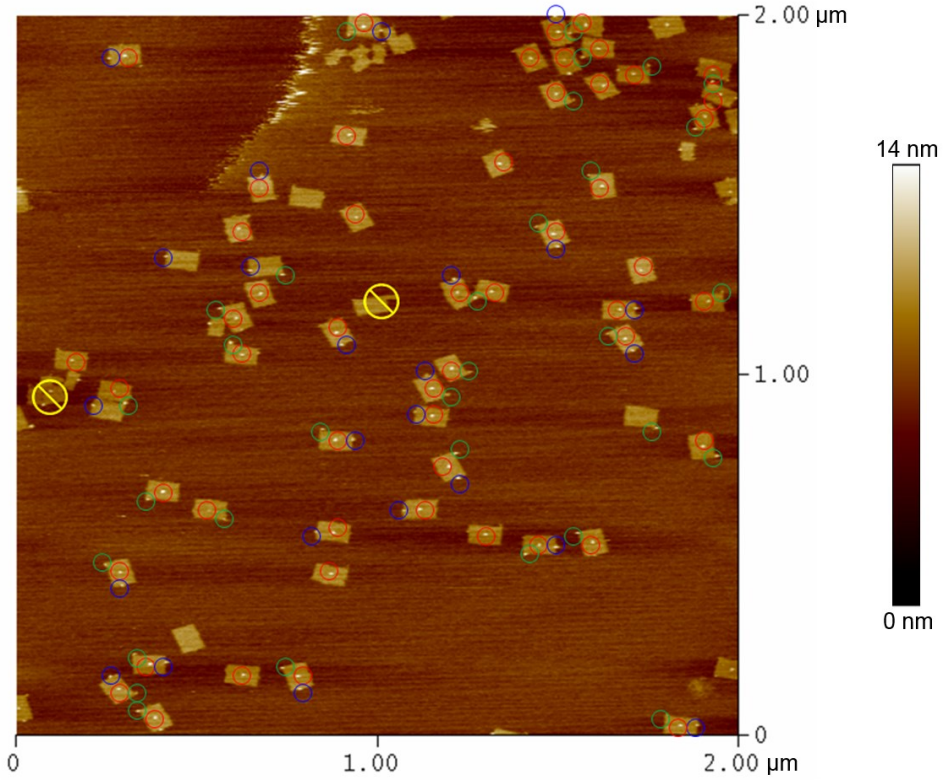
2.00 µm
1.00
0
0
1.00
2.00 µm
14 nm
0 nm

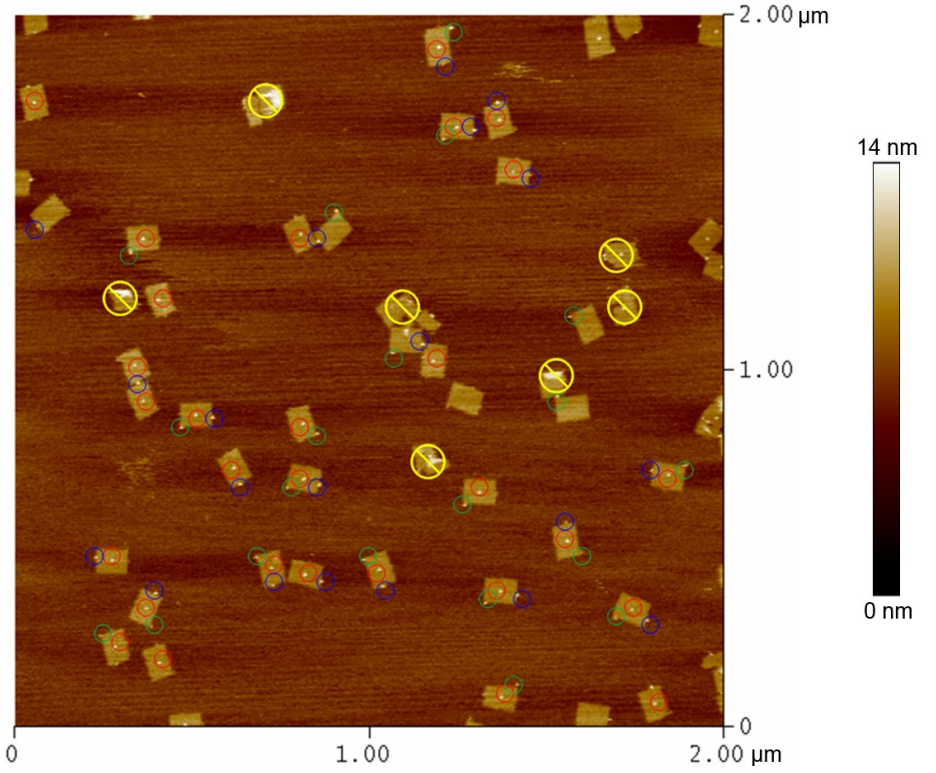
2.00 µm
1.00
0
0
1.00
2.00 µm
14 nm
0 nm

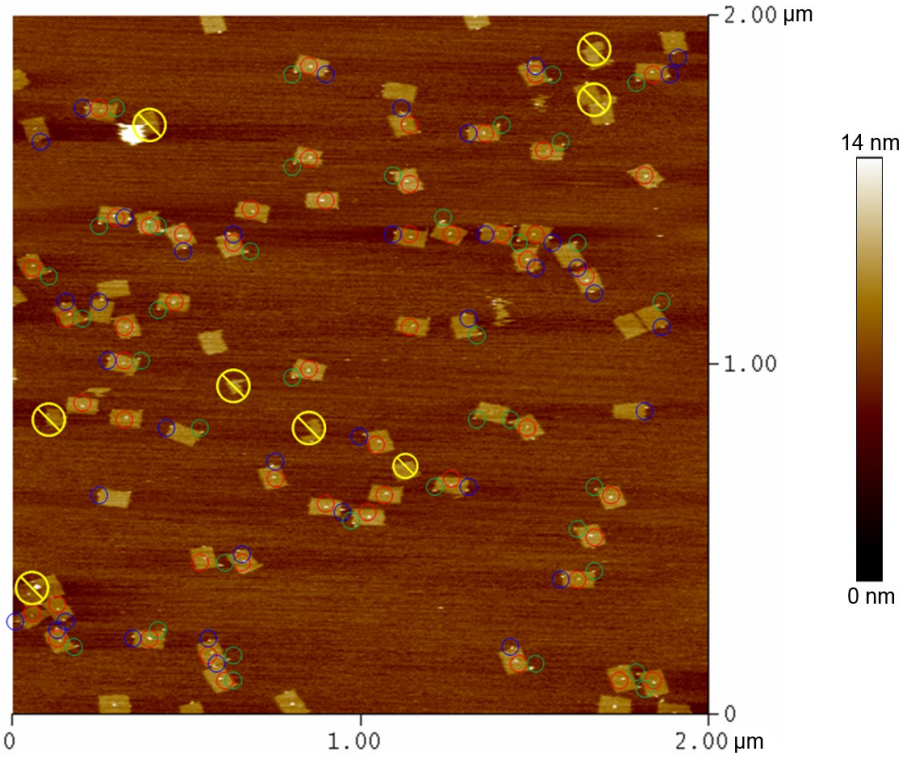
2.00 µm
1.00
0
0
1.00
2.00 µm
14 nm
0 nm

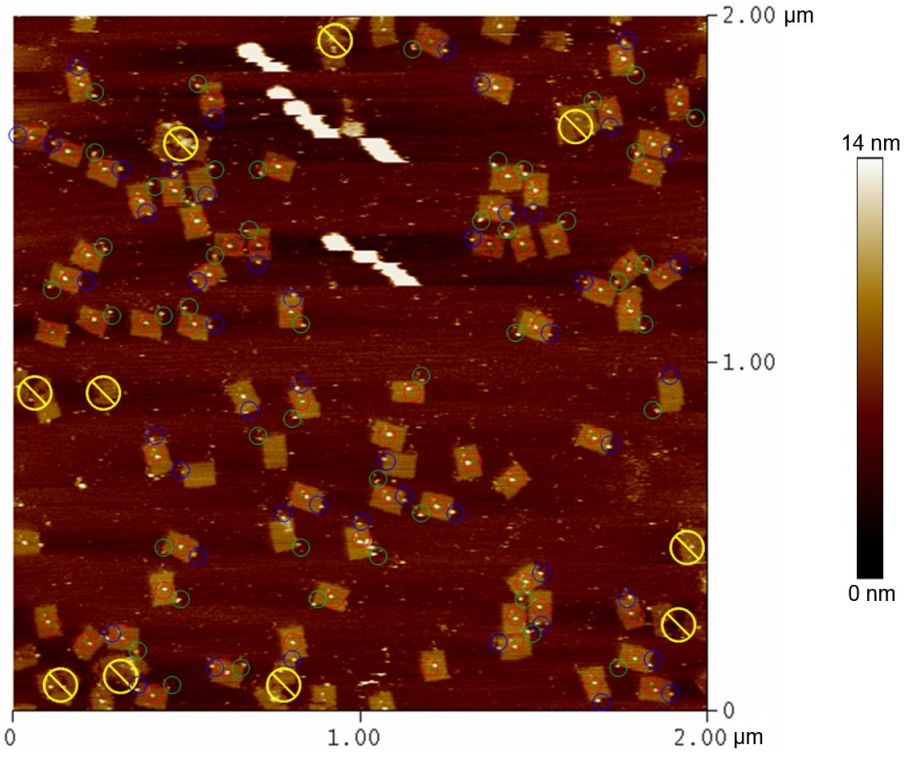
2.00 µm
1.00
0
0
1.00
2.00 µm
14 nm
0 nm

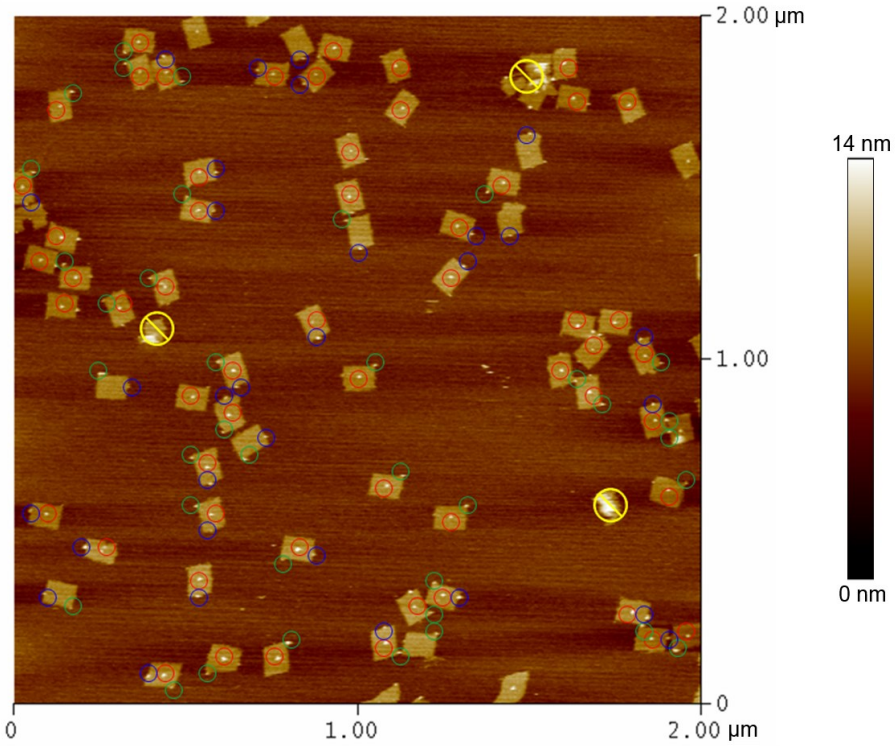
2.00 µm
1.00
0
0
1.00
2.00 µm
14 nm
0 nm

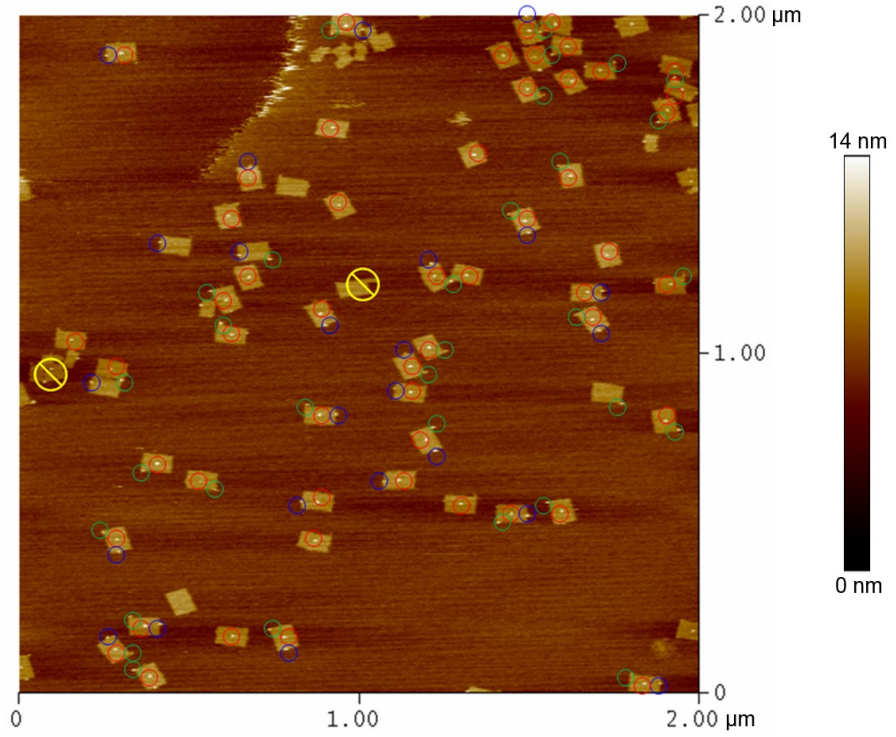
2.00 µm
1.00
0
0
1.00
2.00 µm
14 nm
0 nm

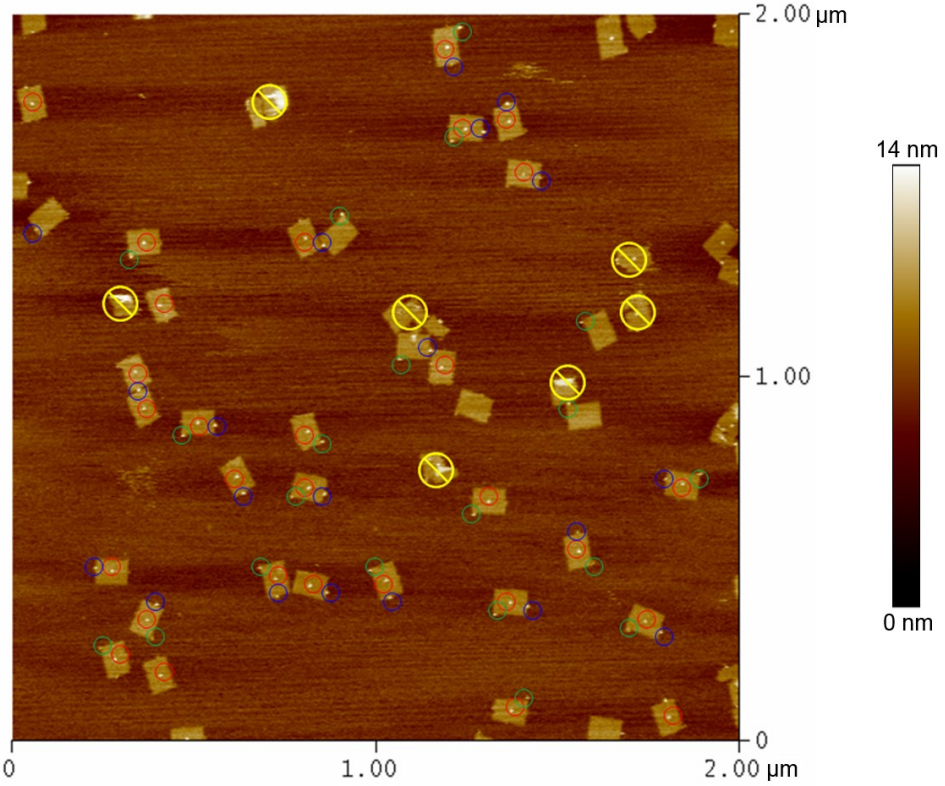
2.00 µm
1.00
0
0
1.00
2.00 µm
14 nm
0 nm

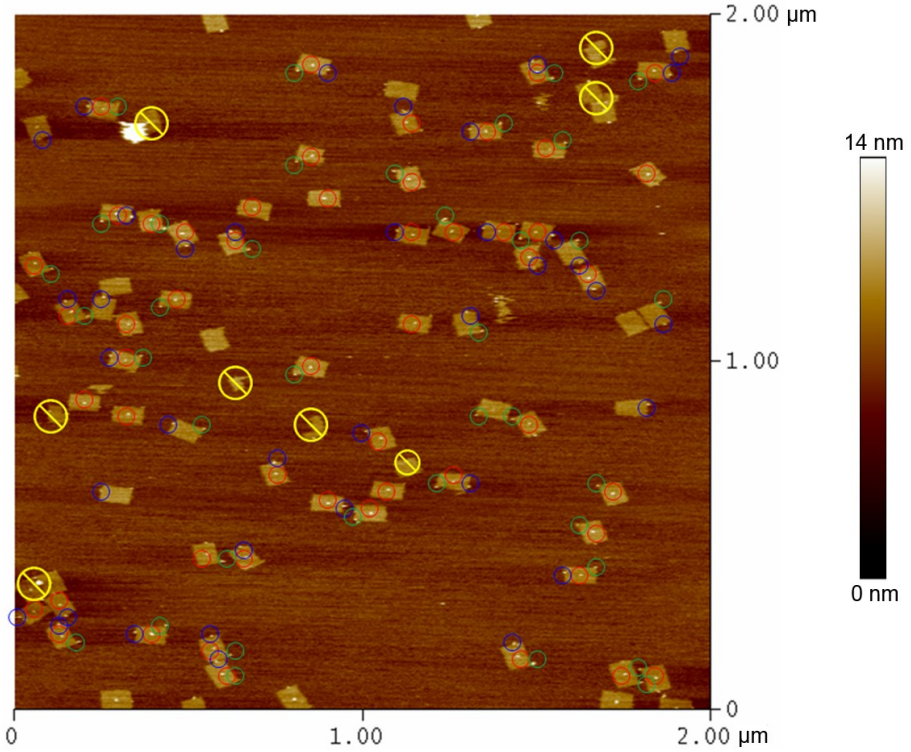
2.00 µm
1.00
0
0
1.00
2.00 µm
14 nm
0 nm

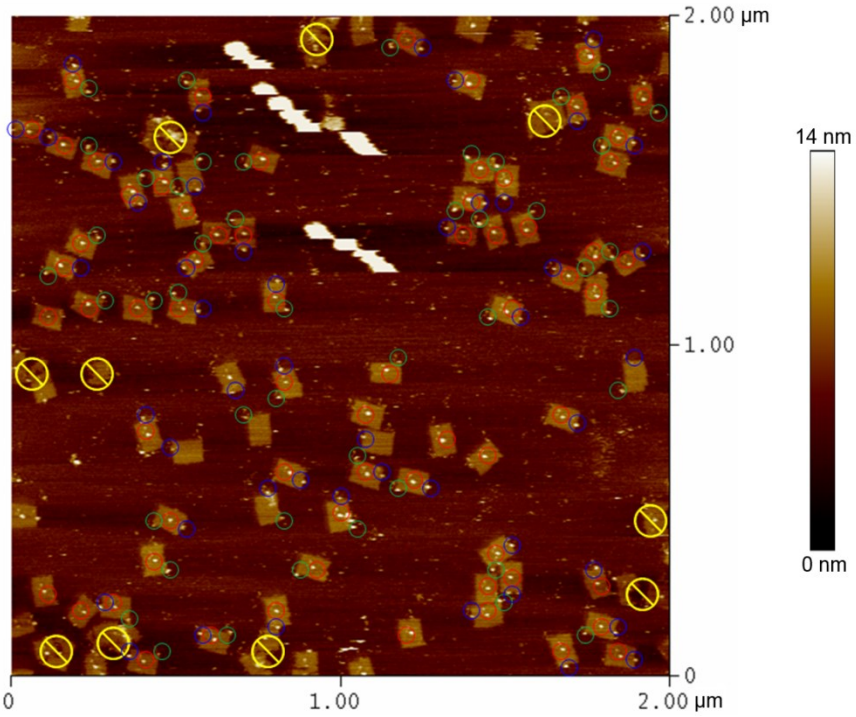
2.00 µm
1.00
0
0
1.00
2.00 µm
14 nm
0 nm

AFM Micrographs of Biotinylated DNA control Incorporated in Origami

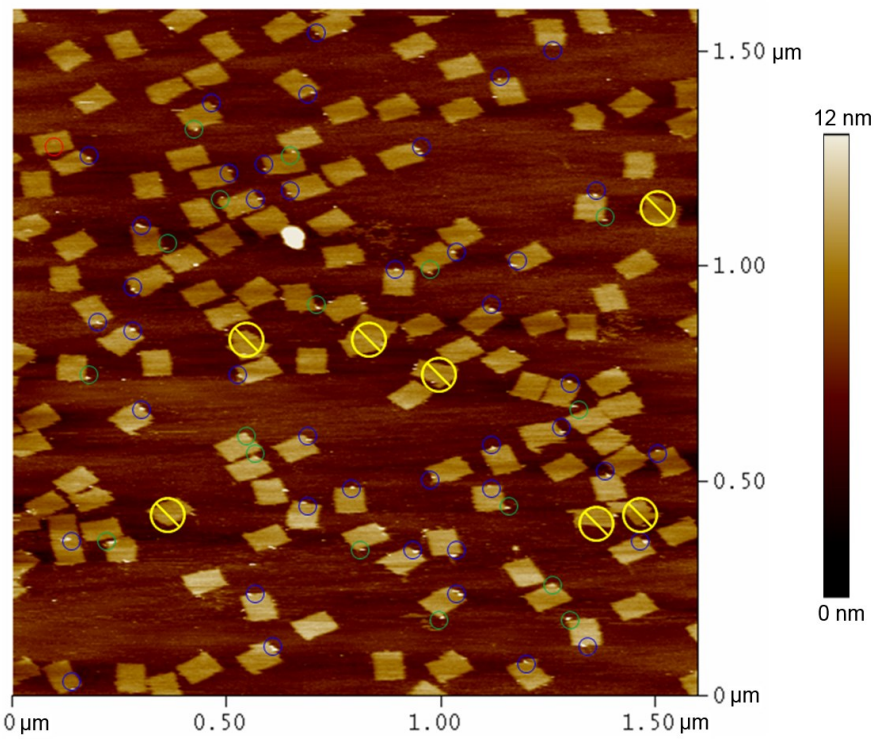

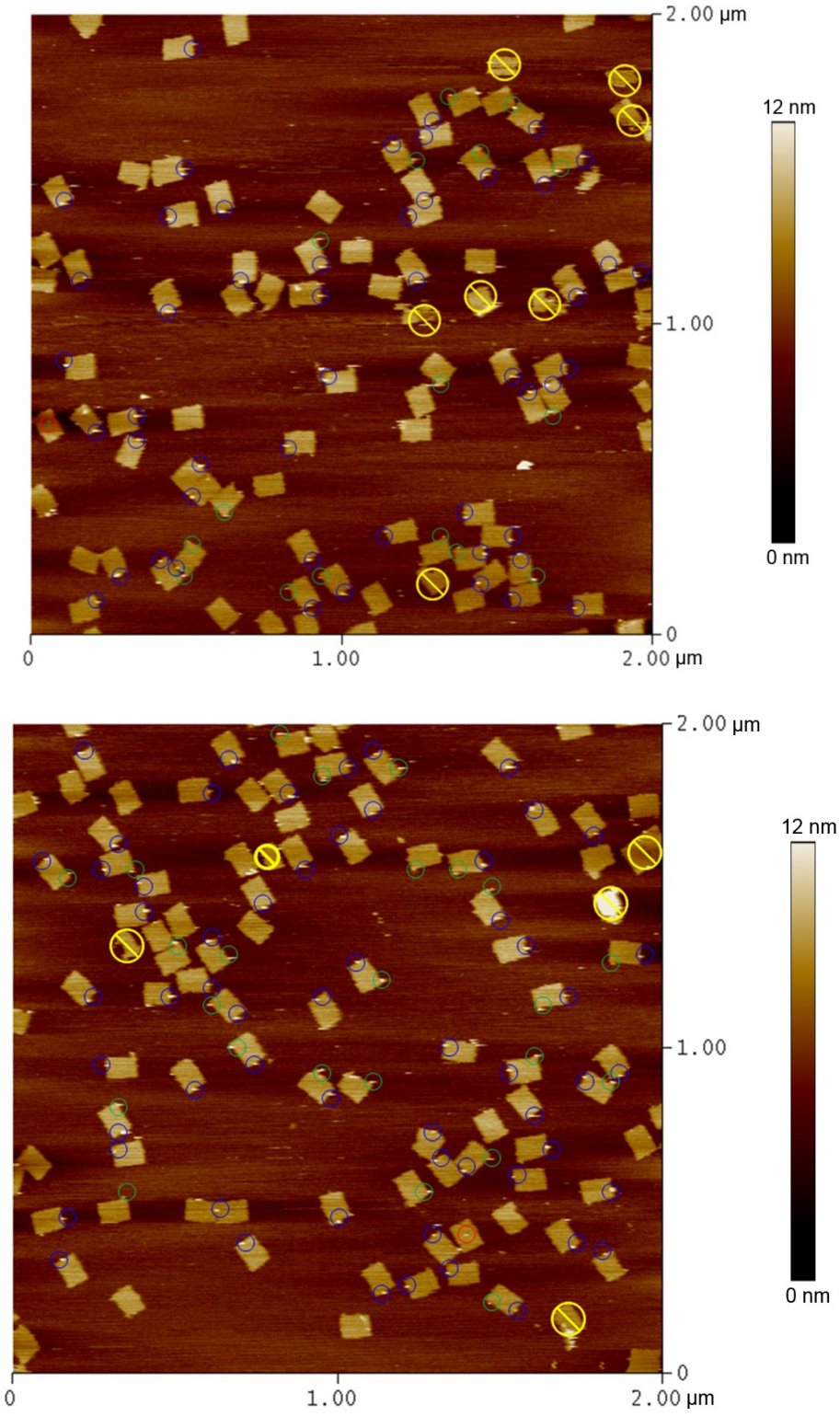
2.00 µm
1.00
0
0
1.00
2.00 µm
12 nm
0 nm
2.00 µm
1.00
0
0
1.00
2.00 µm
12 nm
0 nm

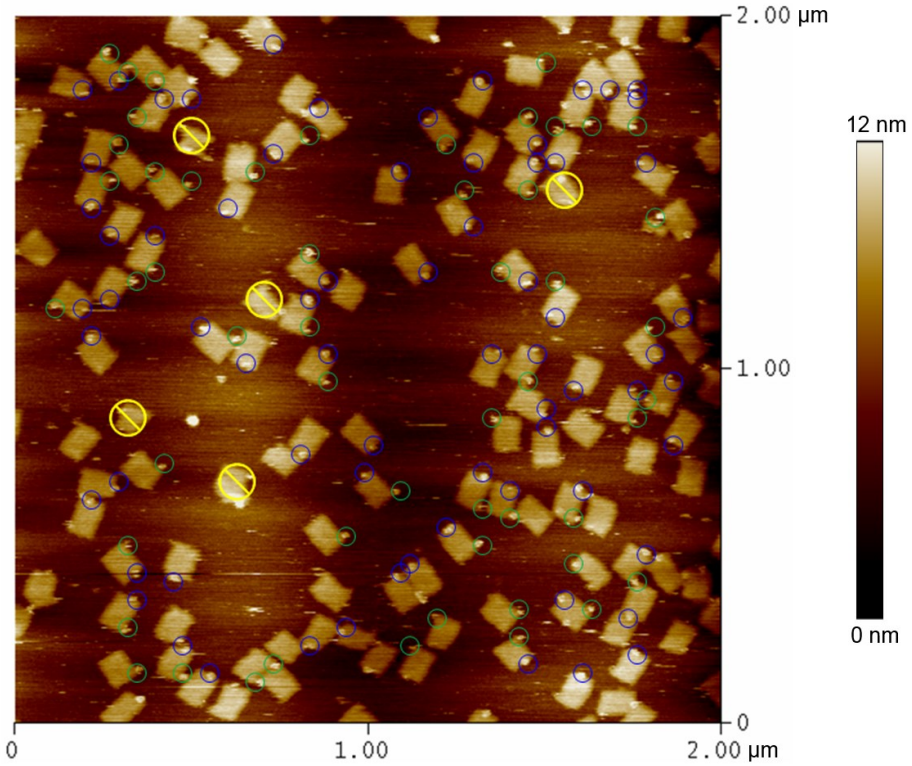
2.00 µm
1.00
0
0
1.00
2.00 µm
12 nm
0 nm

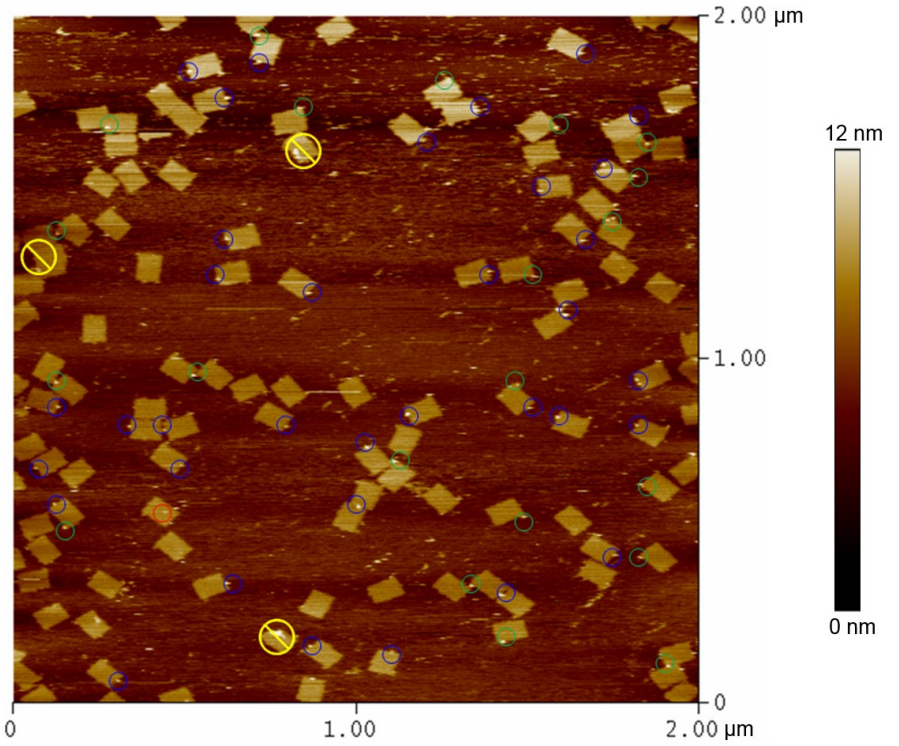
2.00 µm
1.00
0
0
1.00
2.00 µm
12 nm
0 nm

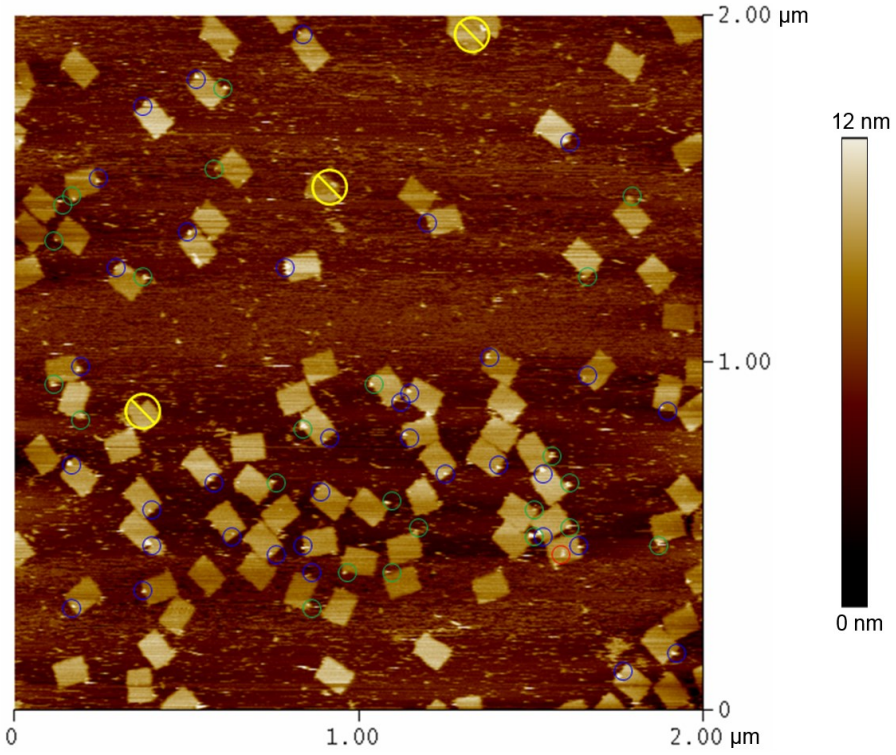
2.00 µm
1.00
0
0
1.00
2.00 µm
12 nm
0 nm

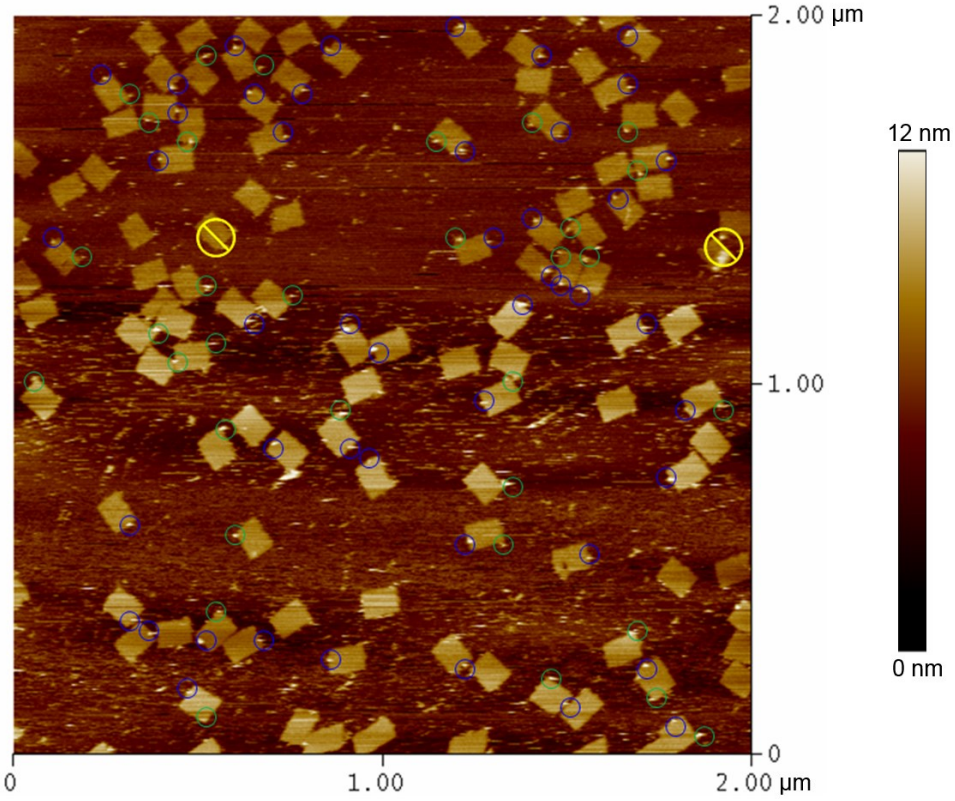
2.00 µm
1.00
0
0
1.00
2.00 µm
12 nm
0 nm

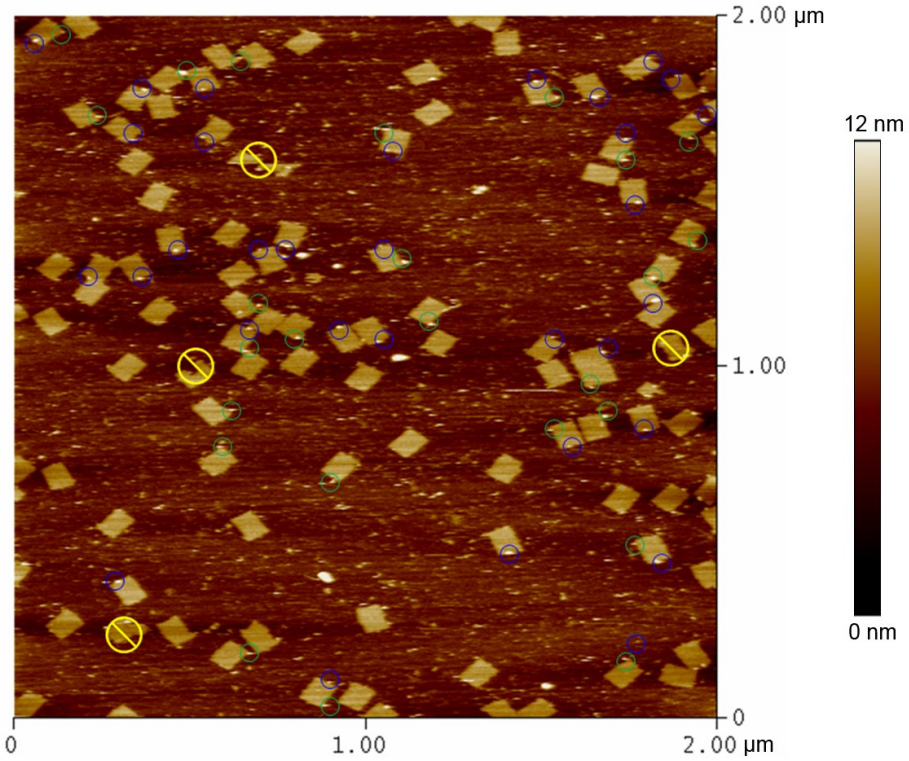
2.00 µm
1.00
0
0
1.00
2.00 µm
12 nm
0 nm

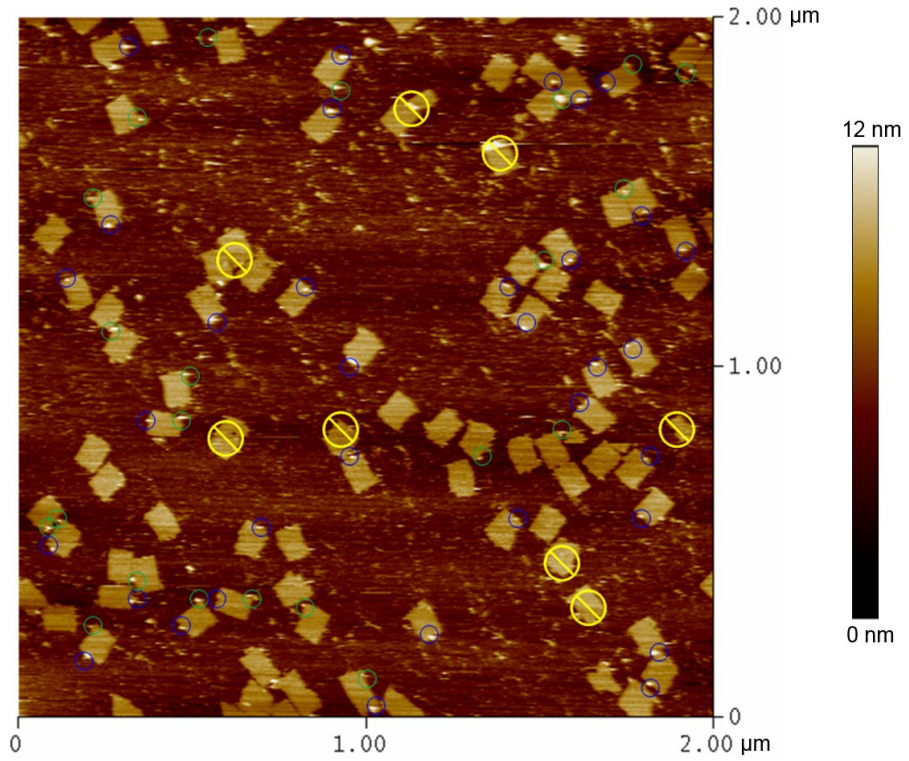
2.00 µm
1.00
0
0
1.00
2.00 µm
12 nm
0 nm

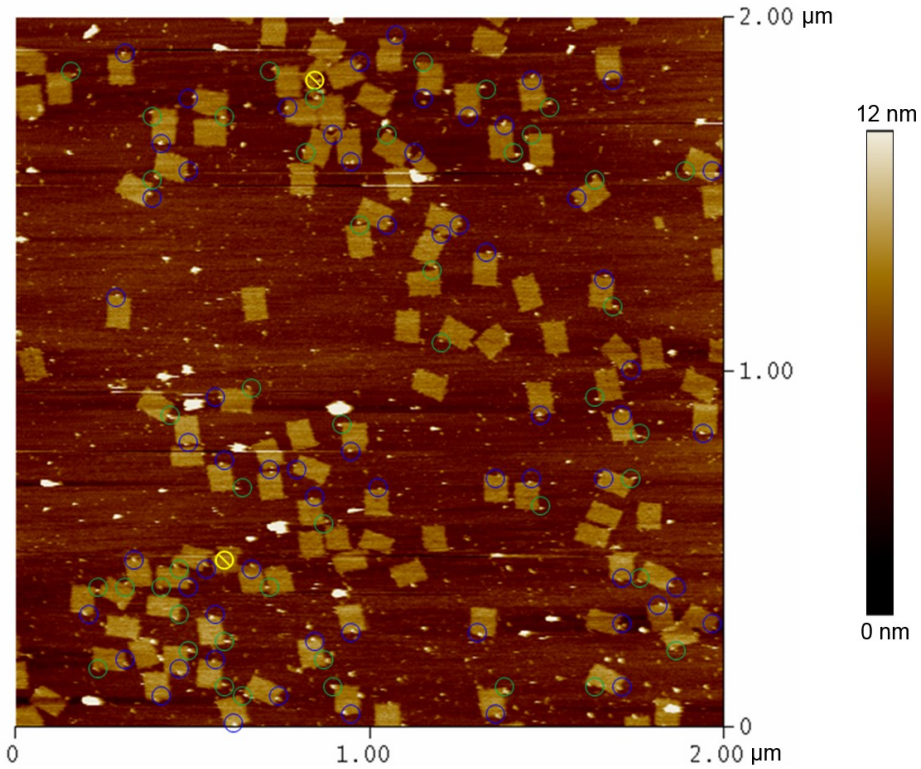

Appendix B – DNA Sequences

TGF-β Origami Sequences

Strands t-1r14f, t-1r16f, t-1r18f, t-1r20f, t-1r14e, t1r14f, t-1r16e, t1r16f, t-1r18e, t1r18f, t-1r20e and t1r20f from the tall rectangle was substituted with the following strands:

A_CR: biotin-TT AA AGC GAA AGT TTC AT TCC ATA TAT TTA GTT T

B_CR: biotin-TT GA CCA TTA AGC ATA AAGCT AAA TCC TTT TGC G

C_CR: biotin-TT GG AGA AGC CCG GAG AG GGT AGC TAT TGC CTG A

AS1: AAG AGG AAC GAG CTT C

AS2: GA GTC TGG TTA AAT CA

D_CR: biotin-TT GA CTT CAA CAA GAA CG- GGT ATT AAT CTT TCC T

E_CR: biotin-TT TT CCC AAT ATT TAG GC-AGA GGC ATA CAA CGC C

F_CR: biotin-TT CA AAA ACA CAA ATA TA-TTT TAG TTC GCG AGA A

G_CR: biotin-TT AG ATC TAC CCT TGC TT-CTG TAA ATA TAT GTG A

AS3: GT GAA TAA AAA GGC TA-TCA GGT CAT TTT TGA G

H_CR: biotin-TT TA TCA TTC ATA TCG CG-TTT TAA TTG CCC GAA A

I_CR: biotin-TT AA CAT GTA TCT GCG AA-CGA GTA GAA CAG TTG A

J_CR: biotin-TT AA CTT TTT TTA TGA CC-CTG TAA TAG GTT GTA C

Zinc Finger DNA Sequences

TX Tile Sequences

Strand 1:

GCAGACCGTAGAATCGCCTGCTCTGTATGTCACTGCGGCTCCGGCCCCAGTTT

TCTGGGGCCGGAGCCGCAGTGACTTTGCCGAACTGG-ACACTTACCTCTA

Strand 2:

ACGACTAATCCGTCTTGTGGCGATTCTACGG

Strand 3:

ATGTCGCACCAGTTCGGCAATACAGAGCACCAGTGGCATTCGGAGAT

Strand 4:

TCTGCTAGAGGTAAGTGTGGAGTGGAACAAGTAACCGCAACGCACCAAGGCT

Strand5:

GTCGTTATCGTGGACTCCTGCGACATAGCCTTGGACTGGACAAGACGGATTA

Strand 6:

GGCTTACAATGAACGGCACCACGATA

Strand 7:

AAGCCATCTCCGAATGCCTGCGTTGCGGTTGGGAGCCGGAGCCGGAGTCAGT

TTTCTGACTCCGGCTCCGGCTCCCATTTACTTGTTCC-TGCCGTTCATTGTA

Origami Sequence

The staple strand t-5r2f is substituted with the two strands below:

5′ t-5r2f:

TGAGTTTCAAAGGAACTTTTGGCCACTGCGGCTCCGGCCCCGAGTTTTCTCGGG

GCCGGAGCCGCAGTGGCC

3` t-5r2f:

AACTAAAGATCTCCAA

PNA DNA sequences

Origami Strands

Centre strands t-1r16e and t1r16f were substituted with

PNA_E_CR_V: TCAACCCT - TT CCC AAT ATT TAG GC-AGA GGC ATA CAA CGC C

PNA_I_CR_V: AA CAT GTA TCT GCG AA-CGA GTA GAA CAG TTG A TACTTATA

Corner strand t7r29f was substituted with

PNA_7: CTA CAT TTT GAC GCT CAC GCT CAT GGA AAT AC TTT

TACTTATATCAACCCT

For the side position on the M13 scaffold the staple stran; t1r0g was left out

References

1. Drexler, K. E. (1981) Molecular engineering: An approach to the development of general capabilities for molecular manipulation., *Proceedings of the National Academy of Sciences of the United States of America 78*, 5275-5278.

2. Seeman, N. C., and Belcher, A. M. (2002) Emulating biology: Building nanostructures from the bottom up, *Proceedings of the National Academy of Sciences of the United States of America 99*, 6451-6455.

3. Mittal, A., and Acharya, C. (2013) Protein folding: is it simply surface to volume minimization?, *Journal of Biomolecular Structure & Dynamics 31*, 953-955.

4. Watson, J. D., and Crick, F. H. (1953) Molecular structure of nucleic acids; a structure for deoxyribose nucleic acid., *Nature 171*, 737-738.

5. Baker, B., Mahmoudabadi, G., and Milam, V. T. (2013) Strand displacement in DNA-based materials systems, *Soft Matter 9*, 11160.

6. Tobin, J. *To Conquer the Air: The Wright Brothers and the Great Race for Flight;* Free Press: New York, 2004.

7. Crick, F. (1970) Central dogma of molecular biology, *Nature 227*, 561-563.

8. Woese, C. R., Kandlert, O., and Wheelis, M. L. (1990) Towards a natural system of organisms : Proposal for the domains, *Proceedings of the National Academy of Sciences of the United States of America 87*, 4576-4579.

9. Sapp, J., Bacteria, S., and Stanier, R. Y. (2006) Two faces of the prokaryote concept, *International Microbiology 9*, 163-172.

10. Lessard, J. C. (2013) Molecular cloning., *Methods in Enzymology 529*, 85-98.

11. Bourniquel, A., and Bickle, T. (2002) Complex restriction enzymes: NTP-driven molecular motors., *Biochimie 84*, 1047-1059.

12. O'Neill, P., Rothemund, P. W. K., Kumar, A., and Fygenson, D. K. (2006) Sturdier DNA nanotubes via ligation., *Nano Letters 6*, 1379-1383.

13. Pellicer, J., Fay, M. F., and Leitch, I. J. (2010) The largest eukaryotic genome of them all?, *Botanical Journal of the Linnean Society 164*, 10-15.

14. Derelle, E., Ferraz, C., Rombauts, S., Rouzé, P., Worden, A. Z., Robbens, S., Partensky, F., Degroeve, S., Echeynié, S., Cooke, R., Saeys, Y., Wuyts, J., Jabbari, K., Bowler, C., Panaud,

O., Piégu, B., Ball, S. G., Ral, J.-P., Bouget, F.-Y., Piganeau, G., De Baets, B., Picard, A., Delseny, M., Demaille, J., Van de Peer, Y., and Moreau, H. (2006) Genome analysis of the smallest free-living eukaryote Ostreococcus tauri unveils many unique features., *Proceedings of the National Academy of Sciences of the United States of America 103*, 11647-11652.

15. Zentner, G. E., and Henikoff, S. (2013) Regulation of nucleosome dynamics by histone modifications., *Nature Structural & Molecular Biology 20*, 259-266.

16. Tammen, S. a., Friso, S., and Choi, S.-W. (2013) Epigenetics: the link between nature and nurture., *Molecular Aspects of Medicine 34*, 753-764.

17. Cunningham, E. L., and Berger, J. M. (2005) Unraveling the early steps of prokaryotic replication., *Current Opinion in Structural Biology 15*, 68-76.

18. Vos, S. M., Tretter, E. M., Schmidt, B. H., and Berger, J. M. (2011) All tangled up: how cells direct, manage and exploit topoisomerase function., *Nature Reviews. Molecular Cell Biology 12*, 827-841.

19. Balakrishnan, L., and Bambara, R. (2013) Okazaki fragment metabolism., *Cold Spring Harbor Perspectives in Biology 5*.

20. Sahu, S., LaBean, T. H., and Reif, J. H. (2008) A DNA Nanotransport Device Powered by Polymerase φ29, *Nano Letters 8*, 3870-3878.

21. Erlich, H. A., Gelfand, D., and Sninsky, J. J. (1991) Recent Advances in the Polymerase Chain Reaction, *Science 252*, 1643-1651.

22. Jin, D. J., Cagliero, C., and Zhou, Y. N. (2013) Role of RNA polymerase and transcription in the organization of the bacterial nucleoid., *Chemical Reviews 113*, 8662-8682.

23. Robinson, A., and van Oijen, A. M. (2013) Bacterial replication, transcription and translation: mechanistic insights from single-molecule biochemical studies., *Nature reviews. Microbiology 11*, 303-315.

24. Schmeing, T. M., and Ramakrishnan, V. (2009) What recent ribosome structures have revealed about the mechanism of translation., *Nature 461*, 1234-1242.

25. Liao, S., and Seeman, N. C. (2004) Translation of DNA signals into polymer assembly instructions., *Science (New York, N.Y.) 306*, 2072-2074.

26. Krejci, L., Altmannova, V., Spirek, M., and Zhao, X. (2012) Homologous recombination and its regulation., *Nucleic Acids Research 40*, 5795-5818.

27. West, Y. L. a. S. C. (2004) Happy Hollidays: 40th anniversary of the Holliday junction, *Nature Reviews. Molecular Cell Biology 5*, 937-944.

28. Seeman, N. (1982) Nucleic acid junctions and lattices, *Journal of Theoretical Biology 99*, 237-247.

29. Kallenbach, N. R., Ma, R.-I., and Seeman, N. C. (1983) An immobile nucleic acid junction constructed from oligonucleotides, *Nature 305*, 829-831.

30. Wang, Y., Mueller, J. E., Kemper, B., and Seeman, N. C. (1991) Assembly and characterization of five-arm and six-arm DNA branched junctions, *Biochemistry 30*, 5667-5674.

31. Wang, X., and Seeman, N. C. (2007) Assembly and Characterization of 8-Arm and 12-Arm DNA Branched Junctions, *Journal of the American Chemical Society 129*, 8169-8176.

32. Fu, T. J., and Seeman, N. C. (1993) DNA double-crossover molecules, *Biochemistry 32*, 3211-3220.

33. Mao, C., Sun, W., Shen, Z., and Seeman, N. C. (1999) A nanomechanical device based on the B-Z transition of DNA., *Nature 397*, 144-146.

34. Winfree, E., Liu, F., Wenzler, L. A., and Seeman, N. C. (1998) Design and self-assembly of two-dimensional DNA crystals, *Nature 394*, 539-544.

35. Yan, H., Park, S. H. H., Finkelstein, G., Reif, J. H., LaBean, T. H., and Ha, S. (2003) DNA-Templated Self-Assembly of Protein Arrays and Highly Conductive Nanowires, *Science 301*, 1882-1884.

36. Park, S. H., Pistol, C., Ahn, S. J., Reif, J. H., Lebeck, A. R., Dwyer, C., and LaBean, T. H. (2006) Finite-size, fully addressable DNA tile lattices formed by hierarchical assembly procedures., *Angewandte Chemie (International ed. in English) 45*, 735-739.

37. Rothemund, P. W. K. (2006) Folding DNA to create nanoscale shapes and patterns, *Nature 440*, 297-302.

38. Samano, E. C., Pilo-Pais, M., Goldberg, S., Vogen, B. N., Finkelstein, G., and LaBean, T. H. (2011) Self-assembling DNA templates for programmed artificial biomineralization, *Soft Matter 7*, 3240-3245.

39. Ke, Y., Douglas, S. M., Liu, M., Sharma, J., Cheng, A., Leung, A., Liu, Y., Shih, W. M., and Yan, H. (2009) Multilayer DNA Origami Packed on a Square Lattice, *Journal of the American Chemical Society 131*, 15903-15908.

40. Douglas, S. M., Marblestone, A. H., Teerapittayanon, S., Vazquez, A., Church, G. M., and Shih, W. M. (2009) Rapid prototyping of 3D DNA-origami shapes with caDNAno., *Nucleic Acids Research 37*, 5001-5006.

41. Douglas, S. M., Dietz, H., Liedl, T., Hogberg, B., Graf, F., and Shih, W. M. (2009) Self-assembly of DNA into nanoscale three-dimensional shapes, *Nature 459*, 414-418.

42. Han, D., Pal, S., Nangreave, J., Deng, Z., Liu, Y., and Yan, H. (2011) DNA Origami with Complex Curvatures in Three-Dimensional Space, *Science 332*, 342-346.

43. de Larco, J. E., and Todaro, G. J. (1978) Growth factors from murine sarcoma virus-transformed cells, *Proceedings of the National Academy of Sciences 75*, 4001-4005.

44. Roberts, A. B., Lamb, L. C., Newton, D. L., Sporn, M. B., De Larco, J. E., and Todaro, G. J. (1980) Transforming growth factors: Isolation of polypeptides from virally and chemically transformed cells by acid/ethanol extraction, *Proceedings of the National Academy of Sciences 77*, 3494-3498.

45. Todaro, G. J., Fryling, C., and De Larco, J. E. (1980) Transforming growth factors produced by certain human tumor cells: polypeptides that interact with epidermal growth factor receptors., *Proceedings of the National Academy of Sciences 77*, 5258-5262.

46. Roberts, A. B., Anzano, M. A., Lamb, L. C., Smith, J. M., and Sporn, M. B. (1981) New class of transforming growth factors potentiated by epidermal growth factor: isolation from non-neoplastic tissues., *Proceedings of the National Academy of Sciences 78*, 5339-5343.

47. De Crescenzo, G., Hinck, C. S., Shu, Z., Zúñiga, J., Yang, J., Tang, Y., Baardsnes, J., Mendoza, V., Sun, L., López-Casillas, F., O'Connor-McCourt, M., and Hinck, A. P. (2006) Three key residues underlie the differential affinity of the TGFbeta isoforms for the TGFbeta type II receptor., *Journal of Molecular Biology 355*, 47-62.

48. Baardsnes, J., Hinck, C. S., Hinck, A. P., and O'Connor-McCourt, M. D. (2009) TbetaR-II discriminates the high- and low-affinity TGF-beta isoforms via two hydrogen-bonded ion pairs., *Biochemistry 48*, 2146-2155.

49. Zúñiga, J. E., Groppe, J. C., Cui, Y., Hinck, C. S., Contreras-Shannon, V., Pakhomova, O. N., Yang, J., Tang, Y., Mendoza, V., López-Casillas, F., Sun, L., and Hinck, A. P. (2005) Assembly of TbetaRI:TbetaRII:TGFbeta ternary complex in vitro with receptor extracellular domains is cooperative and isoform-dependent., *Journal of Molecular Biology 354*, 1052-1068.

50. Radaev, S., Zou, Z., Huang, T., Lafer, E. M., Hinck, A. P., and Sun, P. D. (2010) Ternary complex of transforming growth factor-beta1 reveals isoform-specific ligand recognition

and receptor recruitment in the superfamily., *The Journal of Biological Chemistry 285*, 14806-14814.

51. Massagué, J., Seoane, J., and Wotton, D. (2005) Smad transcription factors., *Genes & Development 19*, 2783-2810.

52. Wrana, J. l., Attisano, L., Wieser, R., Ventura, F., and Massague, J. (1994) Mechanism of activation of the TGF-β receptor, *Nature 370*, 341-347.

53. Huse, M., Muir, T. W., Xu, L., Chen, Y. G., Kuriyan, J., and Massagué, J. (2001) The TGF beta receptor activation process: an inhibitor- to substrate-binding switch., *Molecular Cell 8*, 671-682.

54. Wu, G. (2000) Structural Basis of Smad2 Recognition by the Smad Anchor for Receptor Activation, *Science 287*, 92-97.

55. Tsukazaki, T., Chiang, T. a., Davison, a. F., Attisano, L., and Wrana, J. L. (1998) SARA, a FYVE domain protein that recruits Smad2 to the TGFbeta receptor., *Cell 95*, 779-791.

56. Chacko, B. M., Qin, B. Y., Tiwari, A., Shi, G., Lam, S., Hayward, L. J., De Caestecker, M., and Lin, K. (2004) Structural basis of heteromeric smad protein assembly in TGF-beta signaling., *Molecular Cell 15*, 813-823.

57. Inman, G. J., and Hill, C. S. (2002) Stoichiometry of active smad-transcription factor complexes on DNA., *The Journal of Biological Chemistry 277*, 51008-51016.

58. Jayaraman, L., and Massague, J. (2000) Distinct oligomeric states of SMAD proteins in the transforming growth factor-beta pathway., *The Journal of Biological Chemistry 275*, 40710-40717.

59. Inman, G. J., Nicolás, F. J., and Hill, C. S. (2002) Nucleocytoplasmic shuttling of Smads 2, 3, and 4 permits sensing of TGF-beta receptor activity., *Molecular Cell 10*, 283-294.

60. Aitchison, J. D., and Rout, M. P. (2012) The yeast nuclear pore complex and transport through it., *Genetics 190*, 855-883.

61. Hill, C. S. (2009) Nucleocytoplasmic shuttling of Smad proteins., *Cell Research 19*, 36-46.

62. Watanabe, M., Masuyama, N., Fukuda, M., and Nishida, E. (2000) Regulation of intracellular dynamics of Smad4 by its leucine-rich nuclear export signal., *EMBO Reports 1*, 176-182.

63. Sirard, C. (2000) Targeted Disruption in Murine Cells Reveals Variable Requirement for Smad4 in Transforming Growth Factor beta -related Signaling, *Journal of Biological Chemistry 275*, 2063-2070.

64. BabuRajendran, N., Palasingam, P., Narasimhan, K., Sun, W., Prabhakar, S., Jauch, R., and Kolatkar, P. R. (2010) Structure of Smad1 MH1/DNA complex reveals distinctive rearrangements of BMP and TGF-beta effectors., *Nucleic Acids Research 38*, 3477-3488.

65. Shi, Y., Wang, Y. F., Jayaraman, L., Yang, H., Massagué, J., and Pavletich, N. P. (1998) Crystal structure of a Smad MH1 domain bound to DNA: insights on DNA binding in TGF-beta signaling., *Cell 94*, 585-594.

66. Chai, J., Wu, J.-W., Yan, N., Massagué, J., Pavletich, N. P., and Shi, Y. (2003) Features of a Smad3 MH1-DNA complex. Roles of water and zinc in DNA binding., *The Journal of Biological Chemistry 278*, 20327-20331.

67. Mullen, A. C., Orlando, D. a., Newman, J. J., Lovén, J., Kumar, R. M., Bilodeau, S., Reddy, J., Guenther, M. G., DeKoter, R. P., and Young, R. a. (2011) Master transcription factors determine cell-type-specific responses to TGF-β signaling., *Cell 147*, 565-576.

68. Massagué, J. (2012) TGFβ signalling in context., *Nature Reviews. Molecular Cell Biology 13*, 616-630.

69. Derynck, R., and Zhang, Y. E. (2003) Smad-dependent and Smad-independent pathways in TGF-β family signaling, *Nature 425*, 577-584.

70. Choi, M. E., Ding, Y., and Kim, S. I. (2012) TGF-β signaling via TAK1 pathway: role in kidney fibrosis., *Seminars in Nephrology 32*, 244-252.

71. Groppe, J., Hinck, C. S., Samavarchi-Tehrani, P., Zubieta, C., Schuermann, J. P., Taylor, A. B., Schwarz, P. M., Wrana, J. L., and Hinck, A. P. (2008) Cooperative assembly of TGF-beta superfamily signaling complexes is mediated by two disparate mechanisms and distinct modes of receptor binding., *Molecular Cell 29*, 157-168.

72. Seeman, N. C. (2010) Nanomaterials based on DNA., *Annual Review of Biochemistry 79*, 65-87.

73. Linko, V., and Dietz, H. (2013) The enabled state of DNA nanotechnology., *Current Opinion in Biotechnology*, 1-7.

74. Li, H. Y., Carter, J. D., and LaBean, T. H. (2009) Nanofabrication by DNA self-assembly, *Materials Today 12*, 24-32.

75. Rajendran, A., Endo, M., and Sugiyama, H. (2012) Single-molecule analysis using DNA origami., *Angewandte Chemie (International ed. in English) 51*, 874-890.

76. Saaem, I., and LaBean, T. H. (2013) Overview of DNA origami for molecular self-assembly., *Wiley Interdisciplinary Reviews. Nanomedicine and Nanobiotechnology 5*, 150-162.

77. Mei, Q., Wei, X., Su, F., Liu, Y., Youngbull, C., Johnson, R., Lindsay, S., Yan, H., and Meldrum, D. (2011) Stability of DNA origami nanoarrays in cell lysate., *Nano Letters 11*, 1477-1482.

78. Keum, J.-W., and Bermudez, H. (2009) Enhanced resistance of DNA nanostructures to enzymatic digestion., *Chemical Communications (Cambridge, England)*, 7036-7038.

79. Shen, X., Jiang, Q., Wang, J., Dai, L., Zou, G., Wang, Z.-G., Chen, W.-Q., Jiang, W., and Ding, B. (2012) Visualization of the intracellular location and stability of DNA origami with a label-free fluorescent probe., *Chemical Communications (Cambridge, England) 48*, 11301-11303.

80. Rangnekar, A., Zhang, A. M., Li, S. S., Bompiani, K. M., Hansen, M. N., Gothelf, K. V., Sullenger, B. A., and LaBean, T. H. (2012) Increased anticoagulant activity of thrombin-binding DNA aptamers by nanoscale organization on DNA nanostructures, *Nanomed-Nanotechnol 8*, 673-681.

81. Conway, J. W., McLaughlin, C. K., Castor, K. J., and Sleiman, H. (2013) DNA nanostructure serum stability: greater than the sum of its parts., *Chemical Communications (Cambridge, England) 49*, 1172-1174.

82. Koyfman, A. Y., Braun, G. B., and Reich, N. O. (2009) Cell-Targeted Self-Assembled DNA Nanostructures, *Journal of the American Chemical Society 131*, 14237-14239.

83. Ko, S., Liu, H., Chen, Y., and Mao, C. (2008) DNA Nanotubes as Combinatorial Vehicles for Cellular Delivery, *Biomacromolecules 9*, 3039-3043.

84. Chang, M., Yang, C.-S., and Huang, D.-M. (2011) Aptamer-conjugated DNA icosahedral nanoparticles as a carrier of doxorubicin for cancer therapy., *ACS Nano 5*, 6156-6163.

85. Jiang, Q., Song, C., Nangreave, J., Liu, X., Lin, L., Qiu, D., Wang, Z.-G., Zou, G., Liang, X., Yan, H., and Ding, B. (2012) DNA origami as a carrier for circumvention of drug resistance., *Journal of the American Chemical Society 134*, 13396-13403.

86. Li, J., Pei, H., Zhu, B., Liang, L., Wei, M., He, Y., Chen, N., Li, D., Huang, Q., and Fan, C. (2011) Self-assembled multivalent DNA nanostructures for noninvasive intracellular delivery of immunostimulatory CpG oligonucleotides., *ACS Nano 5*, 8783-8789.

87. Verena J. Schuller, S. H., Nadja Sandholzer, Philipp C. Nickels, Nina A. Suhartha, Stefan Endres, Carole Bourquin, Tim Liedl†. (2011) Cellular Immunostimulation by CpG-Sequence-Coated DNA Origami Structures, *ACS Nano 5*, 9696-9702.

88. Aldaye, F. A., Senapedis, W. T., Silver, P. A., and Way, J. C. (2010) A Structurally Tunable DNA-Based Extracellular Matrix, *Journal of the American Chemical Society 132*, 14727-14729.

89. Horiguchi, M., Ota, M., and Rifkin, D. B. (2012) Matrix control of transforming growth factor-β function., *Journal of biochemistry 152*, 321-329.

90. Li, L., Orner, B. P., Huang, T., Hinck, A. P., and Kiessling, L. L. (2010) Peptide ligands that use a novel binding site to target both TGF-β receptors., *Molecular BioSystems 6*, 2392-2402.

91. Li, L., Klim, J. R., Derda, R., Courtney, A. H., and Kiessling, L. L. (2011) Spatial control of cell fate using synthetic surfaces to potentiate TGF-beta signaling., *Proceedings of the National Academy of Sciences of the United States of America 108*, 11745-11750.

92. Le Trong, I., Wang, Z., Hyre, D. E., Lybrand, T. P., Stayton, P. S., and Stenkamp, R. E. (2011) Streptavidin and its biotin complex at atomic resolution., *Acta Crystallographica. Section D, Biological Crystallography 67*, 813-821.

93. Miller, J., McLachlan, A. D., and Klug, A. (1985) Repetitive zinc-binding domains in the protein transcription factor IIIA from Xenopus oocytes., *The EMBO Journal 4*, 1609-1614.

94. Branden, C., and Tooze, J. (1999) *Introduction to Protein Structure*, Garland Science.

95. Liu, Q., Segal, D., Ghiara, J., and Barbas, C. (1997) Design of polydactyl zinc-finger proteins for unique addressing within complex genomes, *Proceedings of the National Academy of Sciences of the United States of America 94*, 5525-5530.

96. Beerli, R. R., Segal, D. J., Dreier, B., and Barbas, C. F. (1998) Toward controlling gene expression at will: specific regulation of the erbB-2/HER-2 promoter by using polydactyl zinc finger proteins constructed from modular building blocks, *Proceedings of the National Academy of Sciences of the United States of America 95*, 14628-14633.

97. Li, H., LaBean, T. H., and Kenan, D. J. (2006) Single-chain antibodies against DNA aptamers for use as adapter molecules on DNA tile arrays in nanoscale materials organization., *Organic & Biomolecular Chemistry 4*, 3420-3426.

98. Nakata, E., Liew, F. F., Uwatoko, C., Kiyonaka, S., Mori, Y., Katsuda, Y., Endo, M., Sugiyama, H., and Morii, T. (2012) Zinc-Finger Proteins for Site-Specific Protein Positioning on DNA-Origami Structures, *Angewandte Chemie (International ed. in English) 51*, 2421-2424.

99. Pinheiro, A. V., Han, D., Shih, W. M., and Yan, H. (2011) Challenges and opportunities for structural DNA nanotechnology, *Nature Nanotechnology 6*, 763-772.

100. Endo, M., Yang, Y., and Sugiyama, H. (2013) DNA origami technology for biomaterials applications, *Biomaterials Science 1*, 347.

101. Seeman, N. C. (2010) Nanomaterials based on DNA, *Annual Review of Biochemisty 79*, 65-87.

102. Pedersen, R. O., Loboa, E. G., and LaBean, T. H. (2013) Sensitization of transforming growth factor-β signaling by multiple peptides patterned on DNA nanostructures., *Biomacromolecules 14*, 4157-4160.

103. Liu, X., Xu, Y., Yu, T., Clifford, C., Liu, Y., Yan, H., and Chang, Y. (2012) A DNA nanostructure platform for directed assembly of synthetic vaccines., *Nano Letters 12*, 4254-4259.

104. Ding, B., Deng, Z., Yan, H., Cabrini, S., Zuckermann, R., and Bokor, J. (2010) Gold Nanoparticle Self-Similar Chain Structure Organized by DNA Origami, *Journal of the American Chemical Society 132*, 3248-3249.

105. Pilo-Pais, M., Goldberg, S., Samano, E., Labean, T. H., and Finkelstein, G. (2011) Connecting the nanodots: programmable nanofabrication of fused metal shapes on DNA templates., *Nano Letters 11*, 3489-3492.

106. Chen, Z., Lan, X., and Wang, Q. (2013) DNA Origami Directed Large-Scale Fabrication of Nanostructures Resembling Room Temperature Single-Electron Transistors., *Small 9*, 3567-3571.

107. Endo, M., Yang, Y., Emura, T., Hidaka, K., and Sugiyama, H. (2011) Programmed placement of gold nanoparticles onto a slit-type DNA origami scaffold., *Chemical Communications (Cambridge, England) 47*, 10743-10745.

108. Schreiber, R., Do, J., Roller, E.-M., Zhang, T., Schüller, V. J., Nickels, P. C., Feldmann, J., and Liedl, T. (2014) Hierarchical assembly of metal nanoparticles, quantum dots and organic dyes using DNA origami scaffolds., *Nature Nanotechnology 9*, 74-78.

109. Voigt, N. V., Torring, T., Rotaru, A., Jacobsen, M. F., Ravnsbaek, J. B., Subramani, R., Mamdouh, W., Kjems, J., Mokhir, A., Besenbacher, F., and Gothelf, K. V. (2010) Single-molecule chemical reactions on DNA origami, *Nature Nanotechnology 5*, 200-203.

110. Jahn, K., Tørring, T., Voigt, N. V., Sørensen, R. S., Bank Kodal, A. L., Andersen, E. S., Gothelf, K. V., and Kjems, J. (2011) Functional Patterning of DNA Origami by Parallel Enzymatic Modification, *Bioconjugate Chemistry 22*, 819-823.

111. Yoshidome, T., Endo, M., Kashiwazaki, G., Hidaka, K., Bando, T., and Sugiyama, H. (2012) Sequence-selective single-molecule alkylation with a pyrrole-imidazole polyamide visualized in a DNA nanoscaffold., *Journal of the American Chemical Society 134*, 4654-4660.

112. Dervan, P. B. (2001) Molecular recognition of DNA by small molecules., *Bioorganic & Medicinal Chemistry 9*, 2215-2235.

113. He, Y., Tian, Y., Ribbe, A. E., and Mao, C. (2006) Antibody Nanoarrays with a Pitch of ~20 Nanometers, *Journal of the American Chemical Society 128*, 12664-12665.

114. Chhabra, R., Sharma, J., Ke, Y., Liu, Y., Rinker, S., Lindsay, S., and Yan, H. (2007) Spatially Addressable Multiprotein Nanoarrays Templated by Aptamer-Tagged DNA Nanoarchitectures, *Journal of the American Chemical Society 129*, 10304-10305.

115. Shen, W., Zhong, H., Neff, D., and Norton, M. L. (2009) NTA Directed Protein Nanopatterning on DNA Origami Nanoconstructs, *Journal of the American Chemical Society 131*, 6660-6661.

116. Williams, B. a. R., Lund, K., Liu, Y., Yan, H., and Chaput, J. C. (2007) Self-assembled peptide nanoarrays: an approach to studying protein-protein interactions., *Angewandte Chemie (International ed. in English) 46*, 3051-3054.

117. Saccà, B., Meyer, R., Erkelenz, M., Kiko, K., Arndt, A., Schroeder, H., Rabe, K. S., and Niemeyer, C. M. (2010) Orthogonal Protein Decoration of DNA Origami, *Angewandte Chemie (International ed. in English) 49*, 9378-9383.

118. Meyer, R., and Niemeyer, C. M. (2011) Orthogonal Protein Decoration of DNA Nanostructures, *Small 7*, 3211-3218.

119. Erben, C. M., Goodman, R. P., and Turberfield, A. J. (2006) Single-molecule protein encapsulation in a rigid DNA cage., *Angewandte Chemie (International ed. in English) 45*, 7414-7417.

120. Duckworth, B. P., Chen, Y., Wollack, J. W., Sham, Y., Mueller, J. D., Taton, T. A., and Distefano, M. D. (2007) A universal method for the preparation of covalent protein-DNA conjugates for use in creating protein nanostructures., *Angewandte Chemie (International ed. in English) 46*, 8819-8822.

121. Carter, J. D., and LaBean, T. H. (2011) Organization of inorganic nanomaterials via programmable DNA self-assembly and peptide molecular recognition., *ACS Nano 5*, 2200-2205.

122. Hnilova, M., Oren, E. E., Seker, U. O. S., Wilson, B. R., Collino, S., Evans, J. S., Tamerler, C., and Sarikaya, M. (2008) Effect of molecular conformations on the adsorption behavior of gold-binding peptides., *Langmuir : the ACS Journal of Surfaces and Colloids 24*, 12440-12445.

123. Nielsen, P. E., and Egholm, M. (1999) An introduction to peptide nucleic acid., *Current Issues in Molecular Biology 1*, 89-104.

124. Pellestor, F., and Paulasova, P. (2004) The peptide nucleic acids (PNAs), powerful tools for molecular genetics and cytogenetics., *European Journal of Human Genetics : EJHG 12*, 694-700.

125. De Costa, N. T. S., and Heemstra, J. M. (2013) Evaluating the effect of ionic strength on duplex stability for PNA having negatively or positively charged side chains., *PloS One 8*, e58670.

126. Flory, J. D., Shinde, S., Lin, S., Liu, Y., Yan, H., Ghirlanda, G., and Fromme, P. (2013) PNA-peptide assembly in a 3D DNA nanocage at room temperature., *Journal of the American Chemical Society 135*, 6985-6993.

127. Lukeman, P. S., Mittal, A. C., and Seeman, N. C. (2004) Two dimensional PNA/DNA arrays: estimating the helicity of unusual nucleic acid polymers., *Chemical Communications (Cambridge, England)*, 1694-1695.

128. Chakrabarti, R., and Klibanov, A. M. (2003) Nanocrystals modified with peptide nucleic acids (PNAs) for selective self-assembly and DNA detection., *Journal of the American Chemical Society 125*, 12531-12540.

129. Xiaodi, S., and Kanjanawarut, R. (2009) Control of Metal Nanoparticles Aggregation and Dispersion by PNA and Detection, *ACS Nano 3*, 2751-2759.

130. Ananthanawat, C., Hoven, V. P., Vilaivan, T., and Su, X. (2011) Surface plasmon resonance study of PNA interactions with double-stranded DNA., *Biosensors & Bioelectronics 26*, 1918-1923.

131. Kameshima, W., Ishizuka, T., Minoshima, M., Yamamoto, M., Sugiyama, H., Xu, Y., and Komiyama, M. (2013) Conjugation of Peptide Nucleic Acid with a Pyrrole/Imidazole Polyamide to Specifically Recognize and Cleave DNA, *Angewandte Chemie International Edition 52*, 13681-13684.

132. Stadler, A. L., Sun, D., Maye, M. M., Lelie, D. V. D., and Gang, O. (2011) Site-Selective Binding of Nanoparticles to Double-Stranded DNA via Peptide Nucleic Acid "Invasion", *ACS Nano*, 2467-2474.

133. Sun, D., Stadler, A. L., Gurevich, M., Palma, E., Stach, E., van der Lelie, D., and Gang, O. (2012) Heterogeneous nanoclusters assembled by PNA-templated double-stranded DNA., *Nanoscale 4*, 6722-6725.

134. Ackermann, D., and Famulok, M. (2013) Pseudo-complementary PNA actuators as reversible switches in dynamic DNA nanotechnology., *Nucleic Acids Research 41*, 4729-4739.

135. Yamazaki, T., Aiba, Y., Yasuda, K., Sakai, Y., Yamanaka, Y., Kuzuya, A., Ohya, Y., and Komiyama, M. (2012) Clear-cut observation of PNA invasion using nanomechanical DNA origami devices., *Chemical Communications (Cambridge, England) 48*, 11361-11363.

136. LaBean, T. H., Yan, H., Kopatsch, J., Liu, F., Winfree, E., Reif, J. H., and Seeman, N. C. (2000) Construction, Analysis, Ligation, and Self-Assembly of DNA Triple Crossover Complexes, *Journal of the American Chemical Society 122*, 1848-1860.

137. Li, H., Park, S. H., Reif, J. H., LaBean, T. H., and Yan, H. (2004) DNA-Templated Self-Assembly of Protein and Nanoparticle Linear Arrays, *Journal of the American Chemical Society 126*, 418-419.

138. Tomac, S., Sarkar, M., Ratilainen, T., Wittung, P., Nielsen, P. E., Nordén, B., and Gräslund, A. (1996) Ionic Effects on the Stability and Conformation of Peptide Nucleic Acid Complexes, *Journal of the American Chemical Society 118*, 5544-5552.

139. Ke, Y., Lindsay, S., Chang, Y., Liu, Y., and Yan, H. (2008) Self-Assembled Water-Soluble Nucleic Acid Probe Tiles for Label-Free RNA Hybridization Assays, *Science 319*, 180-183.

140. Jungmann, R., Steinhauer, C., Scheible, M., Kuzyk, A., Tinnefeld, P., and Simmel, F. C. (2010) Single-molecule kinetics and super-resolution microscopy by fluorescence imaging of transient binding on DNA origami., *Nano Letters 10*, 4756-4761.

141. Johnson-Buck, A., Nangreave, J., Jiang, S., Yan, H., and Walter, N. G. (2013) Multifactorial modulation of binding and dissociation kinetics on two-dimensional DNA nanostructures., *Nano Letters 13*, 2754-2759.

142. Wittung, P., Nielsen, P., and Norde, B. (1996) Direct Observation of Strand Invasion by Peptide Nucleic Acid (PNA) into Double-Stranded DNA, *Journal of the American Chemical Society 118*, 7049-7054.

143. Nielsen, P. E., and Christensen, L. (1996) Strand Displacement Binding of a Duplex-Forming Homopurine PNA to a Homopyrimidine Duplex DNA Target Biochemistry Laboratory B, The Panum Institute Molecules that bind sequence specifically to double-stranded DNA in a predictable way are of high interest, *Journal of the American Chemical Society 118*, 2287-2288.

144. Wittung, P., Nielsen, P., and Nordén, B. (1997) Extended DNA-recognition repertoire of peptide nucleic acid (PNA): PNA-dsDNA triplex formed with cytosine-rich homopyrimidine PNA., *Biochemistry 36*, 7973-7979.

145. Nielsen, P. E., and Egholm, M. (2001) Strand displacement recognition of mixed adenine-cytosine sequences in double stranded DNA by thymine-guanine PNA (peptide nucleic acid). *Bioorganic & Medicinal Chemistry 9*, 2429-2434.

146. Frank-Kamenetskii, M. D., and Mirkin, S. M. (1995) Triplex DNA structures., *Annual Review of Biochemistry 64*, 65-95.

147. Betts, L., Josey, J. a., Veal, J. M., and Jordan, S. R. (1995) A nucleic acid triple helix formed by a peptide nucleic acid-DNA complex., *Science (New York, N.Y.) 270*, 1838-1841.

148. Gurtner, G. C., Werner, S., Barrandon, Y., and Longaker, M. T. (2008) Wound repair and regeneration., *Nature 453*, 314-321.

149. Mahdavian Delavary, B., van der Veer, W. M., van Egmond, M., Niessen, F. B., and Beelen, R. H. J. (2011) Macrophages in skin injury and repair., *Immunobiology 216*, 753-762.

150. Moura, L. I. F., Dias, A. M. a., Carvalho, E., and de Sousa, H. C. (2013) Recent advances on the development of wound dressings for diabetic foot ulcer treatment--a review., *Acta Biomaterialia 9*, 7093-7114.

151. Shaw, J. E., Sicree, R. a., and Zimmet, P. Z. (2010) Global estimates of the prevalence of diabetes for 2010 and 2030., *Diabetes Research and Clinical Practice 87*, 4-14.

152. Klapka, N., and Müller, H. W. (2006) Collagen matrix in spinal cord injury., *Journal of Neurotrauma 23*, 422-435.

153. Kohta, M., Kohmura, E., and Yamashita, T. (2009) Inhibition of TGF-beta1 promotes functional recovery after spinal cord injury., *Neuroscience Research 65*, 393-401.

154. Lutton, C., Young, Y. W., Williams, R., Meedeniya, A. C. B., Mackay-Sim, A., and Goss, B. (2012) Combined VEGF and PDGF treatment reduces secondary degeneration after spinal cord injury., *Journal of Neurotrauma 29*, 957-970.

155. Kubo, H., Hayashi, T., Ago, K., Ago, M., Kanekura, T., and Ogata, M. (2014) Temporal expression of wound healing-related genes in skin burn injury., *Legal Medicine (Tokyo, Japan) 16*, 8-13.

156. Douglas, S. M., Bachelet, I., and Church, G. M. (2012) A logic-gated nanorobot for targeted transport of molecular payloads., *Science (New York, N.Y.) 335*, 831-834.

157. Li, H., Park, S., Reif, J., LaBean, T., and Yan, H. (2004) DNA-Templated Self-Assembly of Protein and Nanoparticle Linear Arrays, *Journal of the American Chemical Society 126*, 418-419.

158. Gill, S. C., and von Hippel, P. H. (1989) Calculation of protein extinction coefficients from amino acid sequence data., *Analytical Biochemistry 182*, 319-326.

159. Nielsen, P. E., Ed. *Peptide Nucleic Acids: Protocols and Applications, Second Edition, 2nd Ed.;* Horizon Bioscience: Norfolk, U.K., 2004.

Biography

Ronnie Pedersen was born in Frederikssund, Denmark in 1982. He attended Aarhus University in Aarhus Denmark including a semester abroad at the University of North Carolina Chapel Hill and was awarded his Bachelor degree in Nanoscience in 2008. He continued his studies obtaining a Masters degree in the same field in 2009. He was then accepted to the PhD program at Duke University in Durham USA.

Publications

- (In preparation) **Pedersen, R. O.,** Kong, J., Achim, C., & LaBean, T. Efficient targeting of DNA nanostructures and toehold free strand displacement with short positively charged PNA. (2014)
- **Pedersen, R. O.**, Marchi, A. N., Majikes, J., Nash, J. A., Estrich, N. A., Courson, D. S., Hall, C. K., Craig, S. L., & Labean, T. (2014) Properties of DNA. In B. Bhushan (Ed) *Handbook of Nanomaterials Properties*. New York / Heidelberg: Springer
- **Pedersen, R. O.,** Loboa, E. G., & LaBean, T. H. Sensitization of Transforming Growth Factor-beta Signaling by Multiple Peptides Patterned on DNA Nanostructures. *Biomacromolecules,* (2013) *14*(12), 4157-4160.
- Nielsen, J. T., Bjerring, M., Jeppesen, M. D., **Pedersen, R. O.,** Pedersen, J. M., Hein, K. L., Vosegaard, T., & Skrydstrup, T. Unique Identification of Supramolecular Structures in Amyloid Fibrils by Solid-State NMR Spectroscopy. *Angewandte Chemie* (2009) *48*, 2118-2121.